NANYANG TECHNOLOGICAL UNIVERSITY

Investigation on the Mechanism of Amyloid Beta Peptides Oligomerization and the Process for its Inhibition

Zhao Li Na

School of Physical and Mathematical Sciences

2013

Investigation on the Mechanism of Amyloid Beta Peptides Oligomerization and the Process for its Inhibition

Zhao Li Na

School of Physical and Mathematical Sciences

A thesis submitted to the Nanyang Technological University in partial fulfillment of the requirements for the degree of Doctor of Philosophy

2013

Abstract

Amyloid β (Aβ) plaque, which is a characteristic hallmark of Alzheimer's disease (AD), results from the deposition of Aβ peptides. Amyloid β peptides are prone to self assembly into high-order oligomers, which is the major pathological pathway of AD. It is generally believed that the Aβ oligomers are the main source of toxicity and the leading contributor to neuronal cell death. Amyloid β oligomers are transient structures with no regular secondary structure. They are easily attached to membrane and other molecules. Thus, it is difficult to study them purely based on conventional experimental approaches. Hence, it is the goal of my research to use computational methodologies to reveal the mechanisms of Aβ aggregation in aqueous and membrane environment and the influence of small molecules like curcumin and heme, and the inflammatory proteins like S100A9, on Aβ oligomerization. We have chosen the full-length Aβ peptides as well as the most representative short segments of Aβ and employed the classical molecular dynamics and the sampling-enhanced replica exchange molecular dynamics simulations, to investigate the aggregation and atomic-detailed interaction among Aβ, lipids, small molecules and macromolecules.

We have carried out multiple simulations to study aggregation of the full-length Aβ peptides in the membrane environment. The N-terminus of Aβ was found to interact preferentially with the lipid-aqueous interface region while the C-terminus show inclination to remain inside the bilayer hydrophobic tail region. The interaction between peptides and lipids has facilitated the aggregation of Aβ peptides in the membrane. However, the interaction between cholesterol and peptides is inversely

correlated with the extent of the peptide-peptide interactions. Meanwhile, the formation of a short segment of parallel β-sheet between two peptide chains has been observed.

By studying the effect of curcumin on the stability of Aβ oligomers, we found that curcumin is capable of decreasing the β-sheet secondary structure content within the Aβ oligomers without reducing the contacts between the monomers. The breaking of the β-sheet is found to be preceded by a deformation of the β-sheet structure due to hydrophobic interaction from the nearby curcumin. Furthermore, the π-stacking interaction between curcumin and the aromatic residues of Aβ has also contributed to the diminishing of the β-sheet structure. After examining the paths of curcumin on the Aβ proteins, we have identified the common routes where curcumin lingers as it traverses around the Aβ.

Heme, which is abundant in the hemoglobin and many other hemoproteins, is known to play an important role in electron transfer, oxygen transport, regulation of gene expression, and many other biological functions. It is believed that the formation of Aβ-heme complex is essential in the inhibition of Aβ aggregation as well as in protecting the neurons from degradation. By means of conventional molecular dynamics simulations, we have shed light on this conjecture via the identification of several dominant binding motifs. We found that the hydrophobic residues of Aβ peptide have a high affinity to interact with heme instead of the residue histidine. We conclude that hydrophobic interaction plays a dominant role in the Aβ-heme complex formation which indirectly serves to physically prevent Aβ aggregation.

S100A9 is one of the pro-inflammatory protein abundant and over-expressed in the inflammation sites of AD. By means of replica exchange molecular dynamics simulations, we examine the role of S100A9 in the oligomerization process of Aβ peptides. The pro-inflammatory S100A9 protein interacts with the Aβ peptides directly, mainly through strong hydrophobic interactions with the Aβ central hydrophobic core region. The more straight Aβ_{12-24} peptide with a higher β-content may function as a template to induce the folding of new incoming Aβ peptides, which leads to the formation of aggregation-prone oligomer. Once such oligomer is formed, it may further serve as a seed to accelerate the aggregation of amyloid fibrils. Furthermore, our results show that amyloid oligomerization is mainly induced by S100A9 rather than Aβ peptides.

Overall, our studies have gained insights into the complex interaction pictures of Aβ with lipids, small molecules and macromolecules, which I hope, would lead to an enhanced understanding of the etiology and pathogenesis of AD.

Contents

Acknowledgements

I would like to thank all the people whose guide and help have made this thesis possible. First and foremost, I wish to express my deepest gratitude to my supervisors, Prof. Chew Lock Yue and Prof. Mu Yuguang, for their enormous support, guidance, patience, understanding and invaluable advice. Both of them are very great and super nice person to work with. They have ingrained in me with spirit of scientific research, and guided me in so many things, which have made my PhD journey a most enriching experience.

I would like to thank two colleagues I once worked with: Dr. Qu Xiaohui and Dr. Jerome Benoit. Thanks to Xiaohui for teaching me write my first python program. Thanks to Jerome for his patience in guiding me to build lots of software routines in development servers and cluster systems and also for introducing me to the Debian world. With great pleasure, I wish to thank my colleagues, group members and friends from the SPMS Nonlinear and Complex System Lab and SBS Computational Biology Lab. To Leong Hon Wai, Huynh Hoai Nguyen, He Chong, Hendrik Santoso Sugiarto, Saw Vee Liem, Han Nanyu, Li Weifeng, Wang Yaofeng, Zhang Tong, Lu Lanyuan, Xia Fei and Tong Dudu, thanks for the inspiring discussions we once had and thanks for sharing of knowledge.

Here, I want to give my special thanks Dr. Chiu See-Wing, a collaborator and friend, for his generous help in my research and for providing me with many valuable insights in my study. Another special thanks Soh Hwee Jin, Melvin for his great support and kindness on rendering me with computational resources that are so essential for my research work.

I am really grateful to my friends from the SRC swimming "club". They were proud even when they saw the little progress that I have made in my research and most important of all, they share my troubles. To Lin Fuchun, Gao Peng, Ren Lei, Wu Qiong, Yu Yao, Yang Hongwang, Hwang Chuan-Yang, Wu Li Ya Si and Wang Zuyuan, thanks for the encouragement that you guys have been giving. I really enjoyed the fun hours that we have together.

I wish to address my thanks to the people who are active in the Debian user list, perl world and Python tutor group. The people from those lists have given me so much help regardless of how simple and off-topic my questions were. They have inspired me greatly through their actions. They have also instilled me the philosophy of sharing, openness and the determination to get problems solved.

I would like to thank the Division of Physics and Applied Physics, School of Physical and Mathematical Sciences, Nanyang Technological University for the academic support and opportunities.

Finally, I would like to thank my family for their love and continuous support.

List of Figures

List of Tables

Chapter 1 Introduction

1.1 A brief overview of the background

Alzheimer's disease (AD) is characterized by the extra-neuronal Amyloid β (Aβ) plaque and intra-neuronal fibrillar tangles. The Aβ plaques consist of Aβ peptides, which are cleaved by the β- and γ-secretase from amyloid precursor protein (APP).[1,2] It is generally believe that the Aβ oligomers are one of the main culprit which causes the neurotoxicity.[3–7]

The oligomers usually have no regular but transient secondary structures. They are easily attach to the membrane or other macromolecules, rendering them insoluble.[8] It is thus very difficult for conventional experimental approach to study the toxicity mechanism. Molecular dynamics simulation, which is a complementary to the experimental methods, may serve as a theoretical tool to provide atomic-level study of Aβ aggregation. In addition, its results would serve as a guiding roadmap on Aβ interaction with specific small molecules of interest.

Research has found that Aβ peptide is generated in the cholesterol-rich membrane area and it is generally believed that an elevated level of cholesterol has a greater risk of Alzheimer's disease.[9] In this respect, it is important for us to examine the binding effect of cholesterol to the Aβ peptide during the peptide aggregation in the membrane environment.

On the other hand, it is known that certain molecules possess inhibitory effects on Aβ peptide aggregation. One such molecule is curcumin. Curcumin, [(1,7-

bis-(4-hydroxy-3-methoxyphenyl)-1,6-heptadiens-3,5-dione)], possesses significant therapeutic potential due to its antioxidant, anticarcinogen, anti-inflammation,[10] and intrinsic non-toxicity properties. Recent research have revealed strong connections between curcumin and AD. For example, one case shows that the risk of getting AD reduces if one takes a regular diet of curcumin,[11] while another case indicates that curcumin can regulate the production of Aβ via indirectly suppressing presenilin 1 gene expression.[12] Furthermore, curcumin's unique physicochemical properties make it easy to pass the blood-brain barrier and interact with Aβ directly[13] to block aggregation and disrupt plaque formation.[14–17] Despite recent studies being done and several mechanisms being proposed[18] on the inhibitory effects of curcumin, the detailed mechanism on how curcumin interacts with the Aβ oligomers are still awaiting further identification and elucidation.

In addition to curcumin, another molecule that possesses significant interaction with the Aβ peptide is the heme molecule. Heme consists of an iron atom in the center of its four substituted pyrrole rings interconnected via methiane bridges.[19,20] It is very hydrophobic, and easily "stick" to protein or some other macromolecules. Heme has been reported to stick to one or more intracellular Aβ histidine residues which decreases its own bioavailability. The consequence is a deficiency of the functional heme.[16,21] On the other hand, the heme-Aβ_{1-40} complex, which is formed by the exogenous heme and Aβ, shows the potential of inhibiting Aβ aggregation and alleviating toxicity induced by Aβ.[22] Some identified and putative Aβ-heme motifs have been proposed recently.[23–25] The hydrophilic N-terminal of Aβ has been suggested to be a general binding domain.[16,26] Two residues, His-13 and His-14, have been found to be more significant than other residues with respect to heme binding and peroxidase activity.[27] However, the detailed structure of the Aβ-heme complex conformation is still missing and the possible role of Aβ-heme complex in Aβ aggregation still needs to be determined.

The deposits of amyloid beta plaques and the occurence of neurofibrillary tangle (NFT) indicate the presence of potential stimuli for inflammation in the AD brain. It is assumed that the inflammation leads to neuronal degeneration and the pathology of AD.[28] Clinical studies have revealed that anti-inflammation drugs can delay the early-onset progression of AD.[29,30] Meanwhile, the neuroprotective effect of inflammation has been considered as a beneficial response of AD.[31–34] The molecule S100A9 belongs to the EF-hand Ca^{2+}-binding protein family. It is one of the inflammation associated proteins in the S100 family, and it is abundantly over-expressed and actively secreted by non-traditional Golgi-route pathway at the inflammation sites.[35] In particular, the enhanced expression of S100A9 is observed in the AD brains. The knockdown of the S100A9 gene has led to a great improvement in cognitive abilities together with a reduced amount of Aβ.[36] Interestingly, the binding of calcium to S100A9 can expose a broad hydrophobic surface to interact with other proteins and further modulate the target. In addition, it can also reciprocally induce S100A9 to self-interact or to interact with S100A8 to assemble into homodimers, heterodimers or even higher-order oligomers. Recent experimental study has shown that the binding of S100A9 to Aβ peptide has promoted the formation of Aβ plaques, which reduces the toxicity of Aβ oligomers accordingly and hence plays a protective response in the AD brains.[34] It is thus important to examine the interaction of S100A9 with the Aβ peptide.

Above all, being inspired by the pioneering work of many groups in their search for understanding of the toxicity of the Aβ peptides aggregation and accumulation process, and being driven by how complex Aβ neurotoxicity is related with many other factors, we attempt to gain insights into a range of unsolved problems of Aβ aggregation. These problems are: the aggregation mechanisms of Aβ in the membrane environment; the role of the cholesterol; the effect of curcumin; the possible motif of the heme-Aβ complex; the diversity of Aβ peptide oligomers; and the influence of the inflammatory proteins. We also take a glimpse on how Aβ starts to accumulate and contribute to pathogenesis, and what are the best antibodies that can be directed at Aβ peptides which will bring hope for a cure of Alzheimer's disease. Meanwhile, there are further problems which are beyond our current scope of research, such as the ability of pan-Aβ antibodies of detect not only Aβ peptides but also the normally more abundant full-length APP, as well as the Aβ-containing APP fragments, namely the β-secretase cleaved APP βCTFs.

In order to address these problems, the following research has been performed in this thesis: a systematic review on the toxicity mechanism of Aβ oligomers in line of its interaction with membrane and receptors, and its intraneuronal aggregation; a study on the structure and aggregation process of Aβ peptides in the membrane environment; an examination on the small molecule curcumin with regards to its effects on Aβ dimer stability; the prediction of possible Aβ-heme complex as well as an examination on the effect of heme on the process of Aβ oligomerization; and a study on the influence of the pro-inflammatory protein S100A9 on Aβ oligomerization via replica exchange molecular dynamics (REMD) simulations.

1.2 Computational methodologies

1.2.1 Computational modeling

Computational modeling has emerged as a powerful tool in varied areas, such as biological system, neuroscience, social science and new materials. The most salient goal of computer modeling is to reproduce the experimental phenomena and to reveal the underlying mechanism so as to predict many properties before the conduct of experiments. There are currently many computational protocols being adopted to simulate different systems. A book[37] that provides a comprehensive review on this area is "Introduction to Computer Simulation Methods: Application to Physical Systems" by Tamar Schlick.

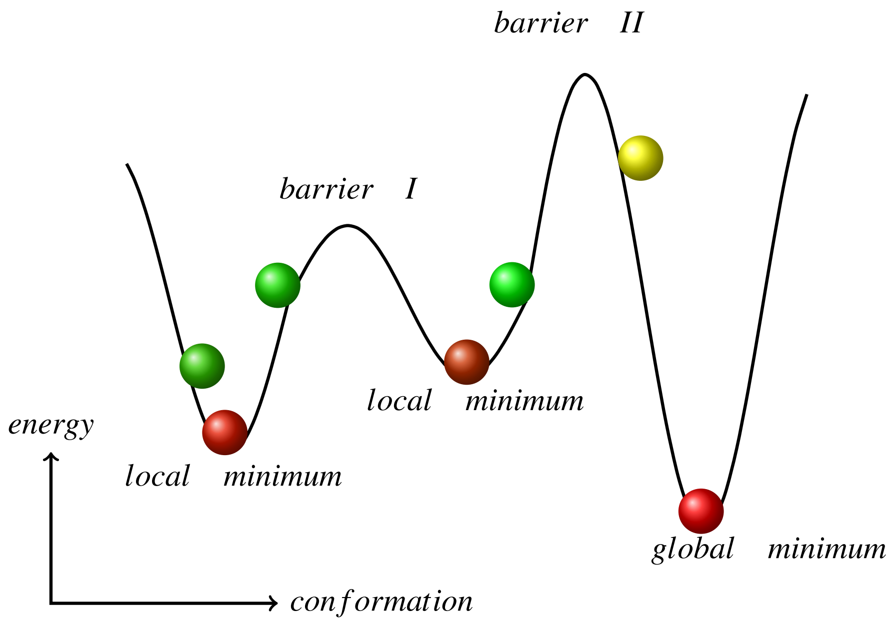

Figure 1.1: Schematic representation of conformational sampling on the potential energy surface.

A widely used simulation protocol which is of interest in this thesis is that of energy minimization (a process to find a local minimum) and molecular dynamics simulation (a process to find a global structural features) (see Figure 1.1). Currently, most popular energy minimization methods[38–40] involve: the steepest descents methods, conjugated gradient method and Newton-Raphson method. These minimization have their own limitation is that they can only help to find local minimum. For the global structural feature of molecules, molecular dynamics turns out to be a powerful tool to be utilized.

1.2.2 Molecular dynamics simulation

One of the most popular molecular simulation methods for small, large and complex molecular systems is the molecular dynamics simulation, which in essence implements the Newton's laws of motion. In this simulation, the positions and momenta of large number of atoms (particles) in certain isolated box or bulk with periodic boundary conditions, are coupled and updated via Newton's equations. These atoms interact with each other via inter- and intra-molecular forces described by empirical energy functions with the total energy summarized as $E_{total} = E_{bonded} + E_{nonbonded}$, where $E_{bonded} = E_{bond} + E_{angle} + E_{dihedral}$ and $E_{nonbonded} = E_{electrostatic} + E_{vanderWaals}$. A typical force field can be written as:

$$\begin{aligned} U(\{r_i\}) = \sum_j \frac{k_j^l}{2}(l_j - l_j^0)^2 + \sum_j \frac{k_j^\theta}{2}(\theta_j - \theta_j^0)^2 + \sum_{torsions} \frac{Vn}{2}(1 + cos(n\phi - \gamma)) \\ + \sum_{i,j=0}^{N} \frac{q_i q_j}{r_{ij}} + \sum_{i,j=1}^{N} 4\varepsilon\Big[(\frac{\sigma_{ij}}{r_{ij}})^{12} - (\frac{\sigma_{ij}}{r_{ij}})^6\Big], \end{aligned} \tag{1.1}$$

which includes the contribution from bond stretching, valence angle bending, torsional and electrostatic (Coulomb), as well as van der Waals (Lennard-Jones) interactions.

Since 1980, several force fields have been developed by different groups. The Amber force field is first developed, followed by optimized potentials for liquid simulation (OPLS), and then the Chemistry at HARvard using Molecular Mechanics (CHARMM) force field. Subsequently, many empirical force fields, such as: GROMOS, CVFF, ENVYMIX, ECEPP/2, QCFF/PI and UFF, have also emerged as popular force fields for different purposes. In particular, AMBER, GROMOS and CHARMM were developed to target molecular dynamics simulation of macromolecules.

The procedure of running a molecular dynamics simulation begins by assigning the initial positions r (by assessing available structure from existing experimental data or homology modeling) and velocities v (based on thermal temperature) for all atoms in the system. After potential V, which is a function of r and v, is then evaluated, and the new positions and velocities are calculated and updated by solving Newton's equation of motion:

$$\begin{aligned} F_i &= -\frac{\partial V}{T_i}, \\ \frac{d^2 r_i}{dt^2} &= \frac{F_i}{m_i}, \\ \frac{dr_i}{dt} &= v_i, \\ \frac{dv_i}{dt} &= \frac{F_i}{m_i}. \end{aligned} \tag{1.2}$$

The net force on each atom is then calculated by summing the force due to bonded interactions, the force between nonbonded interactions, as well as the external forces (refer Eq. 1.1), i.e., $F_i = -\sum F_{ij}$.

1.2.3 Replica exchange molecular dynamics

During molecular dynamics simulation, we treat time average obtained through temporal simulation as "ensemble average" based on the ergodic hypothesis. To calculate an ensemble average, the molecular dynamics simulations must explore all possible states conformations and go beyond particular thermodynamic constraints. From Figure 1.1, we can see that it is difficult to overcome the energy barrier II than barrier I. In order to enhance sampling, replica exchange dynamics simulation is then performed by having a number of independent replicas running simultaneously at different temperatures, with pairs of neighboring replicas i and j exchanging their states based on the metropolis criterion after a very short time period. According to the Metropolis-Hastings criterion, update will be accepted with probability

$$p = min\left(1, e^{(E_i - E_j)(\frac{1}{\kappa_B T_i} - \frac{1}{\kappa_B T_j})}\right), \tag{1.3}$$

where κ_B is the Boltzmann constant, T_i/E_i and T_j/E_j are the ratio of temperature to energy of replica i and j, respectively. Thus, there will be an exchange between state j and state i if state i has a higher temperature with lower energy while on the other hand state with higher temperature and higher energy still has the chance of coming to the neighbouring low temperature state if it meets the Metropolis-Hastings criterion. In consequence, the sampling can be greatly enhanced through the exchange with higher temperature configurations which help to escape the local minimum.

1.2.4 Define secondary structure and hydrogen bonds

The secondary structure of protein is defined based on the DSSP algorithm[41] developed by W. Kabsch and C. Sander in 1983, which involves the pattern recognition of hydrogen-bonded geometry information. By assigning partial charges on the C, O($+q_1$, $-q_1$) and N, H($-q_2$, $+q_2$), they have calculated the electrostatic energy between two H-bonding groups as:

$$E_{electrostatic} = q_1 q_2 (\frac{1}{r_{ON}} + \frac{1}{r_{CH}} - \frac{1}{r_{OH}} - \frac{1}{r_{CN}}) f, \tag{1.4}$$

where $q_1 = 0.42e$ and $q_2 = 0.20e$ and r_{AB} is the distance from atom A to B with the dimensional factor $f = 332$. Based on the above calculation, a general H bond has $3kcal/mol$ binding energy. They have also chosen the cutoff rather generously once it satisfies the condition $E < -0.5kcal/mol$, which allows for the distance between N and O up to $2.2\AA$. Overall, the secondary structures can be categorized:

- "B" = "β-Bridge"
- "E" = "β-Sheet"
- "G" = "3-Helix (3_{10}-helix)"
- "H" = "α-Helix"
- "I" = "5-Helix"
- "S" = "Bend"
- "T" = "Turn"

- "$\sim$" = "Coil"

Based on the calculation from DSSP, which provides information on the secondary structure of each residues as the simulation evolves, we further calculate the occurence of the α- or β- structure of each residues to determine its propensity to adopt the α- or β-structure. Additionally, in the following chapters, the hydrogen bonds are determined based on cutoffs for the angle acceptor - donor - hydrogen as 30 degrees and the distance of hydrogen-acceptor as $0.35nm$ by default and the propensity are based on the occurence of such atom appeared as donor/acceptor during our simulation time.

1.2.5 Potential of mean forces

The potential of mean force is to be determined by first constructing a one-dimensional grid with bins that give the minimum distance between the high propensity residues and the Fe ion of heme. The number of sampled conformations that fall into each bin N_i is then computed. The potential of mean force V_{pmf} is obtained from:

$$V_{pmf} = -k_B T log(N_i/N_{max}). \tag{1.5}$$

Here k_B is the Boltzmann constant, T is the absolute temperature, and N_{max} is the maximum number of the sampled conformations counted in each bin, i.e. the largest N_i.

1.3 Structure of the dissertation

With this brief overview of biological background and the computational methodologies, the outline of the rest of the chapters is as follows:

In Chapter 2, we introduce Alzheimer's disease from the basis of two pathological hallmarks. One relates to intraneuronal fibrillar tangles, which arises from tau protein and its aggregation. Another involves extraneuronal amyloid plaques, which concerns amyloid β peptides and the Aβ oligomers. We put our focus on the amyloid β peptides, the tau protein and the links between the two. After which, we bring out the current therapeutic strategies that target the different developed stages of AD.

Chapter 3 follows closely on the work that has been published: "L. N. Zhao, H. W. Leong, Y. G. Mu and L. Y. Chew. The toxicity of amyloid β oligomers. Int. J. Mol. Sci., 13, 7303 (2012)." In this chapter, the mechanism of Aβ oligomer toxicity was elucidated via a discussion on the interaction of Aβ oligomers with the membrane through the process of adsorption, insertion, aggregation and ion channel/pore formation, as well as a brief review on the intra-neuronal Aβ toxicity. Furthermore, the relationship between Aβ and the membrane receptors, and the detrimental effects of oxidative stress are also discussed.

Chapter 4 depicts the molecular dynamics simulations that were carried out to investigate the self-assembly of three full-length amyloid peptides in the dipalmitoylphosphatidylcholine (DPPC) and cholesterol mixed lipid bilayer. The study has led to the publication: "L. N. Zhao, S. W. Chiu, J. Benoit, L. Y. Chew and Y. G. Mu. Amyloid beta peptides aggregation in a mixed membrane bilayer: a molecular dynamics study. J. Phys. Chem. B, 115(42), 12247-12256 (2011)."

Chapter 5 relates closely to the research work that has been published in "L. N.

Zhao, S. W. Chiu, J. Benoit, L. Y. Chew and Y. G. Mu. The effect of curcumin on the stability of Aβ dimers. J. Phys. Chem. B, 116(25), 7428-7435 (2012)". We have used all-atom explicit solvent molecular dynamics simulations to study the effect of curcumin on the stability of Aβ amyloid protein oligomers. In Chapter 6, we study the interaction of heme with Aβ, via conventional molecular dynamics simulations on the 1 A$\beta + 1$ heme and 2 A$\beta + 4$ hemes system. In Chapter 7, we study the influence of the inflammation associated protein S100A9 on the Aβ segments by replica exchange molecular dynamics simulations.

Chapter 2 and 3 are mainly literature reviews. For Chapters 4 to 7, they are organized in the following format: a brief introduction; simulation methods and protocols as well materials employed; simulation results; and summary and discussion. Note that the heart of each chapter is the result section.

Finally, in Chapter 8, I conclude the thesis and propose possible future directions.

Note that the two appendices list the pKa value of the titratable residues and the curcumin topology respectively. The glossary gives the alphabetical listing of the specialized terms used within this dissertation. The reference section cross-references all the materials being cited in this dissertation. The publication section collects the academic work that have been published as well as those under preparation.

Chapter 2 Alzheimer's disease

Alzheimer's disease was first recognized by Alois Alzheimer as presenile dementia in 1906. It is mainly diagnosed in people whose age is over 65 with the prevalence of AD being shown to grow exponentially with age. However, it is not exactly a ageing-related disease.[42] It is prevalent among the 10% of elderly people, which makes AD an emerging social health issue with the rise of an aging population in the coming decades. AD has been classified into two types. One is gene-related heritable AD, known as early onset familial Alzheimer's disease (FAD). The clinical symptoms can appear in a very young age and it accounts for 25% of all AD cases.[43] Another type is sporadic Alzheimer's disease (sAD), which constitutes the vast majority of AD cases and is also apparently influenced by genetic contributions besides non-genetic environmental factors.[44–46] Several genes have been identified to increase the chance of developing FAD and sAD. However, the pathological role of the only identified $\varepsilon 4$ Apro lipoprotein E (APOE) gene in sAD is still insufficient. In addition, the mutation of APOE $\varepsilon 4$ is not necessary to increase the risk of developing sAD.[47,48] Thus, late-onset AD degenerative process has been speculated to be polygenic with the involvement of multiple risk factors.[45]

The early symptoms of AD include loss of short-term memory, difficulties in executing daily life activities, withdrawal from social life and so on. The behavioral symptoms include progressive decline in memory, spatial reasoning, attention, and languages. AD is mainly characterized by two pathological hallmarks: intracellular NFT formed by hyperphosphorylated tau protein, and extracellular amyloid plaque consisting of amyloid β peptides. Significant selective neuronal degeneration and loss, with neurotransmitter deficits and inflammation are also evident.[49] In the following sections, a short review with regards to the tau protein and tau accumulation, Aβ plaques and Aβ oligomers are discussed.

2.1 Tau protein and tau accumulation

Tau protein arises from the alternative splicing of the microtubule-associated protein tau (MAPT) gene, and is abundant within the central and peripheral nervous system. It is one of the intrinsically unstructured protein (IUP), which exhibits as random coil under physiological conditions, and is capable of folding into a well-defined stable structure, the neurofibrillary tangles in AD, for example. Normally, it is the phosphorylation-modified tau protein that stabilizes axonal microtubules in the centeral nervous sysem (CNS). This protein also with actin cytoskeleton and plasma membrane, serves as enzyme anchoring, helps neurite outgrowth, and transports axoplasm. However, under certain circumstances, tau protein may undergo abnormal phoshorylation, hyperphosphorylation and some other modifications - nitration, ubiquitination, truncation, shift, prolyl isomerization - which may reduce the binding affinity of tau towards microtube, and thus leading to either intraneuronal accumulation of tau protein or its binding to other macromolecules.[50–53]

The mislocalization and accumulation of tau protein in dendrites and dendritic spines brings about a disruption of neuronal cell communication, which precedes neurodegeneration and causes a loss of memory.[54] Tau self-assembles to form straight filaments (SFs) and/or paired helical filaments (PHF) may further aggregate into NFT which is significantly correlated with the severity of AD. Electron microscopy of

PHFs show the appearance of two strands twisting around each other with a cross-over repeat of $75 - 80$ *nm* and a width of $10 - 22$ *nm*.[55,56] It has further revealed the β-sheet as the most dominant structure in the PHFs.

2.2 Amyloid plaque and Aβ peptide

2.2.1 Amyloid precursor protein

The amyloid β plaques results from the aggregation of the amyloid β (Aβ) peptides, which was cleaved by the β- and γ-secreastase from APP. The precise biological function of APP is as yet not well defined even though lots of studies have revealed its biological and physiological importance in the neurite outgrowth modulation,[57] copper homeostasis regulation,[58] synaptic transmission and formation, synaptic function and activity.[59,60] On the other hand, it has been shown that the absence of APP in a mouse model has not caused a significant impairment of cognitive abilities, but instead has led to a decrease in locomotion activity.[61]

2.2.2 Aβ aggregation pathway

Neuronal impairment is observed in patient even before Aβ plaque formation during the early onset AD. It is generally believed that Aβ oligomer is the main culprit of neurotoxicity.[4–7] Due to these oligomers being easily attached to the membrane or other macromolecules and hard to be isolated from these structures, conventional experimental studies on them are very difficult.[8] Some progress has been made recently which shows that Aβ dimers can be measured and strongly associated with dementia.[62] Besides the experimental methods, molecular dynamic simulation is a complementary approach for atomic level study of the unstructured monomer aggregation process, structural evolution and toxicity.

2.2.3 Structural evolution during aggregation

In the recent decades, NMR and X-ray have been performed to determine the structure of Aβ in water and membrane environment (see Table 2.1). One general observation is that Aβ peptides exhibit the characteristic of polymorphism.

Table 2.1: Structural data of amyloid beta peptide obtained from experiments.

PDB ID	Experimental Technique	Resolution	Release Date	Residue Number	DOI
1AMB[63]	SOLUTION NMR	-	1994-12-20	28	-
1AMC[64]	SOLUTION NMR	-	1995-01-26	28	-
1AML[65]	SOLUTION NMR	-	1996-01-29	40	-
1BA4[66]	SOLUTION NMR	-	1998-06-17	40	-
1BA6[67]	SOLUTION NMR	-	1998-06-17	40	10.1021/bi972979f
1BJB[68]	SOLUTION NMR	-	1998-11-04	28	10.1006/jsbi.2000.4267
1BJC[68]	SOLUTION NMR	-	1998-11-18	28	10.1006/jsbi.2000.4267
1HZ3[69]	SOLUTION NMR	-	2001-01-31	26	10.1002/pro.5560060902
1IYT[70]	SOLUTION NMR	-	2003-02-11	42	10.1006/jsbi.2000.4288
1NMJ[71]	SOLUTION NMR	-	2003-01-28	28	10.1038/7562
1QWP[72]	SOLUTION NMR	-	1997-07-07	11	10.1021/bi961598j
1QXC[72]	SOLUTION NMR	-	2004-09-14	11	-
1QYT[72]	SOLUTION NMR	-	2004-12-14	11	10.1021/jm040773o
1ZE7[73]	SOLUTION NMR	-	2005-05-03	18	10.1074/jbc.M504454200
2BP4[73]	SOLUTION NMR	-	2005-04-21	16	10.1074/jbc.M504454200
2LI9[74]	SOLUTION NMR	-	2011-07-20	40	10.1016/j.bbrc.2011.06.133
2LI9[74]	SOLUTION NMR	-	2012-01-18	36	-
2M9S[75]	SOLUTION NMR	-	-	40	10.1016/j.bbagen.2013.06.031
2Y2A[76]	X-RAY DIFFRACTION	-	2011-10-26	6	10.1073/pnas.1112600108
2Y3J[76]	X-RAY DIFFRACTION	1.91	-	6	10.1073/pnas.1112600108
2Y3L[76]	X-RAY DIFFRACTION	2.1	2011-11-02	8	10.1073/pnas.1112600108
2Y3K[76]	X-RAY DIFFRACTION	2.1	2011-11-02	8	10.1073/pnas.1112600108
3Q2X[76]	X-RAY DIFFRACTION	2.1	2011-11-02	6	10.1073/pnas.1112600108
3PZZ[76]	X-RAY DIFFRACTION	2.1	2011-11-02	6	10.1073/pnas.1112600108
2Y3L[76]	X-RAY DIFFRACTION	2.1	2011-11-02	8	10.1073/pnas.1112600108
3OVJ[77]	X-RAY DIFFRACTION	1.8	2011-07-06	24	10.1016/j.molcel.2004.06.037
3OW9[76]	X-RAY DIFFRACTION	1.8	2011-08-31	12	10.1371/journal.pbio.1001080
	SOLUTION NMR	-	2004-09-14	11	10.1021/jm040773o
	SOLUTION NMR	-	2012-01-18	36	10.1016/j.bpj.2011.11.4006
2OTK[78]	3D NMR	-	2013-09-11	40	10.1016/j.bbagen.2013.06.031

In many situations, Aβ is found to easily attach to other protein or to self-assemble into large oligomers or fibrils. The complex involving Aβ peptides, such as the APP, Aβ binding copper ions, Aβ segements with enzymes, as observed by experiment can be found in Table 2.2.

PDB ID	Experimental Technique	Resolution	Release Date	Residue Number	DOI
1AAP[79]	X-RAY DIFFRACTION	1.5	1991-10-15	116	-
1BRC[80]	X-RAY DIFFRACTION	2.5	1994-05-31	279	10.1006/jmbi.1993.1211
1TAW[81]	X-RAY DIFFRACTION	1.8	1997-06-24	281	10.1002/pro.5560060902
1CA0[81]	X-RAY DIFFRACTION	2.1	1997-07-23	590	10.1002/pro.5560060902
1X11[82]	X-RAY DIFFRACTION	2.5	1998-01-14	370	10.1093/emboj/16.20.6141
1MWP[83]	X-RAY DIFFRACTION	1.8	2000-03-15	96	10.1038/7562
1OQN[84]	X-RAY DIFFRACTION	2.3	2003-08-05	336	10.1074/jbc.M304384200
1OWT[85]	SOLUTION NMR	-	2003-05-13	66	10.1074/jbc.M300629200
1TKN[86]	SOLUTION NMR	-	2004-08-03	110	10.1021/bi049041o
1ZJD[87]	X-RAY DIFFRACTION	2.6	2005-08-09	294	10.1074/jbc.M504990200
2BEG[88]	SOLUTION NMR	-	2005-11-22	210	10.1073/pnas.0506723102
2G47[89]	X-RAY DIFFRACTION	2.1	2006-10-24	2060	10.1038/nature05143
2FJZ[90]	X-RAY DIFFRACTION	1.61	2007-01-16	59	10.1016/j.jmb.2006.12.041
2FK1[90]	X-RAY DIFFRACTION	1.6	2007-01-16	59	10.1016/j.jmb.2006.12.041
2FK2[90]	X-RAY DIFFRACTION	1.65	2007-01-16	59	10.1016/j.jmb.2006.12.041
2FK3[90]	X-RAY DIFFRACTION	2.4	2007-01-16	472	10.1016/j.jmb.2006.12.041
2FKL[90]	X-RAY DIFFRACTION	2.5	2007-01-16	132	10.1016/j.jmb.2006.12.041
2FMA[91]	X-RAY DIFFRACTION	0.85	2007-01-16	59	10.1107/S1744309107041139
2IPU[92]	X-RAY DIFFRACTION	1.65	2007-10-09	906	10.1073/pnas.0705888104
2R0W[92]	X-RAY DIFFRACTION	2.5	2007-10-16	450	10.1073/pnas.0705888104
2OTK[78]	SOLUTION NMR	-	2008-02-12	182	10.1073/pnas.0711731105
2ROZ[93]	SOLUTION NMR	-	2008-07-22	168	10.1074/jbc.M803892200
3BAE[94]	X-RAY DIFFRACTION	1.59	2008-04-15	474	10.1016/j.jmb.2007.12.036
3BKJ[94]	X-RAY DIFFRACTION	1.59	2008-04-15	492	10.1016/j.jmb.2007.12.036
3DXC[95]	X-RAY DIFFRACTION	2.1	2008-09-16	350	10.1038/embor.2008.188
3DXD[95]	X-RAY DIFFRACTION	2.2	2008-09-16	350	10.1038/embor.2008.188
3DXE[95]	X-RAY DIFFRACTION	2.0	2008-09-16	350	10.1038/embor.2008.188
3GCI[96]	X-RAY DIFFRACTION	2.04	2009-03-10	126	-
3IFL[97]	X-RAY DIFFRACTION	1.5	2009-11-17	448	10.1074/jbc.M109.045187
3IFN[97]	X-RAY DIFFRACTION	1.5	2009-11-17	481	10.1074/jbc.M109.045187
3IFO[97]	X-RAY DIFFRACTION	2.15	2009-11-17	904	10.1074/jbc.M109.045187
3IFP[97]	X-RAY DIFFRACTION	2.95	2009-11-17	1808	10.1074/jbc.M109.045187
3JQ5[96]	X-RAY DIFFRACTION	2.03	2009-09-29	127	-

3JQL[96]	X-RAY DIFFRACTION	1.2	2009-09-29	125	-
2WK3[98]	X-RAY DIFFRACTION	2.59	2009-11-03	2122	10.1016/j.jmb.2009.10.072
3KTM[99]	X-RAY DIFFRACTION	2.7	2010-02-23	1528	10.1073/pnas.0911326107
3L81[100]	X-RAY DIFFRACTION	1.6	2010-06-02	308	10.1016/j.devcel.2010.01.015
3JTI[101]	X-RAY DIFFRACTION	1.8	2010-07-21	127	-
3L33[102]	X-RAY DIFFRACTION	2.48	2010-09-22	1104	10.1074/jbc.M110.171348
3MOQ[103]	X-RAY DIFFRACTION	2.05	2011-02-16	504	10.1523/JNEUROSCI.4259-10.2011
3MXC[104]	X-RAY DIFFRACTION	2.0	2011-05-11	110	10.1016/j.jmb.2011.09.046
3NYJ[105]	X-RAY DIFFRACTION	3.2	2011-06-01	207	10.1021/bi101846x
3NYL[106]	X-RAY DIFFRACTION	2.8	2011-07-13	210	10.1016/j.molcel.2004.06.037
2Y3J[107]	X-RAY DIFFRACTION	1.99	2011-11-02	48	10.1073/pnas.1112600108
2Y3K[107]	X-RAY DIFFRACTION	1.9	2011-11-02	64	10.1073/pnas.1112600108
3AYU[108]	X-RAY DIFFRACTION	2.0	2011-08-03	177	10.1074/jbc.M111.264176
2LMN[109]	SOLID-STATE NMR	-	2011-12-28	480	10.1021/bi051952q
2LMO[109]	SOLID-STATE NMR	-	2011-12-28	480	10.1021/bi051952q
2LMP[110]	SOLID-STATE NMR	-	2011-12-28	720	10.1073/pnas.0806270105
2LMQ[110]	SOLID-STATE NMR	-	2011-12-28	720	10.1073/pnas.0806270105
2LNQ[111]	SOLID-STATE NMR	-	2012-02-08	320	10.1073/pnas.1111305109
2LOH[112]	SOLUTION NMR	-	2012-05-23	86	10.1016/j.febslet.2012.04.062
2LP1[113]	SOLUTION NMR	-	2012-06-06	122	10.1126/science.1219988
2LLM[114]	SOLUTION NMR	-	2012-06-20	43	PMCID: PMC3347594
3U0T[115]	X-RAY DIFFRACTION	2.5	2012-01-11	894	10.1016/j.jmb.2011.11.047
3UMH[116]	X-RAY DIFFRACTION	2.0	2012-01-25	211	10.1016/j.jmb.2011.12.057
3UMI[116]	X-RAY DIFFRACTION	2.4	2012-01-25	211	10.1016/j.jmb.2011.12.057
3UMK[116]	X-RAY DIFFRACTION	2.6	2012-01-25	211	10.1016/j.jmb.2011.12.057
3SV1[117]	X-RAY DIFFRACTION	3.3	2012-07-11	612	10.1093/jmcb/mjs033
4HIX[118]	X-RAY DIFFRACTION	2.2	2013-03-13	475	10.1038/srep01302
2M4J[119]	SOLUTION NMR	-	2013-09-25	360	10.1016/j.cell.2013.08.035
2LZ3[120]	SOLUTION NMR	-	2013-10-02	56	-
2LZ4[120]	SOLUTION NMR	-	2013-10-02	56	-

Table 2.2: Experimental data of amyloid beta oligomers, fibrills and binding proteins.

The central amyloidogenic step of the oligomerization process is the transition from α-helix rich to β-sheet rich structures. In water environment, REMD simulation had been performed to study the short peptide Aβ_{10-35} dimer and trimer formation[121] and a coarse-grained model of Aβ_{1-42} was used to study the structural diversity of the dimer.[122] In DPPC bilayer environment, a single Aβ_{40} peptide were used to study its structural diversity[123] and the relevant effect of insertion depth and ionic strength on the membrane.[124]

The two alloforms, Aβ_{1-40} and Aβ_{1-42} have distinct effects and pathways during oligomerization.[125] The Aβ_{1-40} is non-amyloidogentic. Hence, it is important to examine a full-length of amyloid β peptide to investigate its toxicity and to determine what kind of role ALA-42 play during aggregation. Another study has shown that Aβ peptides produced in the area with elevated level of cholesterol pose a great risk of Alzheimer's disease.[9] Here, it raises the question on the effect of cholesterol binding to Aβ peptide and the associated mechanisms of Aβ aggregation in the membrane environment.

2.3 Aβ oligomers and tau protein: relationship and link

There are various means in which Aβ oligomers are distributed among cells. These are: diffuse or spread within extracellular parenchymas as oligomers or deposited plaque; adsorption on membrane surface or incorporation into membrane structure forming pores or channels; accumulation within neuronal structure. On the other hand, the tau protein is mainly distributed within the intracellular neuron. One possible direct link between intraneuronal Aβ and protein involves the modulation effect between Aβ and tau pathologies.[126]

Studies have shown that intracellular accumulation appears earlier than amyloid plaque and NFS, and have suggested that intraneuronal Aβ accumulation initiates the caspase-cleavage of tau and precedes the Aβ plaque and NFS formation.[127,128] Meanwhile, tau hyperphosphorylation signal transduction pathways may also be linked indirectly to Aβ oligomers. Recent reviews on the relationship between Aβ pathway and tau pathology can be accessed from Ref. [126, 129] .

2.4 AD progression pathway and current therapeutic strategies

Mild cognitive impairment (MCI) has been used to prescribe the transitional stage between healthy brain and dementia. One impairment subtype is amnestic mild cognitive impairment (aMCI), which may increase the risk of progression to AD. Due to a variation in definitions of MCI based on different clinical criteria, the pathology of aMCI still lacks a strong characteristic profile. In terms of intermediate stages towards AD, mild cognitive impairment (MCI) shares a lot of similarity with AD, i.e. an increase of NFT in the medial temporal lobe (namely, hippocampus) amygdala.

In the last few years, donepezil, rivastigmine, and galantamine are prescribed drugs for AD patients to target acetylcholinesterase which inhibits the breaking down of acetylcholine. Another drug memantine has been used to block glutamate receptors against excitotoxicity as a means to cure AD. To date, the acetylcholinesterase inhibitor is the most widely used AD drugs and have been somewhat successful in slowing down the cognition.

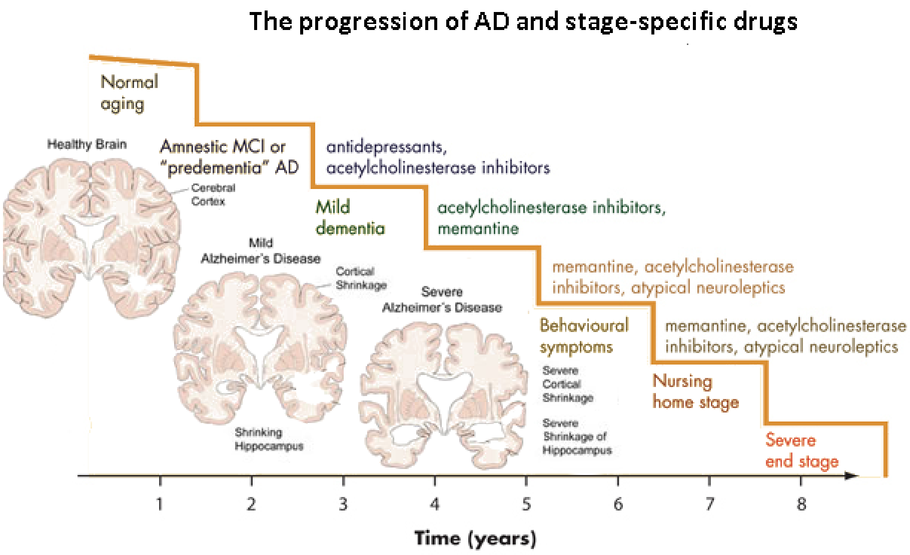

Figure 2.1: The progression pathway of AD and the related clinical treatment. Reproduced from http://pakmed.net/academic/age/alz/alz031.htm and http://www.healthplexus.net/article/alzheimer's-disease-treatments-horizon. With kind permission from Dr. Serge Gauthier.

2.5 Conclusions

In all likelihood the actions of amyloid β peptides and tau proteins are not independent. They are closely related to each other through a series of complicated, but essentially important, processes and events. Despite the strong links between Aβ and tau protein which have been reported so far, it is of paramount importance to uncover the mechanism of Aβ peptide aggregation which will help to decipher the whole story on the pathogenesis of AD.

Chapter 3 The toxic mechanisms of Aβ oligomers

In this chapter, we investigate the mechanisms of Aβ oligomer toxicity which may be the source of Alzheimer's disease. In particular, we perform a systematic review on the interaction of Aβ oligomers with the membrane via the process of adsorption and insertion. The tendency of β-sheet structures to aggregate in the membrane environment are exhibited by means of molecular dynamics simulation, and further insights to the process of membrane induced aggregation are provided. We assume that the aggregated oligomer induces membrane invagination which may serve as a precursor to the formation of pore structures and ion channels. In this review, I will also cover other pathological progressions caused by Aβ oligomers. Specifically, Aβ oligomers interaction with the membrane receptors, their direct versus indirect effects on oxidative stress and intraneuronal accumulation are examined. The comprehensive understanding gained from these current researches on the various toxicity mechanisms shall build a good basis from which to derive better therapeutics and treatment strategies for AD in the near future.

3.1 Introduction

It is well-known that the two apparent pathogenesis hallmarks of Alzheimer's disease are characterized by aggregation of amyloid β peptides leading to extracellular senile plaque, and formation of intracellular neurofibrillary tangle by the hyperphosphorylated tau protein. Amyloid β peptides and hyperphosphorylated tau protein show detrimental effects of causing a significant loss of neurons and synapses, and give rise to the state of Alzheimer's disease. Amyloid β peptide (Aβ), is cleaved from amyloid precursor protein (APP) by β- and γ-secretase, is a peptide of 36-43 amino acids. The self-assembly of Aβ peptides into dimer, trimer and higher-order oligomers is generally believed to be the main reason of toxicity leading to the death of neurons.[4,5] The underlying mechanism of the toxicity has been studied extensively, from both theoretical and experimental perspectives, which can be summarized as follow: (1) formation of membrane pore/channel[130–133] leading to ionic homeostasis alternation[134,135] across membrane; (2) disruption of membrane receptors' function by intimately binding to it;[136] (3) induction of oxidative stress[137] via the formation of metal-Aβ complex;[16,138] (4) activation of inflammatory response by interacting directly with the membrane;[139] and (5) modification of certain DNA structure.[15]

In this chapter, we focus on the oligomers-membrane interaction as well as the related underlying mechanisms of oligomers' toxicity to reveal several general toxic mechanisms. In this respect, we first exhibit the secondary structure information of small oligomers in aqueous environment; the process of Aβ adsorption, insertion and aggregation in membrane environment; and ion channel/pore formation; as well as the aggregation of the intra-neuronal Aβ peptides. We then bring out the relationship between Aβ and the membrane receptors. In addition, we discuss on the role of Aβ in oxidative stress. Experimental evidences and validations, as well as theoretical methods are included.

3.2 Amyloid β oligomers toxic mechanisms

3.2.1 Amyloid β oligomers in aqueous environment

There has been increased interest in elucidating the structural evolution of Aβ oligomers in the past few years. Unlike amyloid fibril, whose structural information has been well developed over the past decade, less is known on the structural evolution of Aβ oligomers in aqueous environment. It is well-known that mature Aβ_{1-42} amyloid fibrils consist of a β-strand-turn-β-strand motif, which is adopted by residues 18-42 with the β-sheet being in a parallel, in-register organization, while the N-terminal (namely residues 1-17) taking a disordered conformation.[88] Amyloid fibrils are formed by the nucleation-dependent self-assembly of Aβ through a series of neuropathogenic cascade process.[140,141] Interestingly, the β-sheet-rich mature amyloid fibril as well as the monomeric Aβ are found to be far less toxic than soluble Aβ oligomers.

The experimental structure of Aβ is undefined due to its propensity to form soluble aggregates in comparison to the amyloid fibrils, and to its readiness to attach to other macromolecules. However, improved understanding has been achieved through computer simulations based on replica exchange molecular dynamics, classical molecular dynamics and Monte Carlo approaches.[121,122,142–146] The formation and conformational properties of Aβ oligomers, ranging from dimers to hexamers (especially the dimers), are intensively studied by these computational methods. These studies have bridged the gap that results from experimental limitation, to explore into the intrinsic toxicity of these oligomers through capturing the transient oligomeric states. Furthermore, these studies have revealed that Aβ_{1-42} oligomers are quasi-spherical in shape, featured with a hydrophobic core and hydrophilic surface, with its N terminal (namely, the region D1 to D7), showing an enhanced exposure to solvent. These results have indicated that oligomerization is heavily driven by hydrophobic effects. It is more favorable energetically for hydrophobic residues to shun away from exposure to solvent and to form inter-molecular contacts with each other. Meanwhile, the electrostatic interactions and π-π interactions are also perceived to play an important role in the aggregation process. These interaction, which dominates Aβ oligomerization and fibrillization, may serve to explain the similar cross-β structure that emerge in the Aβ oligomers (particularly in the toxic Aβ_{1-42} fibrillar oligomers), and the mature amyloid fibril. However, in contrast to amyloid fibril, the antiparallel-β sheets are observed to prevail in the oligomers rather than the fibril-like parallel, in-register β-sheet structure. The consistent reduction in α-helical content as well as an increase in β-sheet structure is one characteristic feature of Aβ dimerization process.[146] Other contributing factors to the Aβ dimer formation involve the salt-bridge formation between D23-k28, and between residues ILE-41 and ALA-42.[145] Interestingly, the free energy landscape of Aβ_{1-42} dimers is found to be more complex and broader than that of Aβ_{1-40}, which indicate Aβ_{1-42}'s greater tendency to form hydrophobic contacts and β-sheet structures than Aβ_{1-40}.[144,145] Furthermore, the "butterfly effect" of chaos is found to occur in the structural evolution of the oligomer. That is, different initial structure can lead to significant differences in the observed end structure. This implies that to fathom or to anticipate the associated toxicity properties of the evolved oligomers solely from a secondary structure point of view is not a straightforward task.

3.2.2 Amyloid β adsorption and insertion mechanism

There are a number of models that are representative of membrane structures, such as the solid surfaces, monolayer bilayers, self-assembled monolayers (SAMs) and implicit membrane. These structures have been employed to study the influence of different types of membrane surfaces on the adsorption and aggregation process of Aβ peptides.[147–152]

It is generally observed that solid surfaces tend to facilitate the self-assembly of Aβ peptides. The main driving force that associate Aβ and the solid surface are the electrostatic interactions and the dehydration effects. A detailed review on Aβ interaction with solid surface can be found in Ref. [147] .

For the self-assembled monolayer surface (SAM), which is capped by COOH, CH3 and the OH groups, the strength and extent of the adsorption of Aβ oligomers (ranging from dimer to hexamer) on the SAMs surface are determined by the binding sites.[148,149] Furthermore, Aβ can change its conformation and reorient itself to adopt a more energetically favorable association during the adsorption process. However, the conformational change of the oligomers is found to be restrained and confined by the SAMs, and the secondary structure is found to evolve slowly in comparison to oligomers that are placed solely in the aqueous environment. Extensive MD simulation studies have revealed that trimers as well as tetramers possess well-preserved β-sheet structures which may act as seed to initiate the process of oligomerization and fibrillization. Electrostatic and hydrophobic interactions as well as water-mediated dewetting transition are the main driving force for the Aβ aggregation and adsorption on the membrane surfaces.[140,153–155]

Short Aβ fragments and their mutants have been employed to study the interaction of Aβ with the membrane as well as the folding process of Aβ in the membrane environment via the implicit membrane-water model calculated by means of the replica-exchange methods.[150] One interesting observation in this study is that the hydrophilic headgroup region of the membrane, the C-terminus of Aβ(25-35), first forms an α-helical structure before it attempts to knock into the hydrophobic membrane core via its hydrophobic residues.

One interesting observation on the study of Aβ peptides association and adsorption on different membrane monolayers is that, the adsorbed Aβ is prone to adopt a β-sheet structure and orientate itself to align parallel to the air-water interface.[151] In addition, the adsorption of Aβ with the monolayer has increased the surface pressure of the monolayer. Meanwhile, both the order and fluidity of the bilayer are affected by the interaction of Aβ peptides with the membrane bilayer, which is observed during the incorporation of the two fragments Aβ_{1-28} and Aβ_{25-40} into the bilayer. Specially, the hydrophobic region of Aβ_{25-40} is observed to tend to locate inside the hydrophobic core region of the bilayer, while the Aβ_{1-28} has a propensity to interact with the hydrophilic headgroup region of the membrane.[152] In addition, Aβ_{25-40} is observed to induce a larger membrane alteration and perturbation relative to Aβ_{1-28}.

In our investigations, we have considered two pre-formed Aβ dimers, which consist of 4 Aβ peptide chains: A, B, C and D. The peptides are represented by the GROMOS96 43a1 force field. The dipalmitoylphosphatidylcholine (DPPC) and cholesterol (CHOL) mixed membrane model is represented by the 43A1-S3 parameter set.[156–160] These β-sheet-rich peptides are arranged at each side of the pre-equilibrated mixed bilayer, with an initial 2 nm distance from the membrane surface. 31777 water molecules as well as 103 Na^+ and 95 Cl^- ions were added to neutralize the system and reach an ion concentration of 0.1 mol/L. In our simulation, all the bonds are constrained by the linear constraint solver (LINCS) algorithm[161] with a $2\,fs$ integration time step at a temperature of $323\,K$ using the Nosé-Hoover coupling scheme.[162,163]

During the $1.2\ \mu s$ simulations, our results have indicated that the dimers mainly adsorb and reside on the membrane surface. Furthermore, we have uncovered that while the N-terminus tends to bury inside the DPPC headgroup, the C-terminus of the Aβ peptide remains outside the membrane as a result of the strong protein-lipid interactions. The partial density functions of Aβ peptides, water molecules, and the constituents of the mixed bilayer during the last $100\,ns$, are plotted in Figure 4.2. The result here shows that while the C-terminus remains outside the membrane, the N-terminus of chain A, namely the residues $1-22$ and $26-33$, is fully inserted into the DPPC headgroup. Meanwhile, chain B and chain A have reduced its interactions with the membrane. Similar trends hold for chain A. The N-terminus of chain C and D, namely residues $1-33$ and $1-24$ respectively, are totally buried within the DPPC hydrophilic headgroup. However, their C-termini are found to stay outside of the membrane. Figure 3.2 shows that the dimer formed by chain C and D is less stable than the dimer formed by chain A and B. Furthermore, Aβ peptides that adsorbed onto membrane surface do not always have stronger protein-protein interaction within the dimer. Indeed, the association of Aβ dimers to the membrane appears to be an insignificant perturbation of the bilayer.

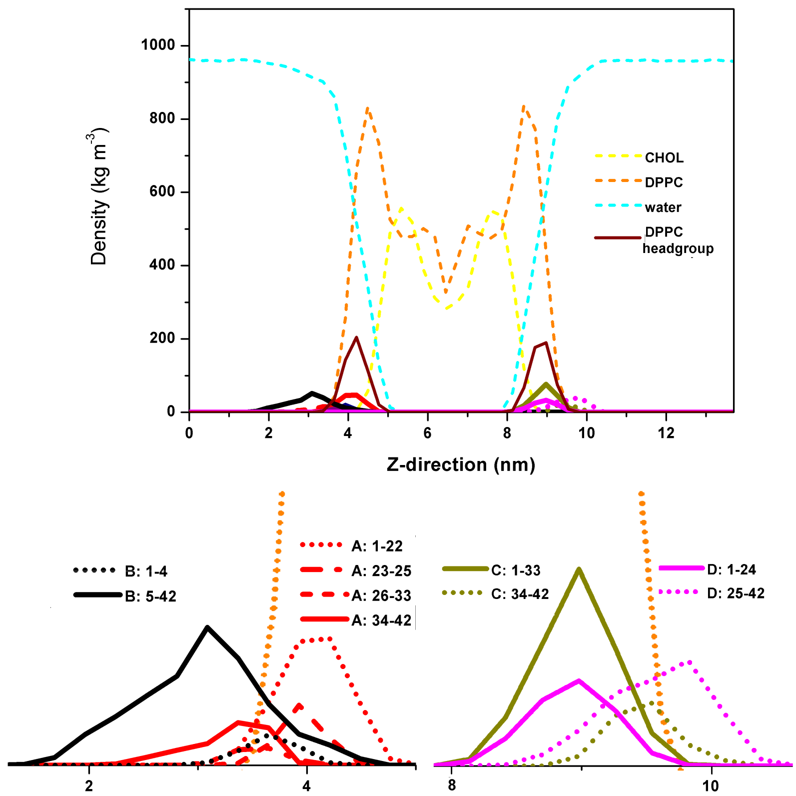

Figure 3.1: Partial density function along the Z-direction.

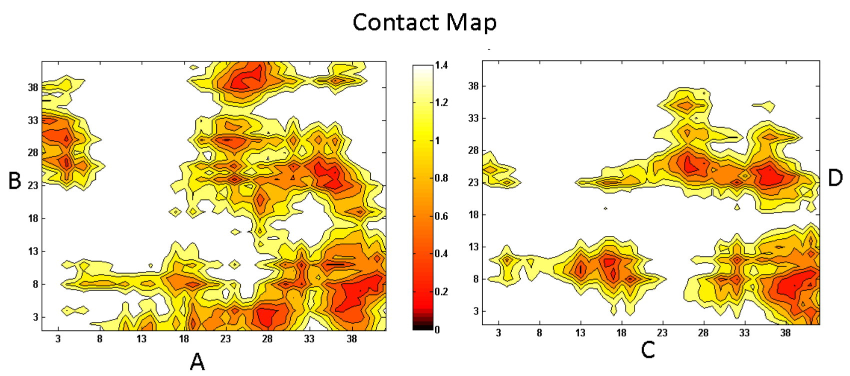

Figure 3.2: The residue contact map of each dimer. The contacts involving hydrogen bond forming are indicated by dark red.

3.2.3 Amyloid β membrane-mediated aggregation mechanism

Aβ peptides originates from the cleavage of APP. The cleaved peptides which fail to exit and release from the membrane into the extracellular space may recede into intracellular space, and form neurofibrillary tangle. The excessive Aβ peptides in the extracellular space may deposit on the membrane surface to form neuronal plaque, which is the main source of Aβ toxicity. Thus, a good understanding on the Aβ toxicity mechanisms requires detailed knowledge on the possible transmembrane structures of the Aβ peptide as well as the post-cleavage scenario of APP.[164]

In particular, in order to explore the possible aggregation behavior inside the membrane,[142] it is necessary to examine the interaction of Aβ within the membrane. In fact, cumulative evidence have suggested that elevated cholesterol level in the membrane can lead to a greater risk of Alzheimer's disease.[9] Recently, research has found that a high concentration of Aβ peptides in the cholesterol-rich area of the membrane known as the lipid rafts. The raft-like heterogeneous membrane environment, which mainly consists of cholesterol and ganglioside,[165–167] has been extensively employed to examine the detailed interaction of Aβ within the membrane environment. Indeed, the lipid rafts has been proposed to accelerate the Aβ aggregation process.[168] Furthermore, the cholesterol within the raft is reported to promote the interaction of Aβ with 1-palmitoyl-2-oleoylphosphatidylcholine (POPC) bilayer[169] while it inhibits the interaction of Aβ with the gangliolipids.[170] Our study has shown that the interaction between Aβ and lipids has promoted the aggregation of the Aβ peptides. However, the interaction between cholesterol and Aβ is negatively correlated with the extent of the peptide-peptide interactions.[142] The depletion of gangliosides or cholesterol has been shown to significantly reduce the amount of

Aβ as well as its aggregation.[167,171] Furthermore, the aggregation of Aβ to fibrils is mediated by the gangliosides on the lipid rafts, at which the transition from the α-helix-rich conformation to the β-sheet-rich conformation is observed. In this way, the constituents of the raft-like membrane controls the amyloid formation.[172]

To gain a better understanding on the underlying mechanism of the interaction between Aβ, cholesterol and lipids, as well as the aggregation process of Aβ in a raft-like environment, we have aligned three full-length Aβ peptides in a parallel fashion in the vicinity of a DPPC and cholesterol mixed bilayer, with residues 1-27 on the surface of the membrane and 28-42 inside the membrane. In chapter 4, we are going to illustrate the detailed simulation protocol and aggregation mechanism of Aβ in the cholesterol and DPPC mixed bilayer membrane environments. Our simulation indicates that residues 1-27 predispose to interact with the aqueous-membrane interface region, while residues 28-42 incline to remain inside the hydrophobic core region (see Figure 3.3).[142] The oligomer is found to attach to the sunken raft-like membrane surface forming a conglomerate of defects and disordered cholesterol molecules. Cholesterol further enhances the pre-existing hydrogen-bond network between Aβ and DPPC and promotes the incorporation of Aβ into the membrane.[173] However, the interaction between cholesterol and Aβ competes with the Aβ peptide-peptide interactions such that cholesterol hardly facilitates the aggregation of Aβ once Aβ has been immersed into the membrane.[142] Nonetheless, cholesterol is observed to facilitate the formation of pore/channel in the membrane by binding directly to the Aβ during the adsorption process.[174]

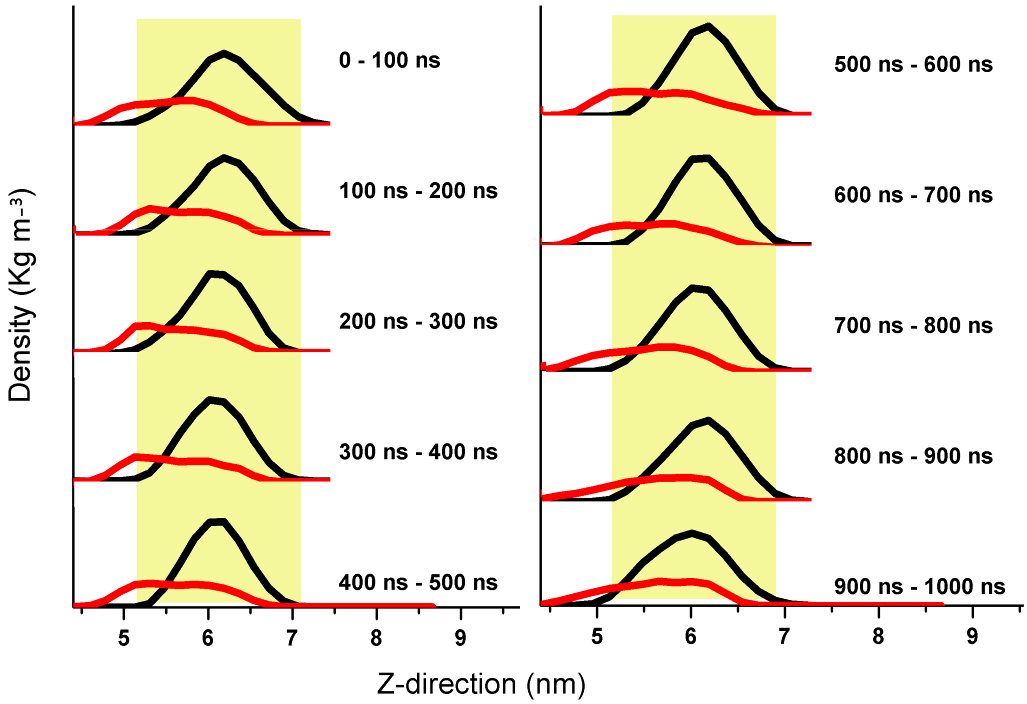

Figure 3.3: The density function of Aβ in the mixed bilayer environment along the Z-direction. 1-27 are indicated by black line, and residues 28-42 is red line. The light yellow background shows the DPPC headgroup region.

3.2.4 Intraneuronal Aβ accumulation mechanism

It is possible for the intraneuronal accumulation of Aβ to occur prior to the deposition of Aβ plaque and before the formation of neurofibrillary tangles.[127] At the moment, it is inconclusive as to whether intraneuronal Aβ accumulation can result in a series of pathological alterations such as cognitive impairment, selective neuron loss, and axonopathy.[175,176] Nonetheless, it is suggested that intraneuronal Aβ_{17-42} secreted by α- and γ-secretases from APP is a normal product of neuronal metabolism. Thus, it is controversial to conclude that the presence of intracellular Aβ is a sign of neuronal pathology. Notwithstanding all these results, the behavior of Aβ in the intraneuronal space is still poorly understood.

Currently, there are two theories of Aβ intraneuronal accumulation. One assumes that Aβs get inside the neuron directly after cleavage, which then lead to the death of the neuron. In lieu of that, the Aβs are released into the extracellular space and subsequently deposit as amyloid plaques.[177] The second theory suggests that the Aβ is first released into the extracellular space of the neuron before being re-uptake into the neuron through endocytosis or membrane receptors. Meanwhile, several receptors, such as alpha 7 nicotinic acetylcholine receptors (nAChRs),[178,179] the low-density lipoprotein receptor-related protein associated protein 1 (LRPAPL),[180] and scavenger receptor for advanced glycation end products (RAGE),[181] have been reported to be able to mediate and internalize the Aβ from extracellular space. A comprehensive review on different uptake and internalization mechanisms and processes can be found in Refs. [182, 183] .

Next, let us discuss on the toxicity of intraneuronal Aβ accumulation. The accumulation of intraneuronal Aβ has been speculated to disrupt fast axonal transport[184] which adversely affects intracellular trafficking.[185] Furthermore, the intracellular Aβ can cause early synaptic deficits, cholinergic neuron loss, and hippocampus atrophy in APP/PS1KI mouse AD models.[186–189] In addition, the intraneuronal Aβ accumulation may indirectly contribute to the disruption of neuronal functions as well as neuronal survival.[190]

3.2.5 Ion channels/pore formation by the incorporation of Aβ into the cell membrane

The toxicity of Aβ oligomers arises from the disruption of membrane integrity through an alteration its dielectric propriety, to the binding and activation of membrane receptors, and the formation of pores that leak Ca^{2+} ions which leads to an enhanced level of cytosolic calcium. From the point of ions transportation, the pores formed by Aβ oligomers are much less efficient than the other membrane pores, such as the ion channels, the nuclear pore, and the bacterial pores, which have all undergone the process of optimization during evolution.[191] Here, our focus is riveting on the pores formed by Aβ oligomers on the cellular and synthetic membrane based on experimental observations, as well as those built from computational models.

In 1992, Arispe *et. al* first proposed the possibility of Aβ forming an ion channel[192] which relates to the observation of an elevated level of intracellular Ca^{2+} ions. In the following years, the researchers proposed several models, such as the helix-turn-helix,[134] and beta-sheet-twist-antiparallel-beta-sheet[132,133] morphologies, for the membrane-bound Aβ pore structures. Many factors,[165,193] such as the pH, peptide concentration, the constituents and propriety of the membrane, are found to influence the secondary structure of the membrane-bound Aβ pore conformation. The strand-turn-strand motif has been identified, by basin-hopping global optimization method, to be the most stable membrane-spanning structure for monomers. These monomers assemble as tetrameric and hexameric beta-sheet subunits to form a pore.[194] The hexamer-of-hexamer ion channel model has been proposed to be a stable 36-stranded β-barrel in the membrane, which is consistent with experimental observations and has been further used to explain the consequent channel selectivity.[134]

Atomic force microscopy (AFM) and solid state nuclear magnetic resonance (NMR) have revealed that the Aβ hexagonal annular channels are present in the membrane structure. A pore-like assembly with 6 subunits (4 subunits in the case of rectangular assembly) is strongly suggested.[195] Zn^{2+} ions, as well as other small molecules like the MRS2481 and its enatiomeric species, have shown its potential in blocking the calcium-permeable channels formed by the Aβ oligomer.[196–198]

3.2.6 The relationship of Aβ with different receptors

In the above sections, the role of adsorption, insertion, aggregation and ion channel pore formation as key determinants of Aβ toxicity via the interaction of Aβ with the membrane, have been discussed. In this section, we shall extend our review to the area where Aβ oligomers serve as pathogenic ligands. Aβ oligomers may bind to different receptors, such as the neuronal insulin receptors, the N-methyl-D-aspartate (NMDA) receptors, with the induction of synapses losses through the redistribution of receptors, leading to the alteration of neuronal plasticity as well as oxidative stress.[199,200] In addition, it is well known that Aβ oligomers tend to bind to several receptors[201–206] with the initiation of numerous signaling cascades and surface expression regulations.

Aβ oligomers can induce impairment to neuronal insulin receptors, affect the normal transduction of signal,[201] and suppress the activation of insulin receptor substrate.[207] However, through down-regulation of the Aβ oligomers binding sites, the insulin receptor impairment and synaptic deterioration can be mitigated.[199] Omega-3 fatty acids and curcumin[207] are able to prevent synaptic dysfunction and neuronal loss by suppressing the inactivation of insulin receptors caused by Aβ oligomers.

A question that one may have is what is the role of NMDA receptors on Aβ toxicity? There are several mechanisms that have been proposed.[208,209] One is that Aβ may activate NMDA receptors directly[210] or indirectly by regulating the downstream NMDA receptors. Experiments have identified that both naturally-secreted and synthetic Aβ peptides possess the ability to reduce surface NMDA receptors. Meanwhile, reducing Aβ would restore the expression of surface NMDA receptors.[202] On the other hand, the activation of NMDA receptors affects the production of the synaptic Aβ peptides[211,212] as well as the elevation of intracellular Ca^{2+} and apoptosis.[206] So far, various NMDA receptor antagonists have been suggested to prevent the Aβ oligomer toxicity.[210,213,214]

Another Aβ oligomer receptor of interest is natively folded cellular prion protein (PrP^C). This protein is involved in the development of nervous system by mediating its synaptic and neuroprotective roles,[215–220] and through promoting neurite outgrowth.[221] It is reported that PrP^C mediates the synaptic dysfunction caused by Aβ oligomers.[222] However, there are some experimental demonstration showing that PrP^C is not essential and has no effects on the impairment of synaptic plasticity induced by Aβ oligomers.[223,224] Currently it is still under debate whether the presence of PrP^C is necessary for synaptic dysfunction to be induced by Aβ oligomers.

nAChRs are cholinergic ionotropic receptors which are directly linked to the ion channels. It is found that the alpha 7 nAChRs receptor has a very high binding affinity towards Aβ,[225] with Aβ directly modulates[226] and blocks the response of these nAChRs.[227] In addition, nAChRs are found to promote intraneuronal Aβ aggregation[178] and exacerbate cognitive deficits and synaptic pathology.[228] However, this view is in conflict with another report which states that the absence of nAChRs can enhance Aβ accumulation[229] and hence worsen the cognitive deficit. Nonetheless, the neuroprotective role of nAChRs by counterbalancing the toxicity of Aβ oligomers has been proposed based on experimental observation.[229] For example, drugs like 2-(2-(4-bromophenyl)-2-oxoethyl)-1-methyl pyridinium (S 24795), which have been assessed to be able to reduce the interaction between Aβ and nAChRs, have been shown to enhance long-term potentiation.[230–232] Interestingly, one research group has found that Aβ does not bind with nAChRs and has no direct relationship with the nAChRs expression and activity. Instead, the Aβ may affect the nAChRs indirectly by attaching to the membrane and altering the propriety of the membrane, which then influences the membrane receptors inadvertently.[233] Finally, note that there are other receptors like serpin-enzyme complex receptor (SEC-R),[234,235] receptor for advanced glycosylation end-products (RAGE),[236,237] P75 neurotrophin receptor (P75NTR),[205,238,239] and scavenger receptor CD36,[240–242] which bind with the Aβ oligomers.

3.2.7 Oxidative stress

An elevated level of oxidative stress is typically observed in AD patient. Oxidative stress is mainly characterized by protein, DNA and RNA oxidation, and lipid peroxidation.[243,244] It may induce the overproduction of Aβ peptides via activation of β-secretase.[245] The excessive Aβ peptides may self-assemble into toxic oligomers which in turn initiate the free radical process. This results in new oxidative stress as well as the increased macroautophagy and lysosomal ensuing apoptosis,[246] and any additional overexpression of oxide synthase can bring about extra neuronal damage.[244] Oxidative stress can change the protein structure and affect its function, leading to physiological alteration and pathological induction.[244,247,248] As a matter of fact, a series of oxidatively modified proteins have been identified in the brain of

AD patients.[244,249–251] Met-35 of Aβ is believed to be the key residue involved in oxidative stress and the mutation of Met-35 has been shown to reduce the effect of toxicity in Aβ.[243,252,253] There are many food and compounds, such as the walnut and turmeric extract, which are anti-oxidant in nature, have been reported to be capable of preventing the oxidative stress induced by Aβ and its associated apoptosis.[254]

3.3 Summary

In this chapter, we have discussed the various mechanisms which contribute to Aβ oligomer toxicity: adsorption, insertion, aggregation and pore formation in the membrane, as well as the interaction of Aβ with the membrane receptors and oxidative stress. The pleiotropic effects of Aβ peptides can be seen in Figure 3.4. Currently, there are lots of therapeutic strategies being proposed to suppress the Aβ induced toxicity, such as the β- and γ-secretase inhibitors whose function is to reduce the production of Aβ peptides. There are also other strategies to overcome Aβ oligomer toxicity, such as the aggregation inhibitors, the pore/channel blockers etc; a detailed review on these therapeutic approaches is available in Ref. [255] . In the next chapter, we are going to examine the mechanisms of Aβ aggregation in the membrane environment.

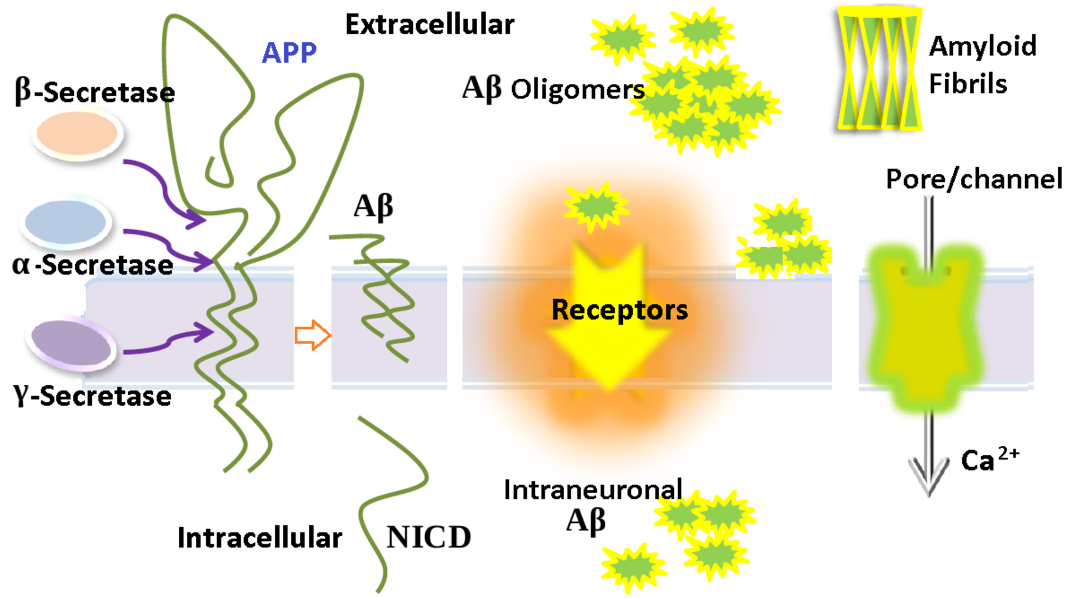

Figure 3.4: The cleavage of APP by α-, β- and γ-secretase and the production of Aβ peptides are shown on the left side of the figure. The following toxic mechanisms are illustrated in the figure: formation of Aβ oligomers and its further conversion to fibrils; disruption of membrane receptors; adsorption on membrane surface which alters the propriety of the membrane; formation of pore which causes the leakage of Ca^{2+}; and the accumulation of intraneuronal Aβ.

Chapter 4 Aβ aggregation in the mixed bilayer environment

The aggregation of amyloid-β peptides resulting in neurotoxic oligomers is an important but yet a mysterious process in the Alzheimer's disease development. Molecular dynamics simulations were carried out to investigate the self-assembly of three Aβ_{1-42} peptides in the zwitterionic DPPC and cholesterol mixed lipid bilayer. During the 1 μs simulation, the residues 1-27 were found to interact preferentially with the lipid-aqueous interface region while residues 28-42 show inclination to remain inside the bilayer hydrophobic tail region. The interaction between peptides and lipids has facilitated the association of Aβ peptides. However, the interaction between cholesterol and peptides is inversely correlated with the extent of the peptide-peptide interactions. Our simulation has uncovered the formation of a short segment of parallel β-sheet between two peptide chains. In another chain, the N- and C-termini came close to each other. All the structural transitions indicate that our simulation has caught a glimpse of the complicated peptide oligomerization process. The full understanding of the underlying mechanism still requires further experimental and theoretical studies.

4.1 Introduction

Alzheimer's Disease is characterized by the extra-neuronal Amyloid β plaque and intra-neuronal fibrillar tangles. Studies show that the Aβ oligomers are the main source of the neurotoxicity.[4–7] The oligomers are prone to attach to the membrane or other macromolecules,[8] which brings extra difficulties for conventional experimental tools to study its pathogenic mechanism. Molecular dynamics simulation, as a theoretical tool for atomic-detailed study, emerged to complement the experimental methods, in the studying on the aggregation process of Aβ.

There exist several hypotheses of the toxicity mechanism.[3,256] One of which suggests that the binding of the excessive Aβ peptides to the membrane receptors, such as glutamate receptor, has affected their functions.[136] Another points to the formation of membrane pore/channel,[130–133] which leads to the alteration of the ionic homeostasis.[134,135] To understand the mechanism of amyloid toxicity, Aβ_{42} oligomers have been studied in an implicit membrane and it was found that the identified β-sheet structure exhibits the typical strand-turn-strand motif.[194] In a DPPC bilayer environment, the structure and the insertion depth of a single Aβ_{40} peptide[123] and the relevant conformational change of the membrane[124] have been studied. In another palmitoyloleoylphosphatidylglycerol (POPG) lipid bilayer environment, six preformed Aβ_{25-35} β-sheets have been inserted into the POPG in different ways. A water-permeable pore is observed to result, which is accompanied by a strongly disturbed local membrane structure.[257]

Replica exchange molecular dynamics simulation has been performed to study the short peptide Aβ_{10-35} dimer and trimer formation.[121] A coarse-grained model has also been employed to study the structural diversity of the dimer in aqueous environment and the diversity of kinetic pathways in fibrillization process.[122,258,259] A discrete molecular dynamics study shows that the C-terminal region of Aβ_{42} plays an important role in its aggregation process.[260] A Monte Carlo simulation has also been used to study the dimer formation of the several mutated Aβ_{42} peptides revealing that the intramolecular antiparallel β-sheet structures are shared by different Aβ variants.[146]

Another replica exchange molecular dynamics simulation study of Aβ_{42} monomer on the surface of DPPC and dioleylphosphatidylserine (DOPS) bilayer indicates that the interactions between Aβ and lipids do not promote structural ordering and the conformational dynamics is possibly restricted because of the interaction between the protein and the lipid.[261] Another all-atomic study of very short peptides (Gly-Ala)$_4$ and (Gly-Val)$_4$ in the presence of water/n-octane mixture indicates that the nonpolar planar octane-water interface facilitates the aggregation by reducing the self-assembly dimension from three to two, thus increasing the concentration of oligomers.[262] A study of the Aβ oligomers adsorption affinity towards the self-assembled monolayers by all-atom MD simulations has revealed the preferential adsorption of the C-terminal regions by monolayers and the main driving force at the interface is the hydrophobic interaction.[263]

Extensive experimental studies have also been carried out focusing on the aggregation and nucleation-elongation mechanism of fibril formation.[264–266] Aβ peptides are being produced in cholesterol-rich areas and it is generally believed that there is a great risk of Alzheimer's disease in the presence of elevated cholesterol level.[9] The relationship between Aβ peptide binding to lipid and its aggregation in the membrane environment is not yet clear. A recent finding showed that the Aβ peptides have the capacity of binding the microbial lipid bilayers as antimicrobial peptides except the incidental amyloidosis.[267] Another experimental study finds that Aβ_{1-28} prefers to interact with the polar headgroup of lipids while Aβ_{25-40} tends to bury itself inside the hydrophobic core region of the membrane.[152] In experiments combining circular dichroism, thioflavin T fluorescence, size-exclusion chromatography and transmission electron microscopy measurements, Aβ peptide was found to change its conformation from an α-helix-rich to a β-sheet-rich structure in a cholesterol-dependent manner.[165,172]

It is important to get a detailed interacting picture of the association of the peptides with the lipid bilayers. Here we have conducted several simulations of the full-length Aβ_{1-42} proteins in the membrane environment formed by mixed DPPC and cholesterol.

4.2 Materials and methods

The initial conformation of the full-length Aβ_{1-42}, whose sequence is *DAEFRHDSGYEVHHQKLVFFAEDVGSNKGAIIGLMVGGVVIA*, was taken from the model 1 of Protein Data Bank (PDB) ID 1IYT.[?] The structure consists of two helical regions encompassing residues 8-25 and 28-38 which are connected by a regular type I β-turn. The protein was represented by the GROMOS96 43a1 force field. The membrane model was proposed by Chiu et al., which consists of the cholesterol and DPPC (http://www.nanoconductor.org/43A1-S3/), and is represented by the 43A1-S3 parameter set.[156–160] The DPPC and cholesterol mixed lipid bilayer were arranged to lie in the *xy*-plane and centered at the origin of the coordinate system. To speed up the simulation, the three Aβ peptides were put in the vicinity of the pre-equilibrium mixed bilayer. 9 cholesterol and 31 DPPC molecules were found steric-clashing with the peptides and were removed from the upper leaflet. The final membrane composition is that there are 118 cholesterol and 96 DPPC in the upper leaflet, and 127 cholesterol and 127 DPPC in the lower leaflet. The DPPC lipid was chosen because it has PC headgroups which are found to be abundant in neural membranes.[268] Three Aβ proteins were solvated in the mixed bilayer and aligned parallel in a cubic box of dimensions $101.57\,\mathring{A} \times 105.03\,\mathring{A} \times 87.82\,\mathring{A}$. The center of mass of each of the proteins were placed at (35.79, 52.52, 65.82), (55.79, 52.52, 65.82) and (75.79, 52.52, 65.82) and were labeled as peptide A, B and C, respectively. 14947 water molecules with 65 Na^+ and 56 Cl^- ions were filled within the box to help neutralize and reach the concentration of 0.1 mol/L. The initial setup is shown in Figure 4.1(a).

All bonds were constrained using the linear constraint solver (LINCS)[161] algorithm with a 2 ps integration time step. The temperature was kept at 323 K using the Nosé-Hoover coupling scheme.[162,163] It was chosen to be above the DPPC gel-liquid transition phase.[269] A semi-isotropic pressure coupling at 1 bar by means of a Parrinello-Rahman barostate with a coupling constant of 2 ps was used in the pressure ensemble. The Van der Waals cutoff was set to 1.6 nm. Particle Mesh Ewald method[270] was used for electrostatic interaction with a sixth-order interpolation and a Fourier grid spacing of 0.15 nm as recommended by the 43A1-S3 force field. 1000 ns simulations were conducted. The simulation and analysis were performed using facilities within the GROMACS package. PyMOL[271] and VMD[272] were used to visualize the structure.

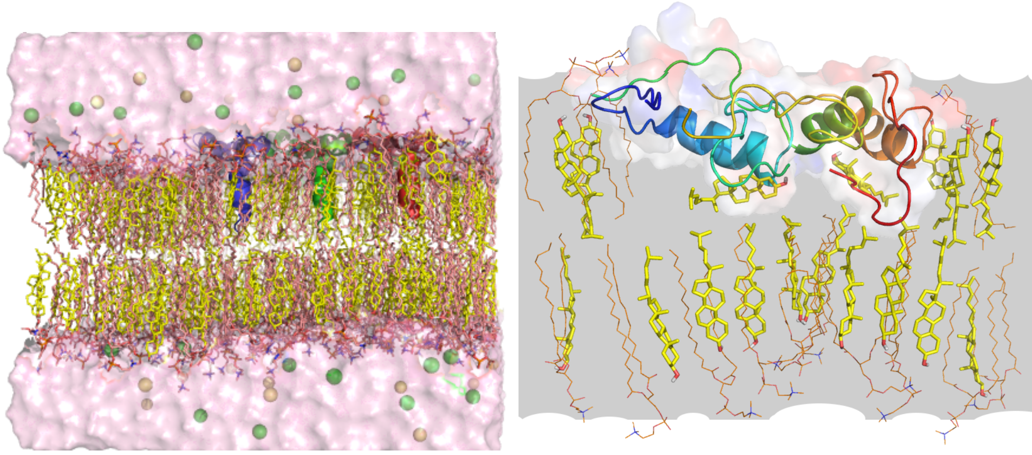

(a) (b)

Figure 4.1: The simulation system. The three peptides are aligned in a parallel fashion in the cubic box as shown in the snapshot (peptide A: blue; peptide B: green; peptide C: red). The cholesterols are represented by yellow lines and the DPPC by orange lines. The green and yellow orange dots are Cl^- and Na^+ ions respectively (a). A schematic representation of the defects of the membrane caused by protein perturbation. The three peptides are represented by cartoon and colored by spectrum. The cholesterol is showed as sticks and colored by elements (C: yellow; O: red; H: grey). The DPPC is represented by lines (b). The images are produced by PyMOL.

4.3 Results

4.3.1 Interaction between Aβ_{42} and DPPC

Initially, residues 1-27 of the peptides were arranged on the surface of the membrane and residues 28-42 were buried inside the membrane. The partial density profile of the water, DPPC headgroups and hydrocarbon tail, cholesterol, residues 1-27 and 28-42 of Aβ_{1-42} during the whole simulation time were plotted along the Z-direction (membrane normal direction). The DPPC carbonyl group atoms (CO) were also plotted to identify the boundary between the polar and hydrophobic regions (see

Figure 4.2). From Figure 4.2, the interface between the DPPC hydrophilic head groups and the hydrophobic tails is clearly shown. The small dip around 4.4 *nm* is the region between the upper and lower monolayers. Due to the fact that the peptides were embedded initially in the upper leaflet, the density of DPPC and cholesterol in the upper leaflet is slightly lower than that of the lower leaflet. At the end of the simulation, the peptides have fully sunk inside the DPPC. Further scrutiny shows that residues 1-27 interact preferentially with the DPPC headgroup, while residues 28-42 prefer to remain inside the DPPC hydrophobic tail region. A recent experimental study by Ionov et al.[152] also showed the same tendency with Aβ_{1-28} interacting with the hydrophilic headgroup and Aβ_{25-40} locating in the hydrophobic tail region of the bilayer.

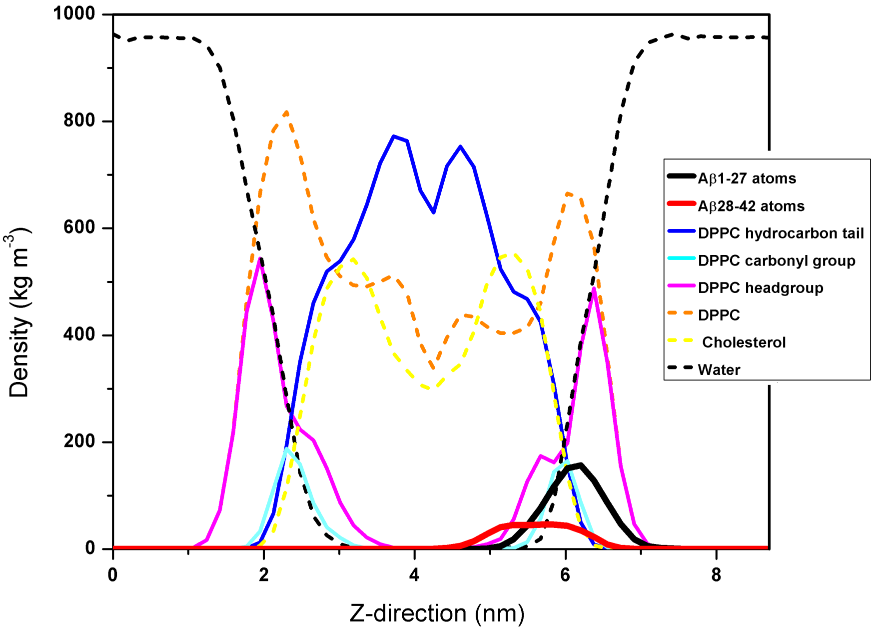

Figure 4.2: Partial density function along the *Z*-direction.

4.3.2 Interaction between Aβ_{42} and cholesterol

The binding of cholesterols onto the peptides has the effect of tilting the cholesterol from its original orientation which can be observed from 4.3. The deuterium order parameter, which is usually used to describe the orientation of lipid chains,[273] is used to quantify this tilt of the cholesterol. The equation of the deuterium order parameters S_{CD} is given as follow:

$$S_{\mathrm{CD}} = \frac{1}{2}\left(\langle 3\cos^2\theta\rangle - 1\right). \tag{4.1}$$

Here θ is the angle between the C-D bond and the bilayer normal. S_{CD} can vary from -0.5 (parallel to the bilayer) to 1 (normal to the bilayer). Due to the rigidity of the cholesterol, only the order parameter for the top and the bottom carbon atoms of the hydrocarbon tail of the cholesterol (CHO) is calculated. From the order parameter in Table 4.1, we can see that CHO-318, CHO-326, CHO-335 and CHO-336 are tilted to such a large extent as to be nearly perpendicular to the normal. The large tilt of the cholesterol at the side where Aβ peptides are bound is caused by the presence of the peptides, but it could also be an artifact or at least be exaggerated by our initial modeling procedure. Nevertheless, for those cholesterols that are located far away from the peptides, they are found to possess higher values of the order parameter which implies that they are not tilted largely and still nearly perpendicular to the bilayer normal. We observed that the cholesterol has a greater tilt at the position where the electrostatic potential of the peptide surface is positive. The same positive potential surface also interacts extensively with the membrane lipids (see Figure 4.3c), while the potential of the interface between the peptides and water molecules is predominantly negative (see Figure 4.3b).

order parameter of cholesterol	
CHO-274	0.49
CHO-294	0.46
CHO-317	0.05
CHO-318	-0.18
CHO-325	0.29
CHO-326	-0.14
CHO-335	-0.14
CHO-336	-0.23

Table 4.1: The order parameter of hydrocarbon tail of cholesterol (from carbon 22 to 25).

4.3.3 Structure of Aβ_{42} embedded in DPPC-CHOL bilayers

The central step of the amyloidogenic oligomerization process is the transition from α-helix rich to β-sheet rich structures. The initial structure of Aβ peptide was determined by 3D nuclear magnetic resonance (NMR) technique in apolar micro-environment, namely, the hexafluoroisopropanol that mimics the lipid phase of membrane, and it turned out to be α-helix predominantly.[?] During our 1 μs simulation, the α-helical structures at the N- and C-terminus of the Aβ were observed to unfold, with the occasional formation of a 3-10-helix, before transforming into random coils and turns. At $t = 500\ ns$ a short segment of parallel β sheet was found to shape up between residues SER-8 and TYR-10 of chain B and residues GLU-3 and ARG-5 of chain C, and at around $t = 800\ ns$, a β hairpin motif appeared at the C-terminus of chain A (see Figure 4.4). It is more likely that the α-helical structure unfolds at both termini, while the middle segment starting from HIS-14 (namely HQKLVFFAED) to ASP-23 remains as an α-helix throughout the whole 1000 ns simulation, based on our DSSP[41] analysis. Interestingly, from $t = 400\ ns$ onwards, the N- and C-terminus of chain A were observed to come close to each other. Such conformation resembles the

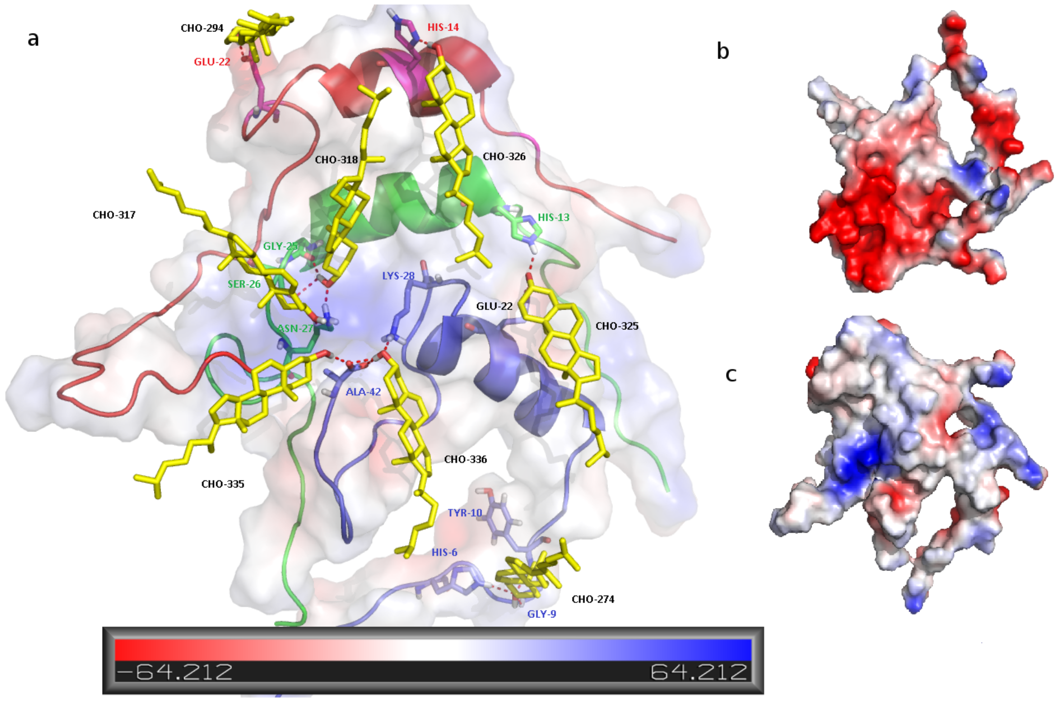

Figure 4.3: A snapshot of the binding of the cholesterol to the protein. The view is directed from the hydrophobic core towards the upper layer. The three peptides are represented in cartoon (peptide A: marine; peptide B: green; peptide C: red). The cholesterols are shown as sticks and colored by element (C: yellow; H: grey; O: red). The residues TYR-10, GLU-22, LYS-28, ALA-42 of peptide A are colored by element (C: marine; N: blue; H: grey; O: red). HIS-13, GLY-25, SER-26, ASN-27 of peptide B are colored by elements with green for carbon to distinguish it from the carbon of peptide A. The carbon atoms of HIS-14 and GLU-22 of peptide C are colored red in order to differentiate from those of peptides A and B's residues, and they are all represented as sticks. The electrostatic surface potential of the protein is represented by the color scheme: red, negative; blue, positive; gray, neutral (a). The electrostatic potential surface of the protein with the view towards the membrane surface (b). The electrostatic potential surface of the protein views from the membrane surface (c).

strand-loop-strand configuration in the structural model of protofibril.[274] It is clear that the time scale needed for the complete conversion from α-helix to β-sheet is far beyond 1000 *ns*. Nevertheless, our 1000 *ns* simulation has caught a glimpse of such a transition.

4.3.4 Peptide-peptide interactions in the membrane

The three peptides were observed to form an invagination in the membrane bilayer (see Figure 4.1(b)). The perturbation of the peptides on the membrane has caused the nearby cholesterol molecules to tilt with a high degree. The void in the middle of the bilayer has induced the elongation of the DPPC chain and also the caving-in of the lower leaflet lipid molecules. The invagination is filled with protein and water. The invagination reaches a depth of 12 $\AA$ from the membrane surface at t =1000 *ns*. From Figure 4.5, we can observe two deep wells in the $P1$ and $P2$ positions, where chain A and B, and chain B and C, make extensive hydrogen-bonding interactions with each other (see Figure 4.6). At the $P1$ site, the NH of amide groups on the GLN-15 side chain and imidazole group of HIS-14 from chain B both act as hydrogen bond donor (2.2 $\AA$ and 2.0 $\AA$) to the side chain and backbone carboxyl groups of ASP-7 of chain C respectively. On the $P2$ site, residues ASN-27, along with the solvent-exposed residues GLU-22 and ASP-23, all from chain A, construct a hydrophilic "floor" and they form hydrogen bonds with TYR-10 and LYS-16 of chain B. The favorable interaction between GLN-15 from chain A and the N-terminus of chain B also stabilizes the parallel β-sheet between chain B and chain C (see Figure 4.4 at snapshots $t = 800$ *ns*, 860 *ns* and 980 *ns*), which might be important for the protofibril formation in the later stage.[275]

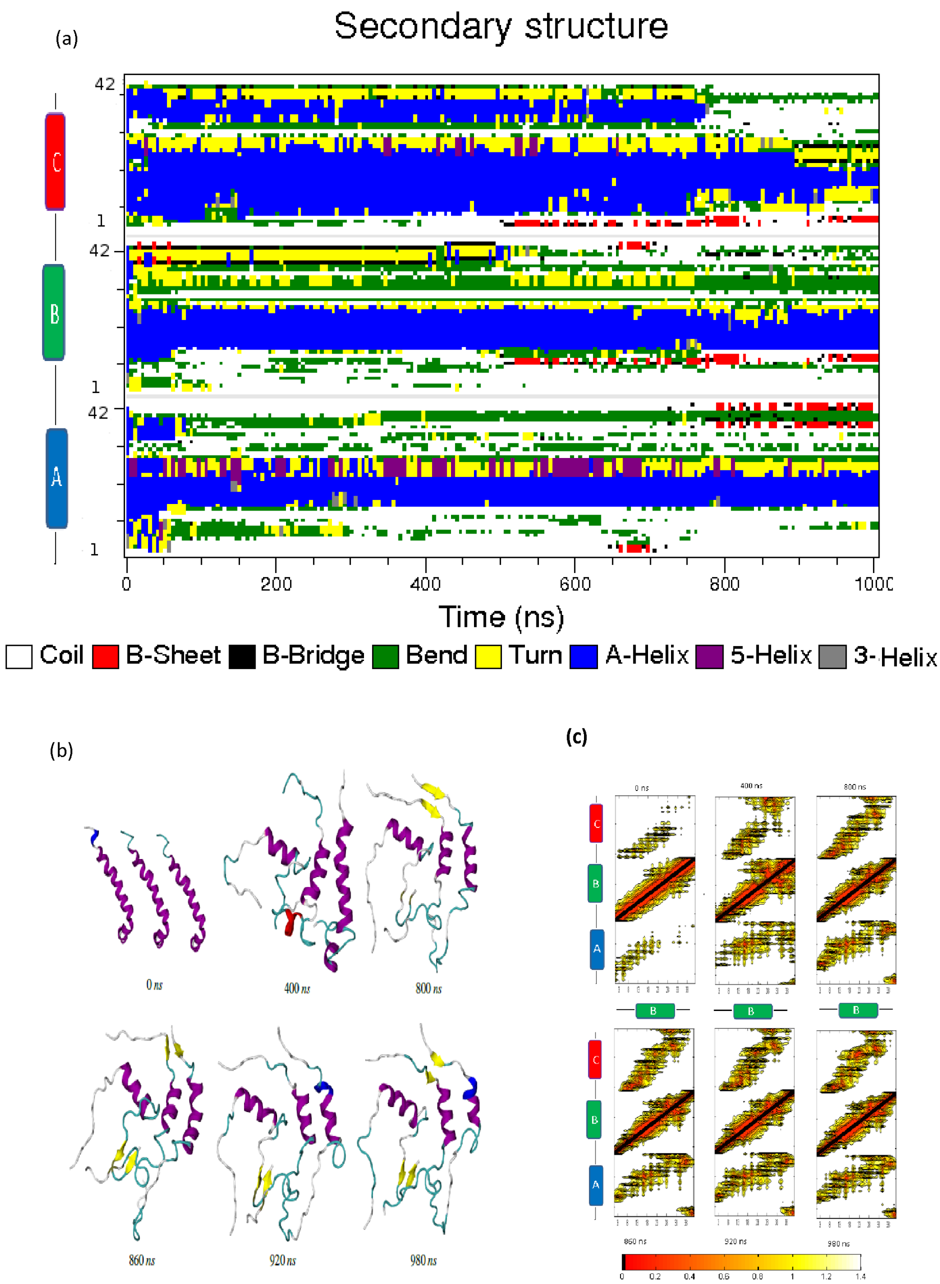

Figure 4.4: Conformational evolution of the Aβ_{1-42} peptides in the mixed bilayer as a function of time. (a) The secondary structure is calculated by DSSP. (b) Snapshots of the secondary structures of peptides are colored based on their default representation in VMD (α-Helix: purple; 3-10-Helix: blue; π-Helix: red; Extended-β: yellow; Bridge-β: tan; Turn: cyan; Coil: white). (c) The contact map of the residues of the three peptides. The contacts that form hydrogen bonding for peptide A and B, B and C, are in dark red.

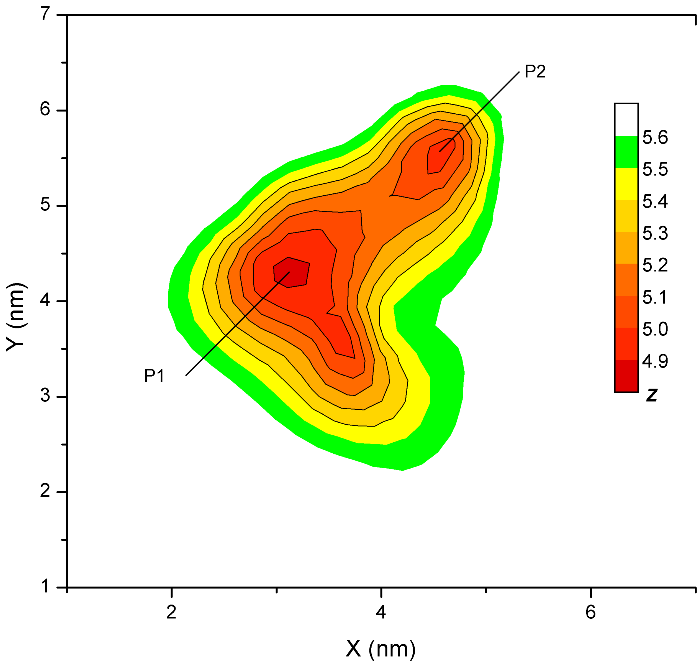

Figure 4.5: The contour map of the invagination. The depth z of the upper surface layer vs. the position x, y as defined in the Methods and Simulation Setup section. Note that the white background is for surface depth $z > 5.6\,nm$.

The ALA-42 at the C-terminus of the two peptides, chain B and C, were found to play an important role in the formation of hydrogen bonds: the main chain amide and carbonyl group of ALA-42 from peptide B forms hydrogen bonds with the side chain carboxyl group and main chain amide group of GLU-3 from peptide A; the carboxyl group of ALA-42 on the peptide C is tightly packed by hydrogen bonds network from main chain amide groups of LYS-28, GLY-29, ALA-30, ILE-31 and ASN-27 of peptide B, of which ASN-27 is located near the end of the α-helix of peptide B (the ASN-27 of peptide A is also located near the end of the α-helix).

4.3.5 Interaction among peptides, cholesterol and DPPC

The asymmetry of the initial arrangement of the peptides on the upper leaflet in our simulation system has made it necessary for us to examine the upper and lower leaflets separately. The order parameter profile (see Figure 4.7) of the DPPC sn-1 (aliphatic

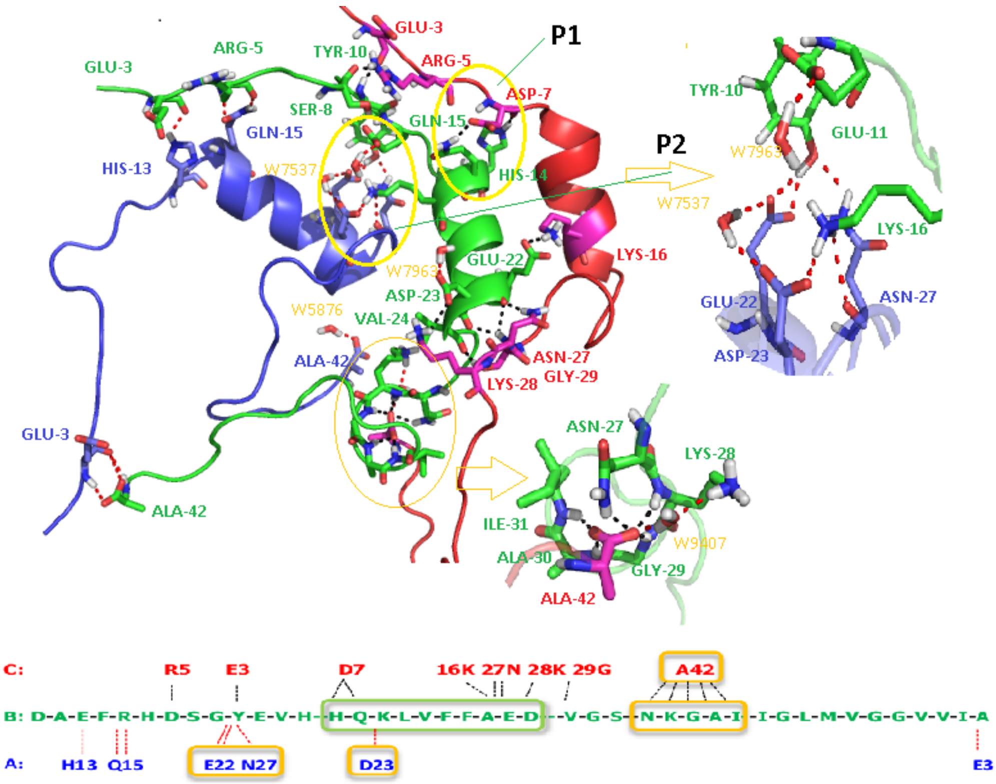

(a)

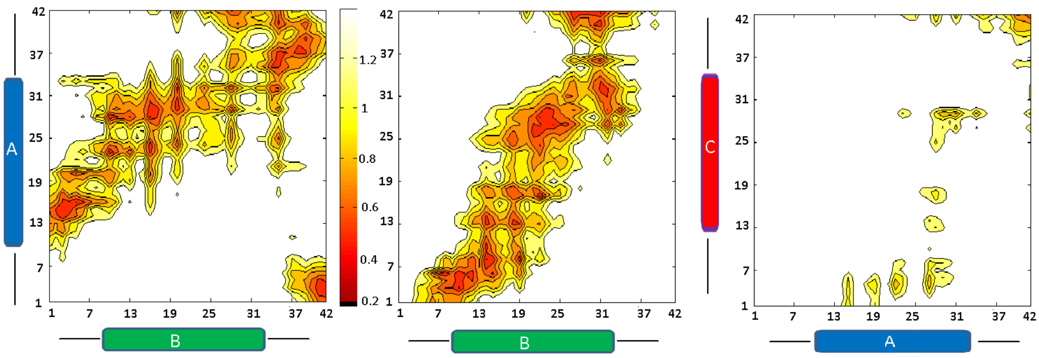

(b)

Figure 4.6: Details of the hydrogen bond configurations between peptide A and B, and peptide B and C. Peptides A, B and C are shown in cartoon and represented in blue, green and red color respectively. The hydrogen bonds between peptide A and B are indicated by red dash lines; the hydrogen bonds between peptide B and C are given by black dash lines; the hydrogen bonds between water and peptides are shown by red dash lines. The two yellow circle depict the $P1$ and $P2$ sites. The sequence below the figure gives a hydrogen bonding map between the three peptides (a). The contact map between the residues of three peptides. Note that the dark red region corresponds to residues connected by hydrogen bonds (b).

carbon atoms C15 to C31 on the tail of DPPC), and sn-2 chains (aliphatic carbon atoms from 34 to 50 on the tail of DPPC) shows that the value of the order parameter of the lower leaflet is higher than that of the upper leaflet: on average the $< S_{\mathrm{CD}} >$ of the upper leaflet is 0.272 ± 0.047 lower than that of the lower leaflet. And the same holds for the cholesterols.

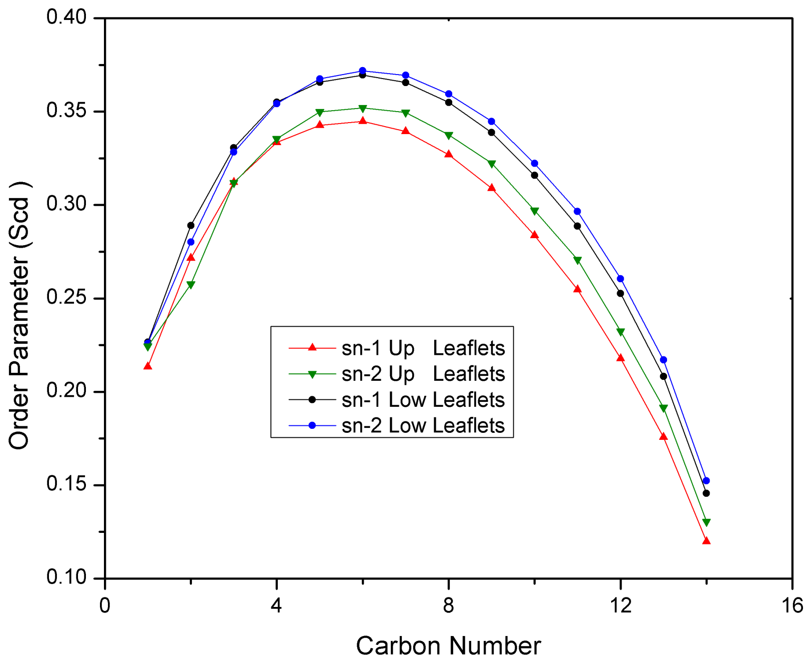

Figure 4.7: The order parameter profile for the DPPC Sn-1 and Sn-2 chains in the upper and lower leaflets.

The radial distribution functions (RDF) of the DPPC and cholesterol with respect to the peptides in the upper and lower leaflets were calculated (see Figure 4.8) with a distance binning of 0.2 $\mathring{A}$. During the whole simulation the peptides remain in the upper leaflet. The pairing of the peptides and cholesterols have a high possibility of locating at the distance of 5-15 $\mathring{A}$ in the upper leaflet, and the pairing between the peptides and DPPC lipids have a high propensity to locate at $4.5 \pm 1.0\,\mathring{A}$ and

$9.0 \pm 1.0\,\AA$. At a distance of $2.4\,\AA$ small peaks are observed at the RDF profile indicating direct contacts (mainly through hydrogen bonds) between peptides and cholesterols and DPPC.

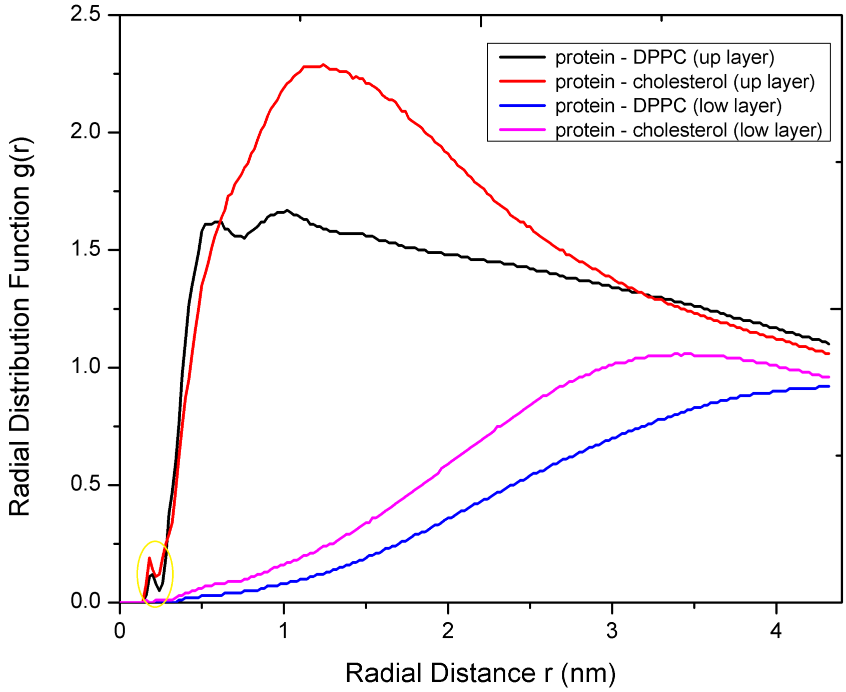

Figure 4.8: A plot of the RDFs of the DPPC and cholesterol with respect to the protein in the upper and lower leaflet.

To further examine the relationship between the protein, DPPC and cholesterol, we have calculated the RDFs between the hydroxyl oxygen atoms of cholesterol, and the DPPC carbonyl oxygen atoms and the phosphate oxygen atoms for both the upper and lower leaflet. From Figure 4.9, one finds that the RDFs have a sharp peak around $2.5\,\AA$ for all the four cases. The study of Chiu et al[276] has shown that the lower the concentration of the cholesterol, the higher the peak of the RDF at $2.5\,\AA$ of the cholesterol oxygen with DPPC carbonyl oxygen. In our simulation, the number ratio of cholesterol to DPPC in the upper leaflet is 118 : 96, and in the lower leaflet, it is 127 : 127. We have also observed that the higher cholesterol concentration (in the upper leaflet) has led to a lower peak height than that in the lower leaflet. The sharp peak around 2.5 $\AA$ reflects the strong binding between the cholesterol and DPPC. The peptides present in the upper leaflet compete with DPPC in the formation of hydrogen bonds with the cholesterol hydroxyl groups. This gives another reason for the decrease of the peak height of CHO-DPPC RDF in the upper leaflet. From the RDFs, we observed that the oxygen atom on the cholesterol has a higher tendency to bind with the carbonyl groups than the phosphate groups of the DPPC. This implies that the cholesterol is predisposed to locate below the DPPC headgroup and agrees well with the study of Chiu et al.[276]

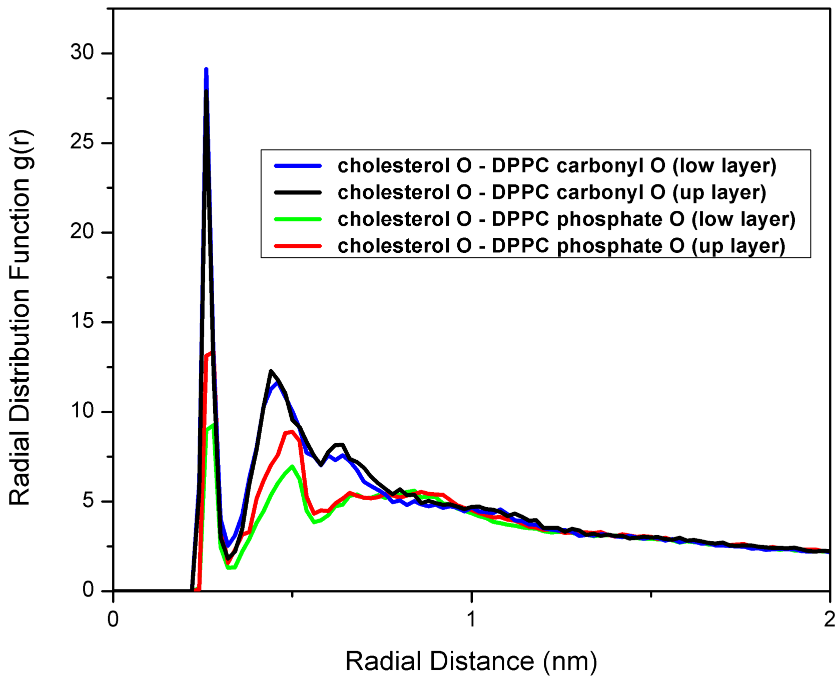

Figure 4.9: A plot of the RDFs between cholesterol O and DPPC phosphate, cholesterol O and DPPC carbonyl O, in the upper and lower leaflet.

In order to examine the hydrogen bonding affinity of the peptides with DPPC and cholesterol, we have also calculated the RDFs of the DPPC carbonyl oxygen group, DPPC phosphate oxygen group, DPPC nitrogen group, cholesterol oxygen group and cholesterol hydroxyl hydrogen with respect to the peptides. The peaks around 1.9 $\AA$ in Figure 4.10 indicate that the peptides prefer to form more hydrogen bonds with cholesterol than with the DPPC. The cholesterol acts as both hydrogen bond donor and acceptor. The length of hydrogen bonds are around 1.9 $\AA$, 2.5 $\AA$ and 3.5 $\AA$. The protein shares the same characteristic as the cholesterol in having a greater tendency to form hydrogen bonds with the carbonyl oxygen group than the phosphate group at around 1.9 $\AA$. No hydrogen bond is observed to form between protein and the DPPC nitrogen group in our study.

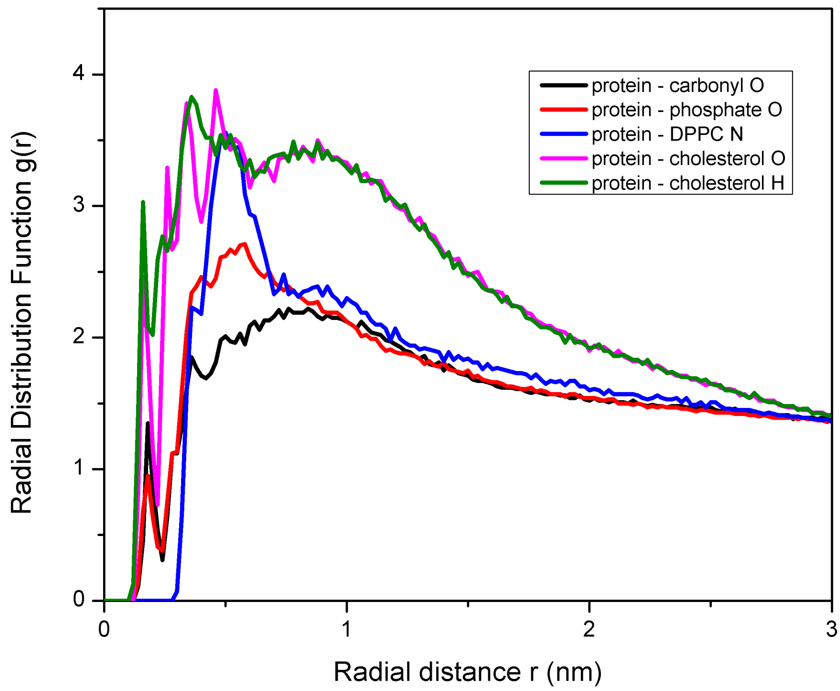

Figure 4.10: The RDFs between protein and DPPC carbonyl oxygen, DPPC phosphate oxygen, DPPC nitrogen, cholesterol oxygen and cholesterol hydrogen of the upper leaflet.

4.3.6 Correlation between peptide aggregation and peptide-lipid interaction

The relationship between peptide aggregation and peptide-lipid interaction is complicated. We try to provide a quantitative description based on the metrics of contact numbers. The number of pairs within 0.35 *nm* between peptides, between peptides and lipids and between peptides and cholesterols were monitored and displayed in Figure 4.11. The interaction between cholesterol and peptides A and B shows a negative correlation in comparison to the interaction between the two peptides (correlation coefficient is around -0.23). The interaction of DPPC with peptides A and B shows a very weak correlation with respect to the interaction between the two peptides according to our contacts number analysis (correlation coefficient is around -0.08). The same negative correlation trend is also observed between cholesterol and chain B and C (correlation coefficient is around -0.28), while for DPPC with peptide B and C, the correlation coefficient is around 0.34. The difference in the correlation coefficient between DPPC with peptide A and B, and DPPC with B and C, reflects the complicated relationship between peptides aggregation and peptide-lipid interactions.

The above analysis indicates that cholesterol molecules compete with peptide-peptide interaction by binding directly with peptides. This implies that monomeric Aβ and/or small Aβ aggregations prefer to locate within cholesterol-rich membranes.[9,277] The binding of lipids with peptides, however, weakly enhances the already-formed aggregation of the peptides. Here through available snapshots we demonstrate some examples of lipid molecules forming hydrogen bonds with two peptide chains (see Figure 4.12). One example shows that DPPC inhibits peptide A and B aggregation (see Figure 4.12(a)). Another example shows that the phosphate oxygen of DPPC-

529 is in close proximity of the backbone amide group of residues ASP-7 (2.8 $\AA$), SER-8 (1.8 $\AA$) and GLY-9 (2.1 $\AA$) from peptide B (see Figure 4.12(b)), which weakly enhances the already-formed aggregation of the peptides. The side chain amide group of GLN-15 from peptide A and the side chain amide group of HIS-6 from peptide B both contribute protons bonded to the non-ester and ester carbonyl oxygens of DPPC-529 respectively. Here the DPPC may enhance the interaction between peptide A and B.

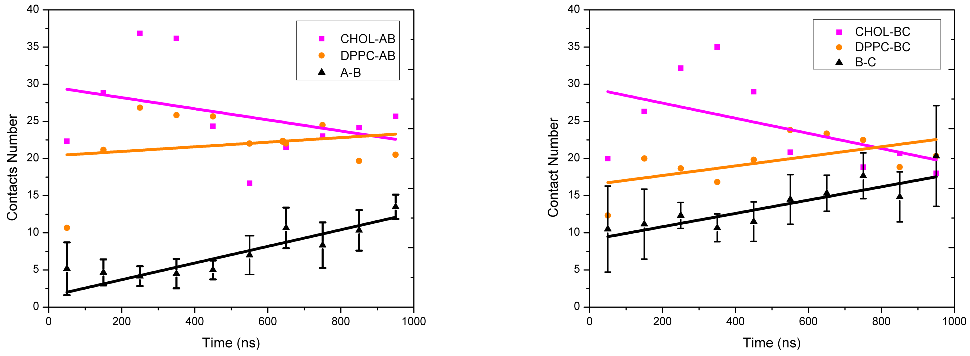

(a) (b)

Figure 4.11: The average contacts number for the pairs within 3.5 *nm* during the time evolution between DPPC and cholesterol with peptide AB, and peptide BC, respectively. Error bars indicate standard deviations of the contact number. The magenta lines are linear fit to the data set for contacts formed between cholesterol and peptide AB, and peptide BC; the orange line is for contacts formed between DPPC and peptides AB, peptide BC. The black lines give the contacts between peptide A and peptide B, and between peptide B and peptide C.

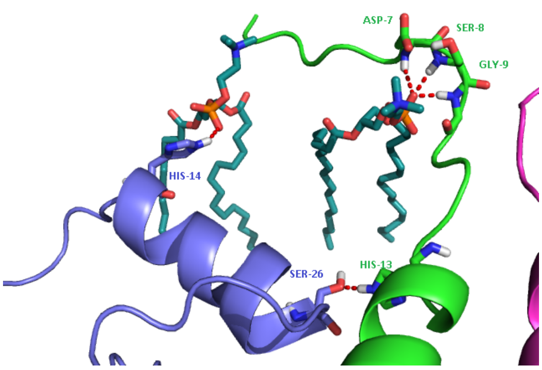

(a)

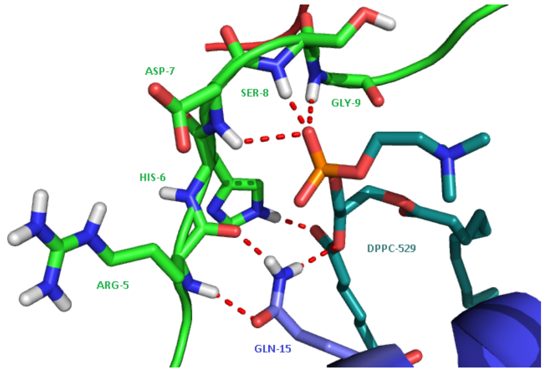

(b)

Figure 4.12: A snapshot of DPPC inhibiting peptide A and B aggregation at 500 *ns* (a). A snapshot of DPPC enhancing peptide A and B aggregation at 1000 *ns* (b).The residues HIS-14, GLN-15 and SER-26 from peptide A are shown as sticks and colored by elements (C: marine; N: blue; H: grey; O: red). The residues ARG-5, HIS-6, ASP-7, SER-8, GLY-9 and HIS-13 from peptide B are shown as sticks and colored by elements (C: green; N: blue; H: grey; O: red). The DPPC is also shown as sticks and colored by elements (C: cyan; N: blue; O: red; P: orange).

4.4 Summary and discussions

It is generally believed that the Aβ oligomers are neurotoxic and one of the main causative factors in Alzheimer's Disease. By studying the aggregation process in mixed bilayers, we show the complicated interaction network among peptides, lipid molecules and cholesterols. The N-terminal part of the peptide prefers to locate at lipid-aqueous interface, while the C-terminal part inclines to bury more deeply inside the hydrophobic tails region of the lipid. A short segment of parallel β-strand is found to form between peptide B and C and another anti-parallel β-strand is observed at the C-terminal of peptide A. Meanwhile the short sequence from 14-23 is found to maintain a well-preserved α-helical structure. This indicates that the force field GROMOS96, which we have used, gives a balanced description of the peptide backbone configuration. This is consistent with the recent finding of Nguyen and collaborators.[278]

All these structural transitions indicate that our 1000 *ns* simulation has caught a glimpse of the mysterious peptide aggregation process together with the peptide secondary structure conversion from α helices to β strand.

In the mixed bilayer environment, the peptides were found to attach to the sunken membrane surface and form a hydrophilic well at the end of the simulation. The presence of the peptides has resulted in the appearance of defects in the membrane and a disordering of the cholesterol molecules. The binding of the lipids with the peptides may enhance the already-formed hydrogen bonds between peptides residues in accordance with our group's previous replica exchange simulation study.[279] The cholesterol molecules interact with the peptides in a competitive way resulting in a negative correlation between cholesterol-peptide interaction and peptide-peptide interaction.

We found that GLN-15 of the peptide shows a considerable importance in the aggregation process. Furthermore, ALA-42 at the C-terminus is also observed to play a noticeable role during the oligomerization in the membrane environment. We observed that sequence HQKLVFFAED maintains a well-preserved α-helical structure in the membrane environment in the final 920 *ns*. Due to limited simulation time, the few small number of peptides used, and the lack of enhanced sampling techniques,[261] the complete picture of conformational transition and amyloid formation is still far beyond the reach of the current study. The aggregation of the full-length Aβ peptides depends on several factors such as pH, ionic strength, etc. The full understanding of the underlying mechanism still requires the joined efforts from both experimental and theoretical studies.

Chapter 5 The curcumin effect on the dimer stability

Aβ oligomers are potential targets for the diagnosis and therapy of Alzheimer's disease. On the other hand, the molecule curcumin has been shown to possess significant therapeutic potential in many areas. There is a strong connection between curcumin and AD. In order to get the detailed mechanism on how curcumin interacts with the Aβ oligomers, we have conducted several all-atom explicit solvent molecular dynamics simulations. In this chapter, we study the effect of curcumin on the stability of Aβ amyloid protein oligomers. We observed that curcumin decreases the β-sheet secondary structural content within the Aβ oligomers without reducing the contacts between the monomers. The breaking of the β-sheet is found to be preceded by a deformation of the β-sheet structure due to hydrophobic interaction from the nearby curcumin. Furthermore, the π-stacking interaction between curcumin (keto-ring and enol-ring) and the aromatic residues of Aβ, which exists throughout the simulations, has also contributed to the diminishing of the β-sheet structure. Our analysis of the under-wrapped amide-carbonyl hydrogen bonds reveals several stable dehydrons of the oligomer, especially the dehydron pair 34L and 41I, with which curcumin tends to hover over. We have examined the paths of curcumin on the Aβ proteins and determined the common routes where curcumin lingers as it traverses around the Aβ. In consequence, our study has provided a detailed interaction picture between curcumin and the Aβ oligomers.

5.1 Introduction

Curcumin with a major polyphenol component, usually extracted from the turmeric, serves as traditional medicine for centuries and is also used as natural food addictive. Curcumin and its derivatives have also been shown to possess significant therapeutic potential as antioxidant, anticarcinogen, with its anti-inflammatory effect[10] well suited for the healing of skin wounds. It is suggested that incorporating curcumin into the cell membrane can induce segmental ordering of the membrane,[280] and modulate diverse membrane proteins by means of the bilayer-mediated mechanism.[281] The increasing attention on curcumin results from its observed therapeutic potential and intrinsic non-toxicity.

Recent research has uncovered a strong connection between curcumin and AD. For example, a regular diet of curcumin can reduce the risk of AD.[11] Curcumin is also found to regulate the production of Aβ by indirectly suppressing the expression of presenilin 1, which is related to γ secretase and the generation of Aβ.[12] With its unique physicochemical properties, curcumin can pass the blood-brain barrier and interact with Aβ.[13] Curcumin may also bind directly to small Aβ oligomers to block aggregation, hence lowering or reversing Aβ oligomer toxicity by disrupting the development of plaques *in vitro* and *in vivo*.[14–17] Curcumin and its derivatives can rescue functional failures such as spontaneous firing inhibition of the hippocampal neurons, and long-term potentiation damages induced by the Aβ oligomers.[282,283] Furthermore, curcumin may protect the neuron from Aβ insult and degeneration.[284,285] However, research has indicated that the neuronal protective effect is concentration-dependent and high dosage of curcumin may result in cell damage in the presence of Cu(II).[138] Some curcumin derivatives have also been used as radioligand for Aβ plaque imaging due to their binding affinities towards the Aβ_{1-42} aggregate.[286] Despite the extensive studies being done and several mechanisms being proposed[18] on the inhibitory effects of curcumin in the last decades, the detailed mechanism on how curcumin interacts with the Aβ oligomers still await further identification and elucidation.

Curcumin consists of two aromatic end groups with a linker region in the middle. Early studies have shown that the predominant tautomer is β-diketone in aqueous environment.[287] However, recent X-ray and NMR studies have found that curcumin tends to exist in solution as an enol-keto tautomer rather than a β-diketone tautomer[288,289] in lieu of the more stable planar structure of the former and also due to energy consideration. Hence, in this article we focus our analysis on the keto-enol form of curcumin. Nonetheless, we have found that the simulation results from the β-diketone tautomer form of curcumin are essentially the same as those of the keto-enol form. The chemical structure of curcumin is displayed in Figure 5.1.

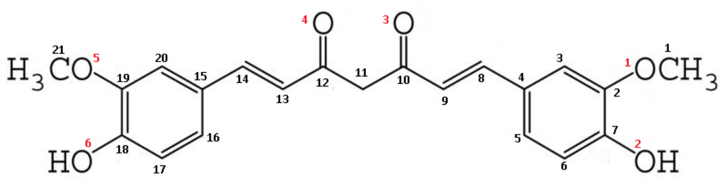

(a)

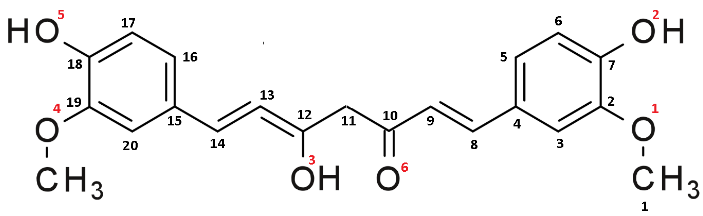

(b)

Figure 5.1: Chemical structure of curcumin (β-diketone tautomer (a) and keto-enol tautomer (b)). The carbon atoms are distinguished by sequential number (black) and oxygen atoms are labeled by red.

5.2 Materials and methods

The initial structure of Aβ_{42}, whose sequence is $DAEFRHDSGY_{10}$ $EVHHQKLVFF_{20}$ $AEDVGSNKGA_{30}$ $IIGLMVGGVVIA_{42}$, was taken from model 1 of the PDB ID: 1IYT.[?] The pKa values of the titratable residues was calculated by the H++ server[290,291] (see Table A1). The default internal and external dielectric constants of 6 and 80 were used in the calculation respectively. The ionic strength was set to 0.1 M with pH 7. The structure of the small curcumin molecule was obtained from the ZINC database[292] (see Figure 5.1). The initial topology and force field parameters of curcumin was generated in the PRODRG2 Server[293] (see Appendix B).

The protein and curcumin were represented by the GROMOS96 53a6 force field, which is able to model the Aβ structural propensities in agreement with experimental NMR results.[294]

5.2.1 Aβ oligomers preparation

Our first set of simulations was performed on a single Aβ peptide in a cubic box of dimensions 52.60 $\mathring{A} \times$ 52.60 $\mathring{A} \times$ 52.60 $\mathring{A}$ for 200 ns. The box was filled with 5582 water molecules, and 13 Na^{+} ions and 11 Cl^{-} ions to neutralize the system. The final Aβ peptide structure was taken as the initial structure for the subsequent simulations.

In our second set of simulations, 5 Aβ of the final conformation from the first set were used and aligned parallel in a cubic box of dimensions 166.86 $\mathring{A} \times$ 46.87 $\mathring{A} \times$ 46.87 $\mathring{A}$. The center of mass of each peptides was placed at (23.43, 23.43, 23.43), (53.43, 23.43, 23.43), (83.43, 23.43, 23.43), (113.43, 23.43, 23.43) and (143.43, 23.43, 23.43), and the peptides were labeled as chain A, B, C, D and E, respectively.

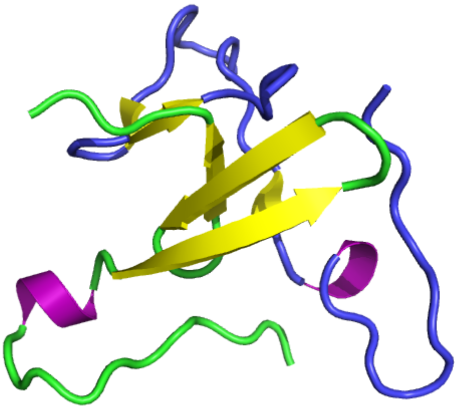

Figure 5.2: The snapshot of the dimer at the end of the set 2 simulation. The dimer was represented as cartoon (β-sheet: yellow; helix: purple; for the others from peptide A: tv_green; for the others from peptide B: tv_blue).

The simulation was conducted for a period of 1000 *ns*.

5.2.2 Docking

In our third set of simulations, we took the dimer (see Figure 5.2) which was formed by peptide A and B at the end of the second simulation to be used as initial structure for docking. AutoDock 4[295] was then employed to dock the curcumin (β-diketone tautomer) onto the preformed dimer. During the docking simulations, gasteiger charge was computed and Autodock type was assigned to the curcumin, and 12 active torsion angles (rotable bonds) were defined as the flexible parts. To explore the possible binding sites, the whole dimer was treated as a blind docking area. The docking space was defined via the dimensions: $106 \times 102 \times 126$, with an autodock default grid spacing of 0.375 $\mathring{A}$. The grid box was centered on the dimer and covered the whole of the dimer. Ten complex conformations (dimer and curcumin) with the lowest docking energy from the most populated clusters were taken as initial structures for further MD simulations. We labeled these conformations as M1 to M10. Similarly, we performed docking for the keto-enol tautomer form of curcumin, and ten complex structures with lowest docking energy were chosen and labeled as M11 to M20.

In Model 1 and 2, curcumin binds both peptide A and B. In Model 5 and 10 curcumin binds to HIS-14, LEU-17 and PHE-19 from peptide B and A respectively. The representative snapshot of the docked diketon curcumin towards Aβ dimer can be seen from Figures 5.3 on page 68 and keto-enol form curcumin towards Aβ dimer can be seen from Figure 5.4 on page 69. The detailed information of the curcumin docked on the specific residues can be seen from Table 5.1.

5.2.3 Molecular dynamics simulations

During the subsequent MD simulations, each of the models was put in the center of a cubic box of dimensions around $62.14\,\AA \times 62.14\,\AA \times 62.14\,\AA$. All the conformations were solved in SPC water model,[296] and 18 Na^+ ions and 14 CL^- ions were added to neutralize the system. Both the protein and curcumin were represented by the GROMOS96 53a6 force field. In our simulations, all bonds were constrained using the LINCS[161] algorithm with a $2\,fs$ integration time step. The temperature was kept at 300 K using the Nosé-Hoover coupling scheme.[162,163] A semi-isotropic pressure coupling at 1 *bar* by means of a Parrinello-Rahman barostate with a coupling constant of $2\,ps$ was used in the pressure ensemble. The van der Waals cutoff was set to $1.0\,nm$. Particle Mesh Ewald method[270] was used for electrostatic interaction with a fourth-order interpolation and a Fourier grid spacing of $0.16\,nm$. The following preparation steps, simulations and analysis were performed using facilities within the GROMACS package. PyMOL[271] and VMD[272] were used to visualize the structure. For each system, $500\,ns$ MD simulation was conducted. Additional analysis and visualization were assisted by WRAPPA,[297] MATLAB, originPro and some in-house scripts.

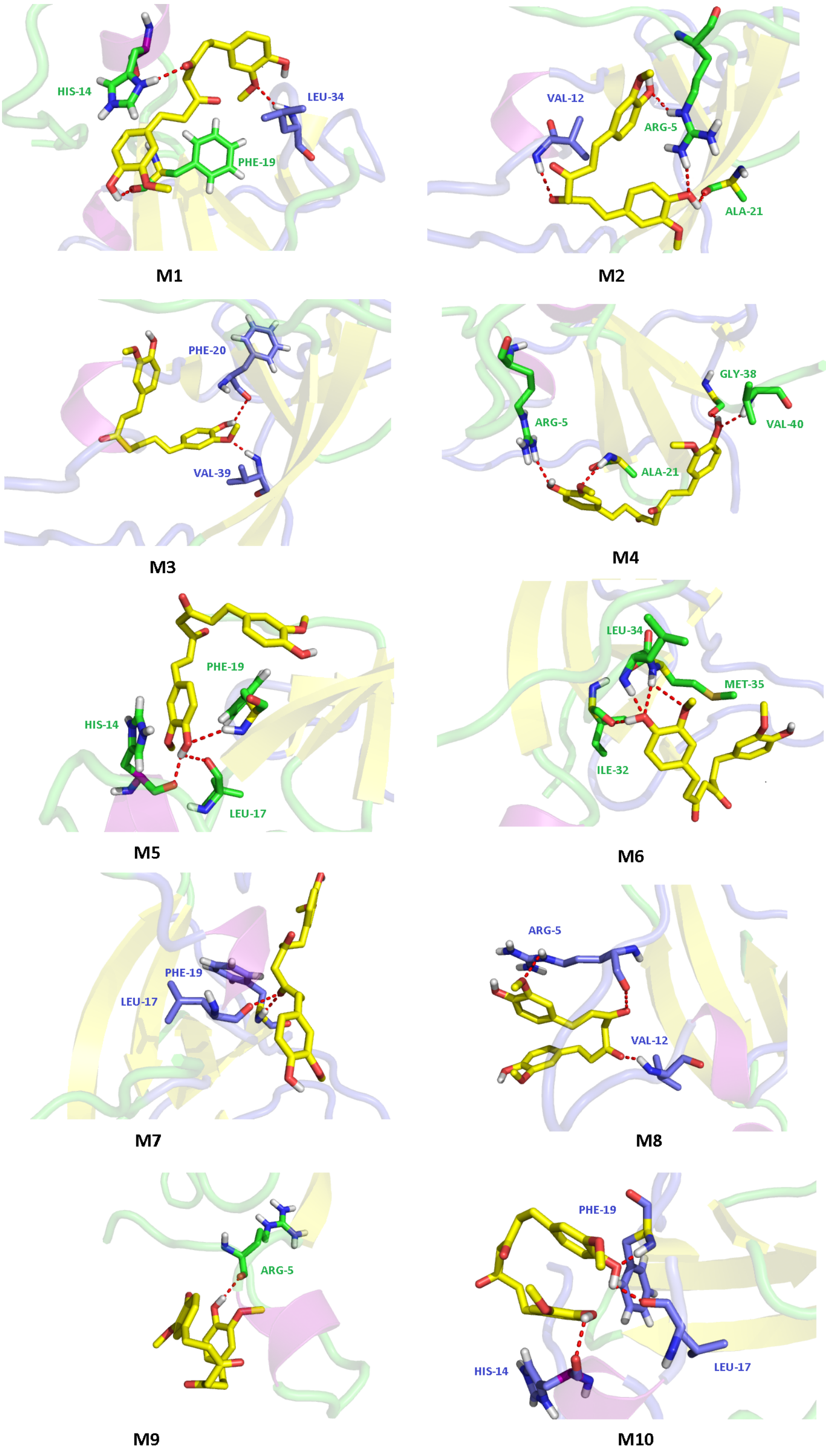

Figure 5.3: The initial M0-10 models. The secondary structure of dimer was represented as transparent cartoon (β-sheet: yellow; α-helix: purple; others for peptide A: tv_blue; others for peptide B: tv_green). The curcumin was shown as stick and colored by element (C: yellow; H: grey; O: red). For the residues from peptide A involved in the contacts with curcumin was represented as stick and colored by element (C: marine; N: blue; H: grey; O: red). For the residues from peptide B involved in the direct contact with curcumin was also represented as stick and colored by the similar element except C atom was colored as green to distinguish from peptide A. Please note for those C_α atom exits in the β-sheet part was colored as yellow, and purple for the Cα atom in α-helix part.

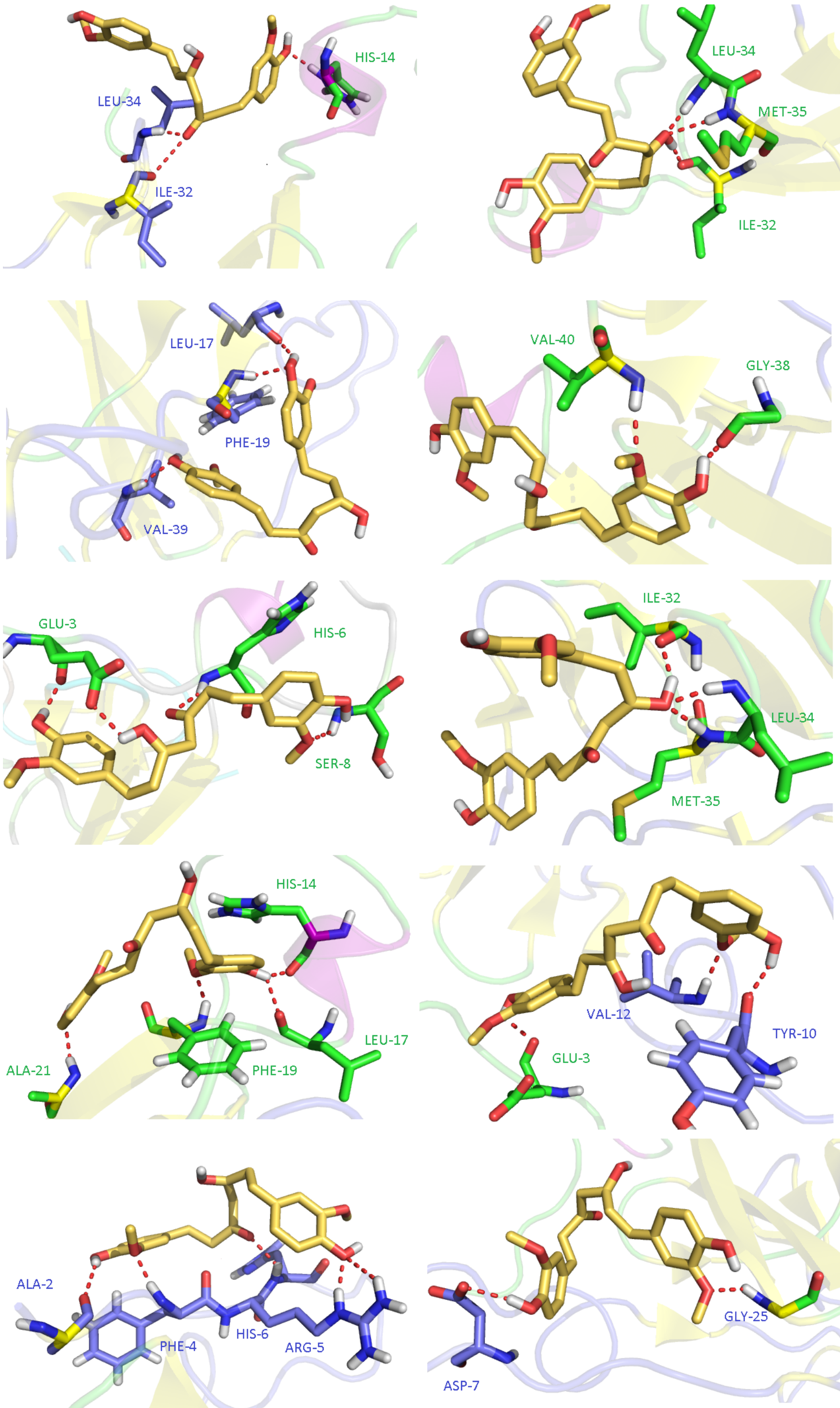

Figure 5.4: The initial M11-20 models.

Table 5.1: Simulation system

β-diketone tautomers					keto-enol tautomers				
Model ID	Potential binding sites	Binding Energy kcal/mol	Rank	Water molecules	Model ID	Potential binding sites	Binding Energy kcal/mol	Rank	Water molecules
M1	A: LEU-34 B :HIS-14$^{\alpha}$, PHE-19$^{\beta}$	-3.84	5	7475	M11	A: LEU-34, ILE-32 B: HIS-14$^{\alpha}$	-4.38	1	8111
M2	A: VAL-12 B: ARG-5, ALA-21$^{\beta}$	-5.30	1	7471	M12	B: ILE-32$^{\beta}$, LEU-34 MET-35$^{\beta}$	-4.14	2	7472
M3	A: PHE-20, VAL-39	-2.82	9	7477	M13	A: LEU-17, PHE-19$^{\beta}$ VAL-39	-3.74	3	7474
M4	B: ARG-5, ALA-21$^{\beta}$ GLY-38$^{\beta}$, VAL-40	-3.04	8	7480	M14	B: GLY-38, VAL-40$^{\beta}$	-3.71	4	7478
M5	B: HIS-14$^{\alpha}$, LEU-17 PHE-19	-4.37	3	7478	M15	B: GLU-3, HIS-6 SER-8	-3.55	5	7468
M6	B: ILE-32$^{\beta}$, LEU-34 MET-35$^{\beta}$	-3.08	7	7474	M16	B: ILE-32$^{\beta}$, LEU-34 MET-35$^{\beta}$	-3.53	6	7479
M7	A: LEU-17, PHE-19$^{\beta}$	-4.79	2	7469	M17	A: HIS-14$^{\alpha}$, LEU-17 PHE-19$^{\beta}$, ALA-21$^{\alpha}$	-2.97	7	7475
M8	A: ARG-5, VAL-12	-2.76	10	7472	M18	A: TYR-10, VAL-12 B: GLU-3	-2.88	8	7471
M9	B: ARG-5	-4.04	4	7466	M19	A: ALA-2$^{\beta}$, PHE-4 ARG-5, HIS-16	-2.77	9	7475
M10	A: HIS-14, LEU-17 PHE-19	-3.66	6	7469	M20	A: ASP-7 B: GLY-25$^{\beta}$	-2.50	10	7471
M0	-	-	-	7495					

- indicates NULL.
$^{\alpha}$ indicates residue sites on α-helix.
$^{\beta}$ indicates residue sites on β-sheet.

5.3 Results

5.3.1 Curcumin as β-sheet breaker

The number of residues that adopt the β-structure conformation in the absence/presence of curcumin and the secondary structure evolution were studied (see Figures 5.5, 5.6 and 5.7). Without curcumin (Model 0), the number of residues with β-structure is found to increase for both peptide A and B. The number of residues forming β-structure in peptide A is relatively stable from 6 at the beginning to 8 in the end of the simulation. In peptide B there is an obvious increase in the number of residues with β-structure from 14 in the beginning to 21 at the end of the simulation with most of the β-structure segments well maintained. In the models with curcumin, both collapse and re-organization of the β-structure happen. We find that the presence of curcumin generally destabilizes the β-structure. The average number of residues of Aβ dimer adopting β-structure without curcumin is around 27.16, while the average number of residues in the presence of curcumin forming β-structure is around 21.48. Here curcumin was found to induce a 21% reduction in the number of β-structure residues. Note that the average here was performed with respect to time and for the case with curcumin, a further average over the time-averaged β-sheet content over the 10 models was carried out (see Figure 5.5). After examining the secondary structure evolution (see Figure 5.6), we detail the secondary structure propensity of Aβ residues in the presence and absence of curcumin as illustrated in Figure 5.7.

The number of contacts, i.e., the number of heavy atom pairs whose distances are smaller than 0.6 *nm*, between peptide A and B were calculated. A weakly negative correlation is found between the number of contacts and the number of β-structure

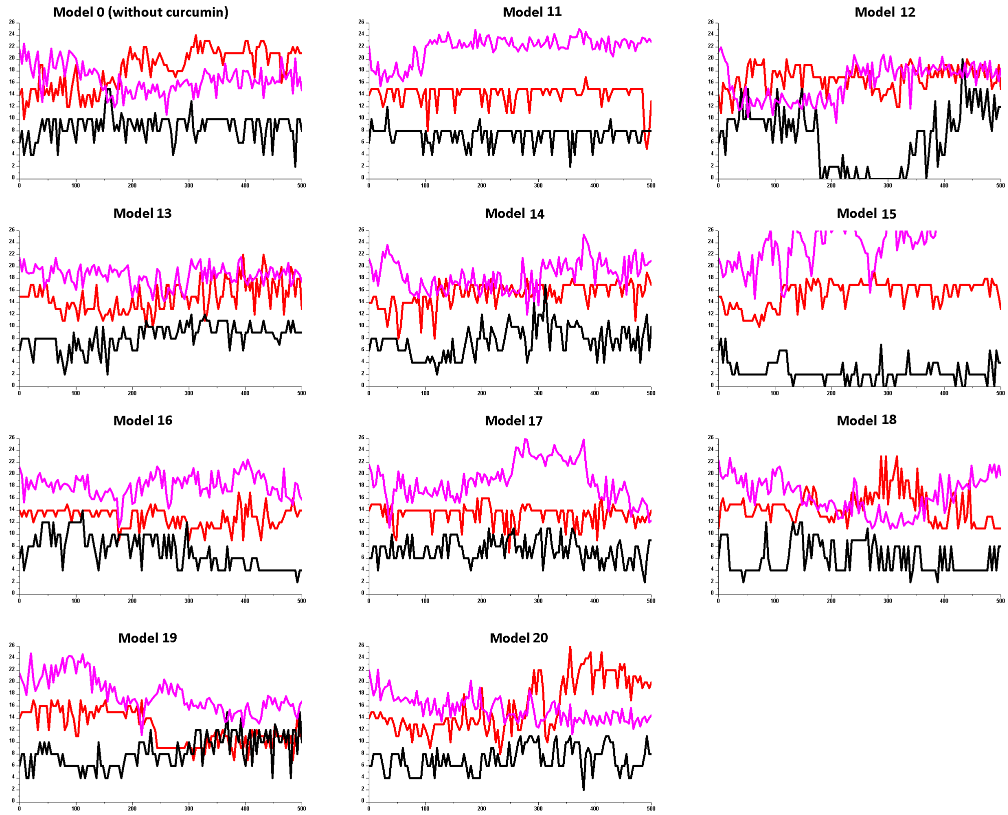

Figure 5.5: Time evolution of the number of residues in β-structure (β-sheet and β-bridge) of peptide A (black line) and B (colored by red) and the contact numbers between peptide A and B (colored by magenta). The data were extracted from each 11 model trajectories and averaged per 4 *ns*. The contact number were divided by 100.

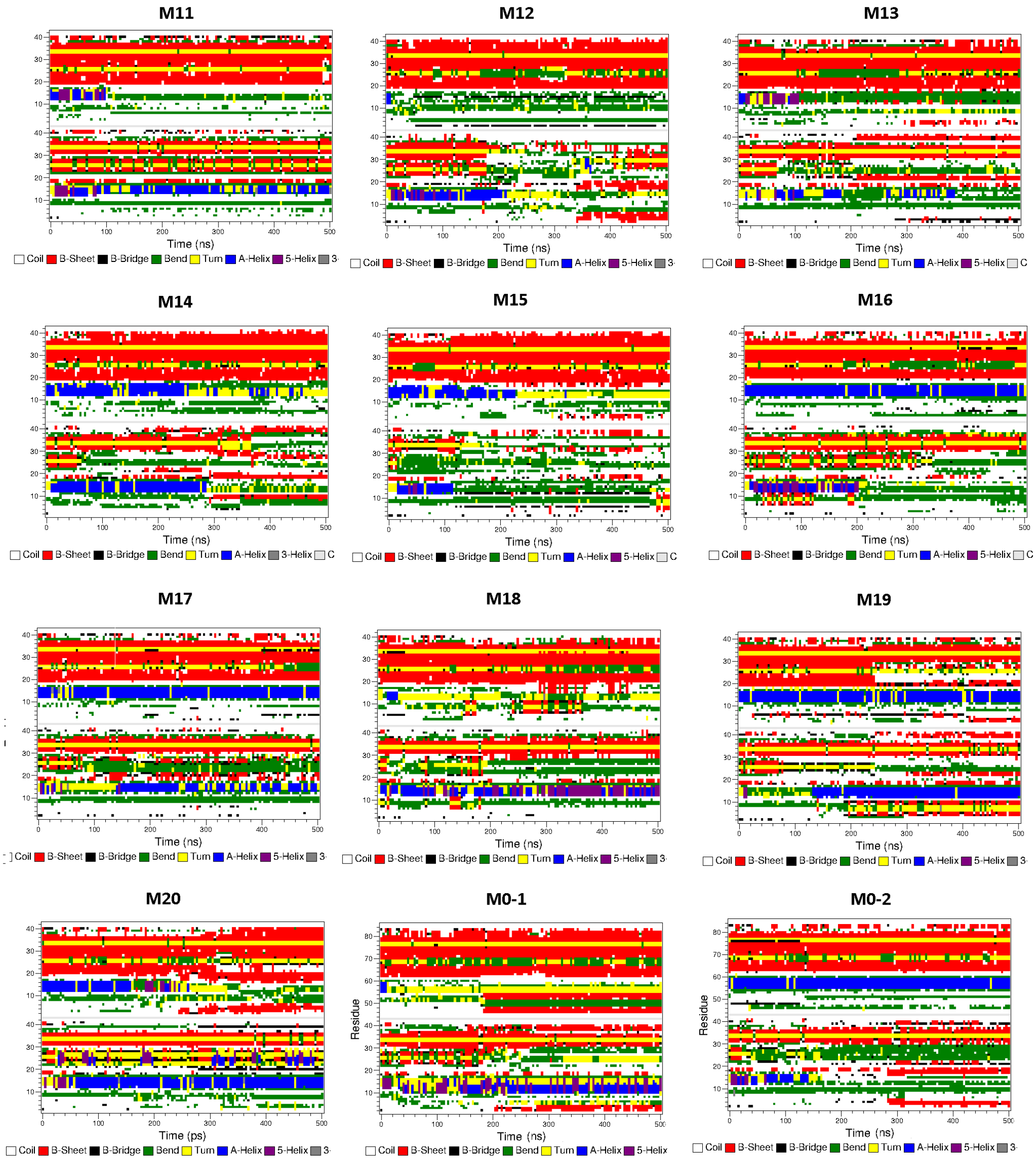

Figure 5.6: Evolution of the secondary structure of protein in the presence of keto-enol conformers and the controlled group M0.

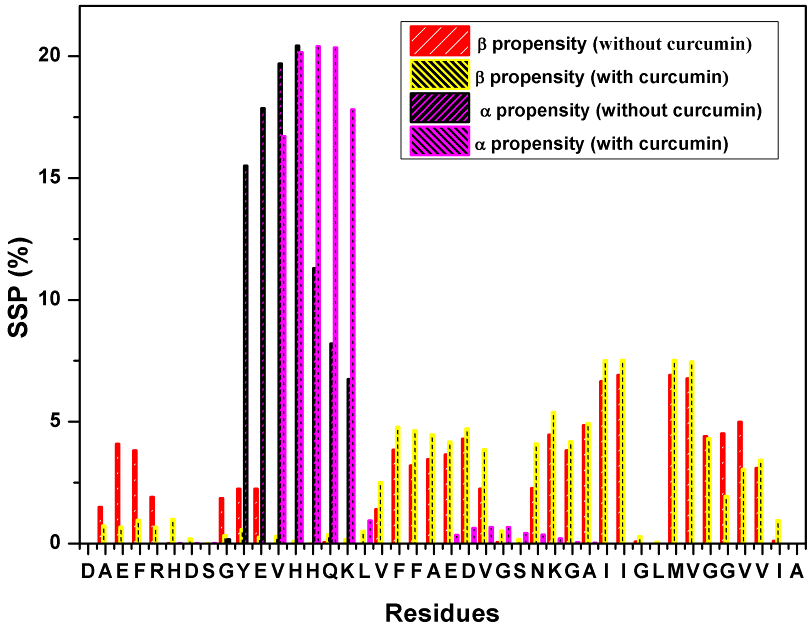

Figure 5.7: The secondary structure propensity of Aβ residues in the presence and absence of curcumin.

residues, with an average Pearson correlation coefficient of -0.13 for all models.

To further examine this phenomenon, we also checked the protein segment of 17-42 which was reported to form well-ordered Aβ fibril that tends to reside in the hydrophobic core of the membranes.[142,152] The correlation between the number of β-structure residues and the contacts number within the segment of 17-42 is also slightly negative with an average Pearson coefficient of -0.22.

The role of curcumin as a β-structure breaker is demonstrated through the evolution of the secondary structure as observed within a trajectory (see Figure 5.8). The secondary structures of 4 segments, SI: $_{3}$E–$_{11}$E; SII: $_{17}$L–$_{20}$F, and SIII: $_{30}$A–$_{42}$V from peptide A and SIV: $_{17}$L–$_{42}$V from peptide B, are shown from 180 *ns* to 210 *ns*. Since the SI remain unchanged as the anti-parallel β-sheet after curcumin depart at around 200 *ns* and segment II (SII) maintain as a loop after 210 *ns*, SI and SII are not displayed in the subsequent snapshot. At 200 *ns*, the anti-parallel β-sheet in segment IV (SIV) starts to deform, and at around 210 *ns*, the two residues, 24V and 27N, from each β-strand detach and join the linking loop of the β-sheets. The presence of curcumin near the SIII region, from 230 *ns* to 240 *ns*, cause the β hairpin structure at SIII to temporarily unfold before being restored at 250 *ns*. After which, the curcumin molecule approaches SIV. The curcumin destabilizes SIV and induces it to transform into an unstructured loop.

In fact, we have noticed similar patterns in the curcumin-Aβ interactions in other trajectories. In some of these trajectories, β-sheets are detected to quickly restore after curcumin leaves the interaction region. The overall β-sheet collapses, however, are not as obvious as those shown in Figure 5.8 on page 76. The binding propensity of both the diketone and keto-enol form of curcumin was illustrated in Figure 5.9. We observed that no specific residues strongly bind to curcumin although some residues have a higher chance of forming hydrogen bonds with curcumin. More specifically, the enol and the phenolic groups (the -OH on the aromatic rings) of curcumin can act as donor/acceptor. Furthermore, we observed that the -OH group of curcumin has more than twice the chance of forming a hydrogen bond than the methoxy group (diketone: -OH $\sim$ 62%, -O-CH3 $\sim$ 17%; keto-enol: -OH$\sim$ 50%, -O-CH3 $\sim$ 20%).[3]

5.3.2 π-stacking between curcumin and Aβ

The π-π nonbonded attractive interaction is prevalent among aromatic residues, DNA, RNA, polyphenol components and carbon nanotubes in biomedical applications.[298–303] This interaction is known to contribute to the stability of tertiary structures of macromolecules. It has served to control molecular recognition in some

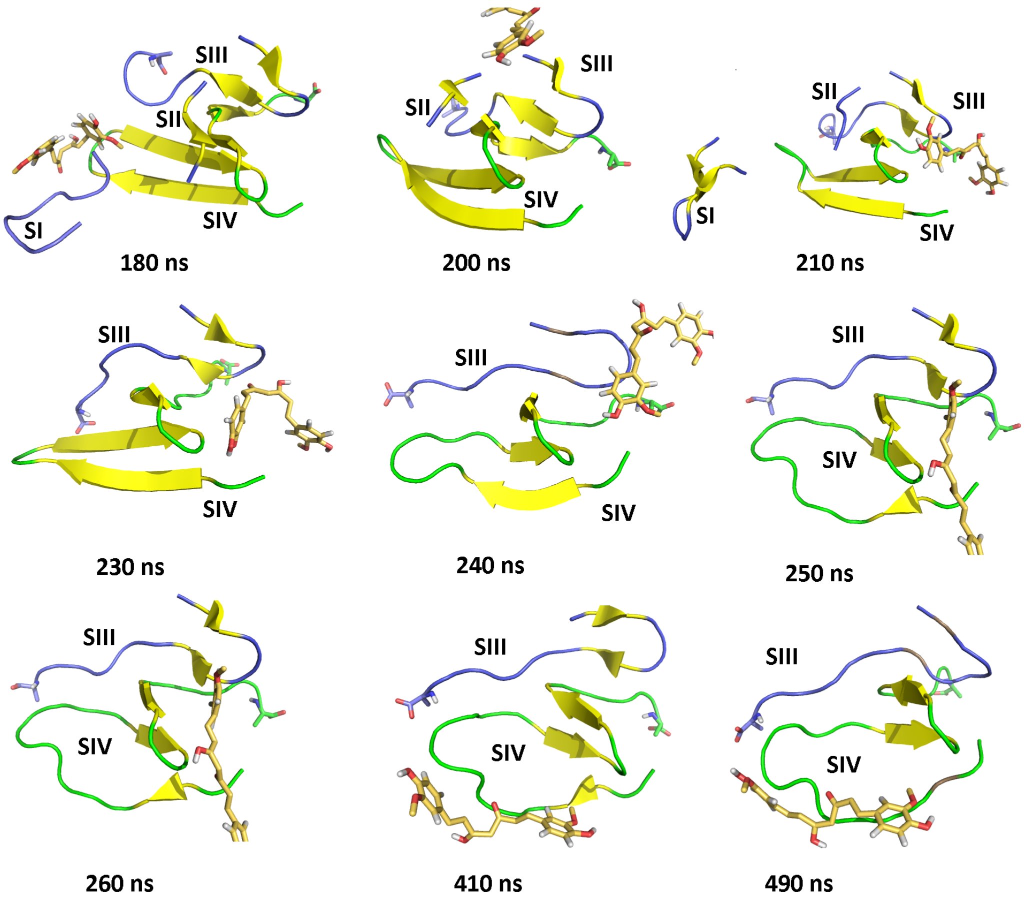

Figure 5.8: The snapshots of the curcumin works as the β-sheet breaker. Here we showed segments of the Aβ peptide, the blue loop indicates the residues are from peptide A. The green loop are the residues from peptide B. The C-terminus, namely residue Val-42 are shown as sticks, and colored blue for peptide A, green for peptide B to distinguish. Curcumin is shown as golden sticks and colored by element.

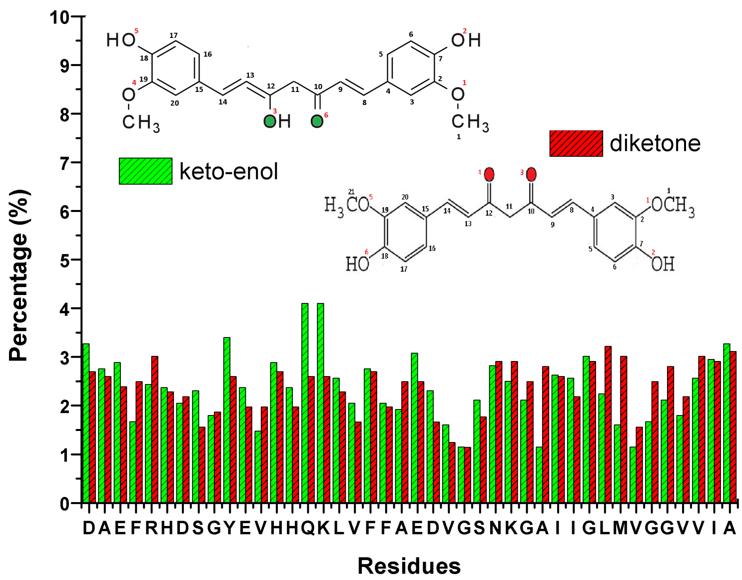

Figure 5.9: The binding propensity of curcumin towards the Aβ dimer.

aromatic substituted drugs and is responsible for the enhancement of adsorption affinity and efficiency.[303,304] In this section, we explore the π-stacking between curcumin and Aβ, whose interaction is determined by calculating the ring-ring distance between the residues TYR, PHE and HIS on Aβ, and the two rings on curcumin. The two rings of curcumin were labeled as R1 (keto-ring) and R2 (enol-ring). Here, we mainly focus on the interaction between pairs of aromatic ring and typically ignore clusters consisting of three or more aromatic rings. At the beginning of the simulation, π-stacking exists between R2 of curcumin and TYR-10 from peptide A (see position ① of Figure 5.10). This is followed by the transient tri-π stacking (see position ② and ③), which is formed among the curcumin R1 ring, and the PHE-4 and PHE-20 from peptide B. There is a very short period of time when π stacking occurs between PHE-4 from peptide A and R2 of curcumin (see position ④). Then from 200 *ns* onwards,

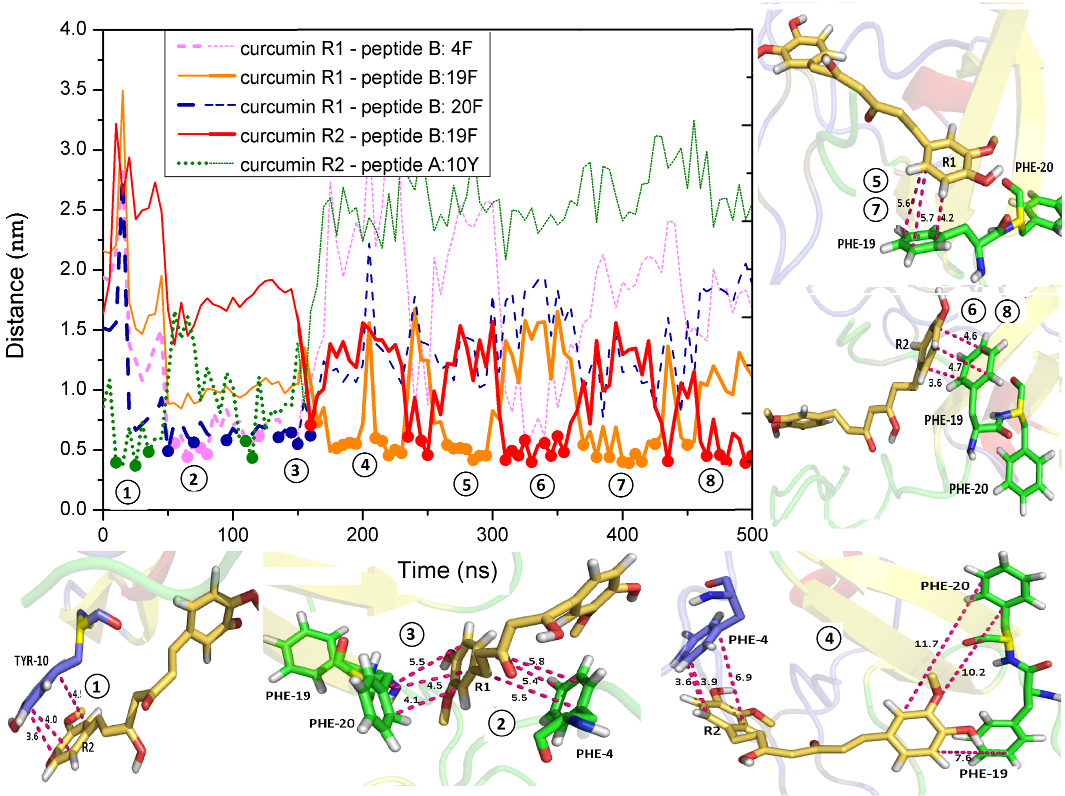

Figure 5.10: A plot of the center of mass distance between the ring of curcumin and the aromatic ring of Aβ residues. The minimum distance is indicated by heavy dots with numbers. Representative snapshots of π-stacking between the ring of curcumin and the aromatic residues of peptide A and B are given (The aromatic ring is colored blue for peptide A and green for peptide B). The red dash highlights the distance between the atoms (unit: $\mathring{A}$). While the residues on Aβ are represented as stick and colored by element (O: red; H: grey; N: blue), the C_α sits on the β-sheet are colored by yellow. The molecule curcumin is represented as stick (C: yellow; O: red; H: grey).

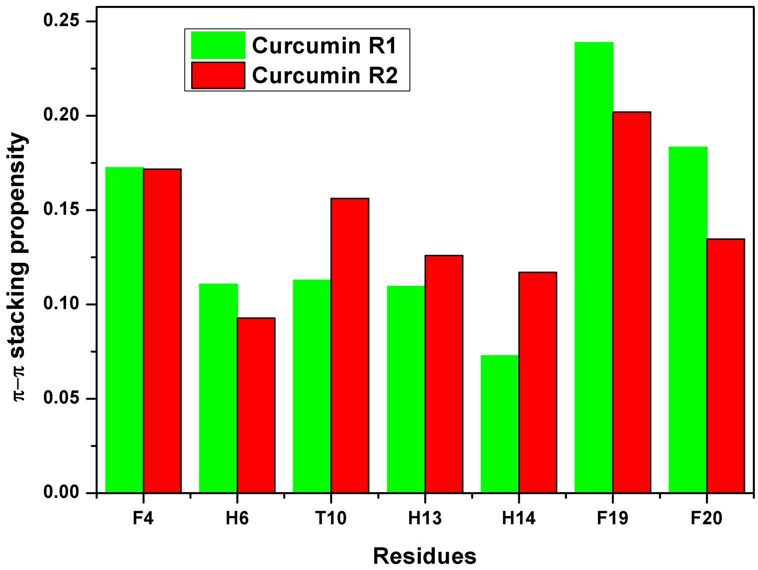

Figure 5.11: The π-π stacking propensity of Aβ residues His, Tyr and Phe with curcumin R1 and R2 respectively.

the R1 and R2 rings of curcumin are observed to interact alternately with PHE-19 of peptide B (see ⑤-⑧) through π-stacking. Indeed, all the computed trajectories with curcumin presence have shown that π-stacking occurs very frequently between the rings in curcumin and the aromatic rings in Aβ.

Although the π-π stacking interactions are transient, they contribute indirectly to a reduction in the β-sheet content in the Aβ dimer. In particular, we observe that the residue PHE demonstrates a higher propensity to be involved in such interaction with the rings of curcumin than the residue HIS (see Figure 5.11).

5.3.3 Dehydron

The concept of dehydron,[305] i.e., the under-wrapped amide-carbonyl hydrogen bonds of proteins, is helpful in the design of pharmaceuticals with improved binding affinities.[306,307] Here, we discuss on the identification of dehydrons of the Aβ dimer and also our investigation on the interactions of dehydron with curcumin. For each of the 10 models (i.e., M11 to M20), we extract the snapshots of dimer plus curcumin structure per 10 *ns* of each trajectory. This leads to a total of 510 structural snapshots. The program WRAPPA[297] is then used to locate the dehydrons without any consideration on the poorly-wrapped C-terminus (ALA-42). Note that we have used a default WRAPPA desolvation domain radius of 6.5 $\AA$ as the cut-off distance between the under-wrapped and the well-wrapped amide-carbonyl hydrogen bonds.[308]

Our analysis on all dehydrons has found that the dehydron with hydrogen bond forming between amide-carbonyl group of the pair 24V and 27N from peptide B appears in 292 of the 510 structures, while that between 24V and 27N from peptide A occurs in 222. A reason for the high frequency of the dehydron pair (24V, 27N) is because 27N is a polar residue. Hence, it prefers to locate on the surface of the protein. Another reason is that the two residues 24V and 27N tends to situate at the end of a strand of anti-parallel β-sheet on peptide B, while the pair from peptide A participates frequently in the short intermittent anti-parallel β-sheet that forms during simulations (see Figure 5.12(a)). Incidentally, 28-Lys and 24-Val are noticed to have a high propensity to act as wrapper residues (see Figure 5.12(b)).

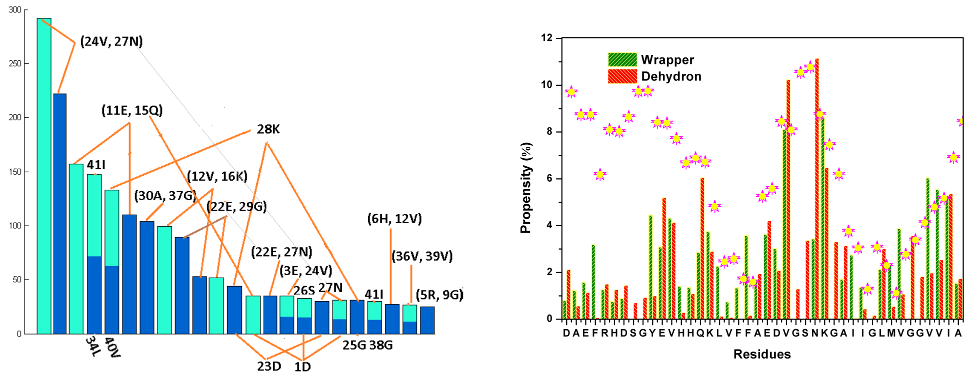

(a) (b)

Figure 5.12: (a) The occurrence of the dehydrons. The blue bar represent the dehydron pairs both from peptide A, the green bar indicates the dehydron pairs both from peptide B. Half blue and half green bar indicates the dehydron pairs one from A, another from B. (b) Wrapper and density propensity is indicated by the color bar, and the stay time of curcumin hanging around Aβ residues is indicated by he scattered maple dots.

The second most popular dehydron pair in rank belongs to residues 11E and 15Q, with 157 structures found in peptide A and 110 structures in peptide B. These residues are polar in nature, with residue 15Q tending to be part of a short α-helical structure (see Figure 5.14). The residue 34L from peptide A and 41I from peptide B with hydrogen bond between them is ranked the third most frequent dehydron pair. This dehydron pair is important due to its frequent interaction with curcumin which will be discussed in greater detail in the next section.

The characteristics of other dehydrons can be found in Table 5.2. In summary, the popular dehydrons are listed as follow: (24V, 27N), (11E, 15Q), (34L, 41I) and (28K, 40V), with residues Lys, Val, Ile and Tyr found to be the most likely neighbours of dehydrons. Scrutinizing the interaction behaviors of curcumin and Aβ, we observed that curcumin tends to stay around several dehydron pairs. More significantly, Figure 5.14 shows that curcumin spends a minimal amount of time around residues that are not dehydrons.

The occurence of dehydron	
pairs	occurence
B: (24V, 27N)	292
A: (24V, 27N)	222
B: (11E, 15Q)	157
B: (34L, 41I)	150
(A: 40V, B: 28K)	133
A:(30A, 37G)	124
A:(11E, 15Q)	110
B:(12V, 16K)	98
A:(22E, 29G)	89
A:(12V, 16K)	53
B:(22E, 29G)	52
A:(6H, 12V)	51
(A:38G, B:41I)	49
A:(23D, 27N)	45
A:(23D, 28K)	44
A:(5R, 9D)	42
(A:36V, B:39V)	37
B:(1D, 15Q)	35
A:(22E, 27N)	35
(A:3E, B:24V)	34
(A:41I, B:28K)	33
(A:1D, B:26S)	32
(A:1D, B:27N)	31
A:(7D, 10Y)	31
A:(28K, 35G)	31
...	< 30

Table 5.2: The occurence of dehydron.

5.3.4 Nomadism – the common routes of curcumin as it travels around Aβ

The interaction between curcumin and Aβ is very dynamic. In consequence, the position of curcumin is not fixed and the molecule travels around the Aβ. Hence, the word "nomadism" is borrowed to characterize such itinerant behavior of curcumin. By labeling the position of curcumin in each structure through the Aβ residue which is closest to it, the location propensity of curcumin on Aβ was calculated from all the trajectories and is illustrated in Figure 5.14. Our results show that curcumin tends to stay close to the residues 34-LEU, 22-GLU and the nearby HIS residues. Indeed, the hydrophobic nature of residues 34-Leu and 32-Ile has rendered them to be the main recognition and binding sites for the curcumin ligand.[309] The residue histidine is known to act as binding sites for protein. Here, it is also observed to be involved as a preferred binding site for curcumin.

Curcumin is observed to be rather mobile around the Aβ dimer. We attempt to find patterns in the paths of curcumin as it traverses about the Aβ. The observed patterns turn out to be the common routes of curcumin. A route is made up of steps, and a step is defined as the movement of curcumin from a position close to one residue of Aβ to a position close to another residue. The common routes must compose of at least 4 steps and are to be shared by two routes from two different trajectories. By making a pairwise analysis on all 10 trajectories, we arrive at the common routes which are shown in Figure 5.13. The most popular routes for the keto-enol form curcumin are: $34L_B \rightarrow 34L_A \rightarrow 32I_A \rightarrow 34L_A (14.5\%)$, $34L_B \rightarrow 34L_A \rightarrow 34L_B \rightarrow 34L_A (9.6\%)$, $34L_B \rightarrow 35M_B \rightarrow 34L_B \rightarrow 35M_B \rightarrow 34L_B (6\%)$, and $32I_A \rightarrow 34L_A \rightarrow 35M_A \rightarrow 34L_A (4.8\%)$. By examining this set of common pathways of curcumin, we see that residue 34L functions as a hub. Recall that 34L is also a popular dehydron (see Figure 5.12(a)) and recognition site on the Aβ. For the β-diketon form, it's also include the following most popular pathway: $34L_B \rightarrow 34L_A \rightarrow 32I_A \rightarrow 34L_A$, $34L_B \rightarrow 34L_A \rightarrow 34L_B \rightarrow 34L_A$ (see Figure 5.13).

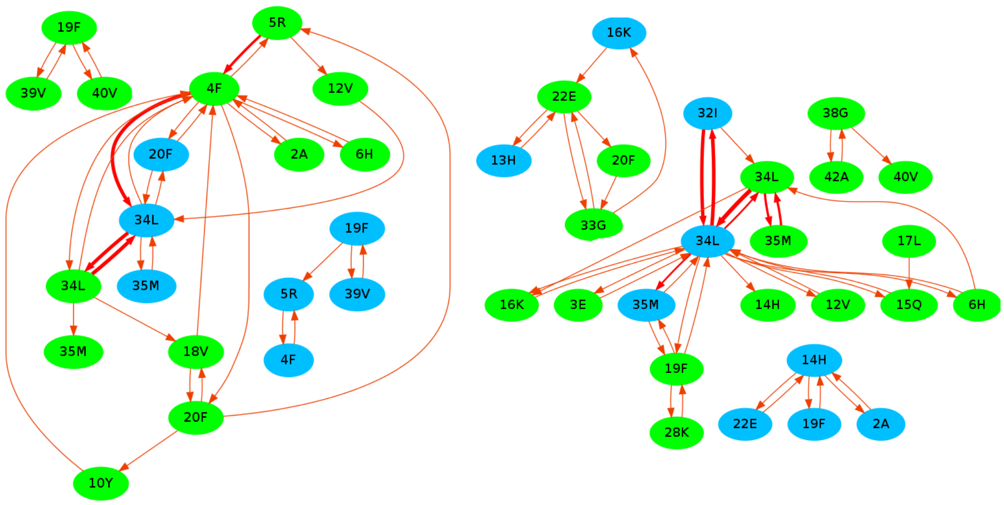

(a) (b)

Figure 5.13: The common pathway of curcumin (a) diketone and (b) keto-enol form. The blue-filled circles represent the residues from peptide A, the green-filled circles represent the residues from peptide B. The thickness of arrow represents the popularity of this pathway. This figure was generated by Graphviz.

The secondary structure propensity (SSP) for each Aβ residue was also analyzed (see Figure 5.14). We see that Val and Ile have a high propensity of forming β-sheet. By comparing the SSP at the last 10 *ns* to the first 10 *ns*, we observe that the presence of curcumin perturbs the conformation of the Aβ secondary structure, resulting in a decrease of β-sheet secondary structure in the last 10 *ns*.

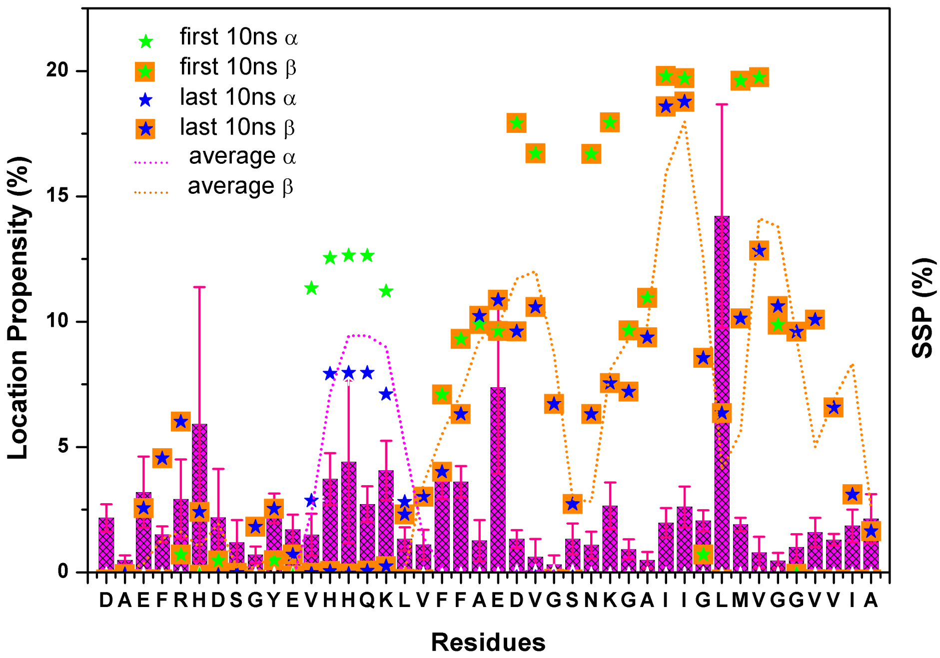

Figure 5.14: Curcumin location propensity on Aβ dimer and Aβ secondary structure propensity. The purple bars were calculated by average all trajectories the curcumin most nearby residues. The helical structures (α-helix, 3-helix and 5-helix) and β-structure (β-sheet and β-bridges) are calculated for all 10 models during each 500 *ns* simulations every 4 *ns*, and the structure propensity of the first 10 *ns* and last 10 *ns* were also plotted. The purple dots line indicated the residues average α propensity during whole simulation, orange dots line indicates the β-propensity. The green stars are the secondary structure propensity in the first 10 *ns*, and blue stars are the secondary structure propensity in the last 10 *ns*. The star were given orange background color to distinguish the β-propensity from α-propensity.

5.4 Summary and discussions

The effect of curcumin on the stability of the Aβ dimer was examined by means of all-atom explicit solvent simulations. We found that curcumin plays the role of an efficient β-sheet breaker by reducing the number of residues adopting the β-sheet secondary structure. There are two possible reasons for its effectiveness. One reason could be due to the hydrophobicity of curcumin. Although curcumin has not been observed to penetrate and break the hydrophobic core of the Aβ dimer apart, the presence of curcumin near the Aβ proteins has perturbed and deformed the β-sheet secondary structure (see Figure 5.8). The other possible reason relates to the π-π stacking interactions. This interaction is speculated to be critical for early molecular recognition and may serve to guide the formation of directionality in the self-assembly process.[298] Note that the polyphenol inhibitors are assumed to be directed to the amyloidogenetic core through specific aromatic interactions.[299] In this study, we have found that the π-stackings between the curcumin keto-ring or enol-ring with the Aβ aromatic rings exist throughout the whole simulation. Thus, we can perceive that the π-stacking interaction, as well as the hydrophobic effects, may play a non-negligible role in the inhibiting effects of curcumin on the Aβ peptides.

In addition, we have used the unwrapped amide-carbonyl hydrogen bonds to predict the potential ligand binding sites. Here, we have found that the amide-carbonyl hydrogen bonds of VAL-24 and ASN-27, GLU-11 and GLN-15, LEU-34 and ILE-41, are very stable dehydrons. As curcumin approaches the Aβ dimer, the dehydrons of the dimer and the hydrophobic centers of curcumin form a complex due to the hydrophobic effect[310] based on a mechanism similar to the nanoscale dewetting transition.[311,312] While the polar groups of curcumin can form hydrogen bonds with the the dimer, the π-π stacking interaction between the curcumin and the dimer partially immobilizes the aromatic arms of the curcumin, and hence strengthen the hydrogen bond network between the two species. The contacts between curcumin and the Aβ proteins are dynamic and the favourite curcumin location sites on Aβ are revealed. The common routes of curcumin as it travels around the Aβ dimer are analyzed. The curcumin molecules are observed to visit the residue LEU-34 regularly and this residue can be treated as a hub within the common routes of curcumin. In conclusion, our study provides a detailed picture on the interaction of curcumin with the dimeric form of the Aβ oligomers.

Chapter 6 Heme prevents Amyloid beta peptides aggregation through hydrophobic interaction based on MD study

Heme, which is abundant in the hemoglobin and many other hemoproteins is known to play an important role in electron transfer, oxygen transport, regulation of gene expression, and many other biological functions. With the belief that the aggregation of Aβ peptides forming higher order oligomers to be one of the central pathological pathways in Alzheimer's disease, the formation of Aβ-heme complex is essential as it inhibits Aβ aggregation and protects the neurons from degradation. In our studies, conventional molecular dynamics simulations were performed on the 1 A$\beta + 1$ heme and 2 A$\beta + 4$ hemes system respectively with the identification of several dominant binding motifs. We found that hydrophobic residues of the Aβ peptide have a high affinity to interact with heme instead of the residue histidine. We conclude that hydrophobic interaction plays a dominant role in the Aβ-heme complex formation which indirectly serves to physically prevent Aβ aggregation.

6.1 Introduction

It is observed that excessive amount of iron and other metals like copper and zinc tends to concentrate inside or around the senile plaques and the NFT. The presence of ionic zinc, iron and copper is known to facilitate the process of Aβ aggregation.[313–316] Meanwhile, the brain is a very aerobically active organ consuming one fifth of the body's oxygen.[317] The activation of molecular oxygen together with the reduction of redox active iron, zinc and copper ion may generate detrimental reactive oxygen species (ROS).[318] Hence, the elevated iron deposition found during the earliest stages of AD may generate the most potent ROS hydroxyl radicals and together with the iron-Aβ complex, may cause significant oxidative stress.[319] Studies have also shown that Aβ bound iron mediates Aβ toxicity, which can be alleviated by iron chelator.[317,320–322]

Heme is a macromolecule consisting of an iron atom in the center of four substituted pyrrole rings interconnected through methine bridges. It is recognized as a member of the prosthetic group which assists the cytochromes family in electron transfer and oxygen transport in globins.[19,20] Its main biological functions are carried out through redox reactions of the ferrous (Fe^{2+}) state of the heme iron. Heme also plays a significant regulatory role as an intracellular signal transduction messenger in gene expression[323] and ion channels function via coordination sphere of the iron to a histidine or cystine.[20]

It has been proposed that heme tends to bind to one or more intracellular Aβ histidine residues. This decreases the bioavailability of heme, and leads to a deficiency of the functional heme[16,21] which results in oxidative stress,[137] electron transport chain defects[324] and mitochondrial complex IV activity decline.[137] On the other hand, the heme-Aβ_{1-40} complex formed by exogenous heme can inhibit Aβ_{1-40} aggregation, and possibly catalyze H_2O_2 decomposition via its peroxidase activity which has the further effect of alleviating Aβ induced toxicity.[22] Aβ-heme complex can also catalyze the oxidation of serotonin[16] and promote protein nitrotyrosination.[27] It shows a stronger peroxidase activity than heme.[16,27] It has been suggested that both the Aβ-heme peroxidase activity and the binding affinity of heme towards Aβ does not depend on the Aβ aggregation stages.[27]

There are several identified and putative heme-binding motif. One is the CxxCH motif in cytochrome c, in which the two cysteine residues form two covalent bonds with the two viny groups ($-CH = CH_2$), while histidine serves as the fifth/proximal axial ligands.[23–25] Another is HxxxY from the heme chaperone protein CcmE. The flexible C-terminus of CcmE facilitates the formation of a transient covalent complex between histidine and heme.[25]

It has been proposed that the hydrophilic N-terminal of Aβ is the binding domain of heme, which involves Arg, Tyr and the three histidine residues (His-6, His-13 and His-14).[16,26] In fact, these residues are found to be in the heme-binding pockets. In particular, His-13 and His-14 are believed to be more significant in heme binding and peroxidase activity than His-6.[27] However, the detailed Aβ-heme complex conformation has yet to be determined.

In this chapter, we investigate into the possible Aβ-heme binding motifs through conventional molecular dynamics (MD) simulation for the 1 A$\beta+$ 1 heme system and the 2 A$\beta+$ 4 hemes system respectively. In addition, the detailed atomic-level interaction between Aβ and hemes, and the role of heme in the Aβ oligomerization process are examined for the 2 A$\beta+$ 4 hemes system. We found that the presence of heme physically serves the possible function of an inhibitor to Aβ self-assembly.

6.2 Materials and methods

The initial structure of Aβ_{42} was taken from model 1 of the Protein Data Bank (PDB) ID: 1IYT.[?] The sequence of Aβ_{1-42} is $DAEFRHDSGY_{10}$ $EVHHQKLVFF_{20}$ $AEDVGSNKGA_{30}$ $IIGLMVGGVVIA_{42}$. The pKa values of the titratable residues was calculated by the H++ server (see Appendices A).[290,291] The default internal and external dielectric constants used in the pKa value calculation are 6 and 80 respectively. The ionic strength was set to 0.1 *M* while the pH was set to 7. The structure of the small heme molecule was obtained from the ZINC database[292] and is displayed in Figure 6.1. Note that all structures as well as their parameters used in our investigation such as the charge of the central Fe atom in Heme were represented by the CHARMM27 all-atom force field (with CMAP) - version 2.0.[325]

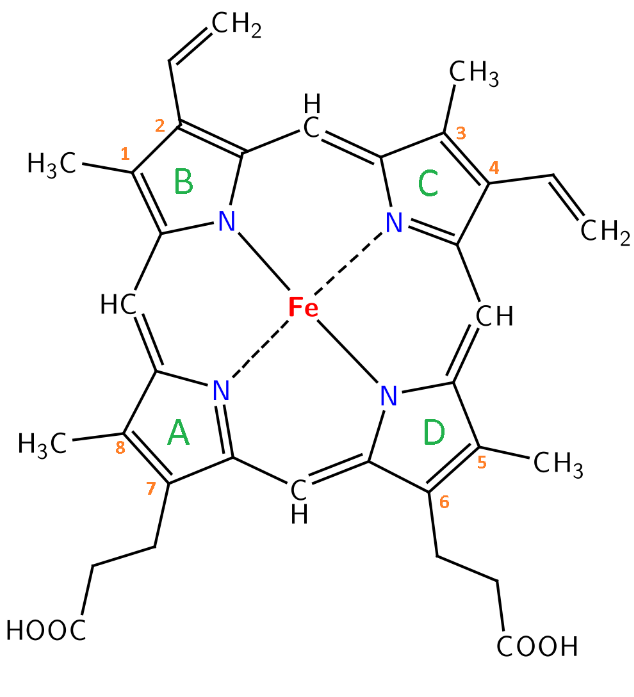

Figure 6.1: The chemical structure of heme.

The LINCS algorithm[161] was used to constrain all bonds with an integration time step of $2\,fs$. The temperature was kept at $300\,K$ using the Nosé-Hoover coupling scheme[162,163] for conventional MD. An isotropic pressure coupling at 1 *bar* by means of a Parrinello-Rahman barostate with a coupling constant of $2\,ps$ was used in the pressure ensemble. A fourth-order interpolation was used in Particle Mesh Ewald method[270] for electrostatic interaction with Fourier grid spacing of $0.16\,nm$. The van der Waals cutoff was set to $1.0\,nm$.

All simulations and analysis were performed using facilities within the GROMACS package version 4.5.3.[326–328] PyMOL[271] and VMD[272] were used to visualize the molecular structures. Additional analysis and visualization were assisted by MATLAB, originPro, GNU image manipulation program (GIMP) and some of our in-house scripts.

Our first set of simulations was performed on a single Aβ peptide in a cubic box of dimensions $52.60\,Å \times 52.60\,Å \times 52.60\,Å$ for $200\,ns$. The box was filled with 5582 water molecules, 13 Na^+ ions and 11 Cl^- ions to neutralize the system and to maintain the ionic strength of $120\,mM$ in the system. The final Aβ peptide structure was taken as the initial structure for the subsequent simulations.

In our second set of simulations, the final conformation of Aβ from the first set of simulation was taken as the initial structure. $5\,ns$ of replica exchange simulation was then performed on 32 different copies of this conformation to get the most random initial structure for the following simulations. Each copy of these Aβ was placed in the center of a box with dimensions $39.42\,Å \times 48.78\,Å \times 55.94\,Å$ with the heme being randomly arranged in the neighborhood of the Aβ. The temperatures of the 32 replicas are as follows: $315.00\,K$, $317.98\,K$, $321.98\,K$, $325.01\,K$, $328.06\,K$, $331.14\,K$, $334.24\,K$, $337.36\,K$, $340.50\,K$, $343.67\,K$, $346.86\,K$, $350.08\,K$, $353.32\,K$, $356.58\,K$, $359.87\,K$, $363.19\,K$, $366.52\,K$, $369.89\,K$, $373.28\,K$, $376.69\,K$, $380.13\,K$, 383.60 K, 387.09 K, 390.61 K, 394.16 K, 397.73 K, 401.33 K, 404.96 K, 408.61 K, 412.29 K, 416.00 K, 419.74 K. Note that 3,276 water molecules, 9 Na^+ ions and 6 CL^- ions were added to neutralize the system. The final conformations of 20 replicas of single Aβ from high temperature were taken as initial structures. Then conventional constant temperature MD simulations at 300 K were performed starting from the 20 configurations. 500 ns trajectory was collected for each system.

In our third set of simulations, two Aβ peptides were taken from our first set of simulation and arranged in a parallel fashion in a cubic box of dimensions 77.84 $\AA \times$ 77.84 $\AA \times$ 77.84 $\AA$. The two Aβ chains were separated 2 nm apart from each other. 4 heme molecules were randomly arranged within the box. 16 initial configurations with different distributions of heme molecules were generated. Each system contains 15,114 water molecules, 40 Na^+ ions and 28 CL^- ions resulting in an ionic concentration of 0.1 M. 100 ns simulation was performed on each system. For the system that serves as a control, with two Aβ chains and without heme molecules, 15,253 water molecules, 32 Na^+ ions and 28 CL^- ions were added to the box to attain the same ionic concentration. MD simulations of the control system were performed 5 times with different initial velocities, with each run lasting 100 ns.

6.3 Results

6.3.1 Aβ-heme complex

In order to uncover the heme-binding Aβ motifs, cluster analysis was performed on each of the last 100 ns of the 20 trajectories (labeled as traj1 to traj20) from the second set of simulation. A C_α-rmsd cutoff of 3 $\AA$ was used to count the number of

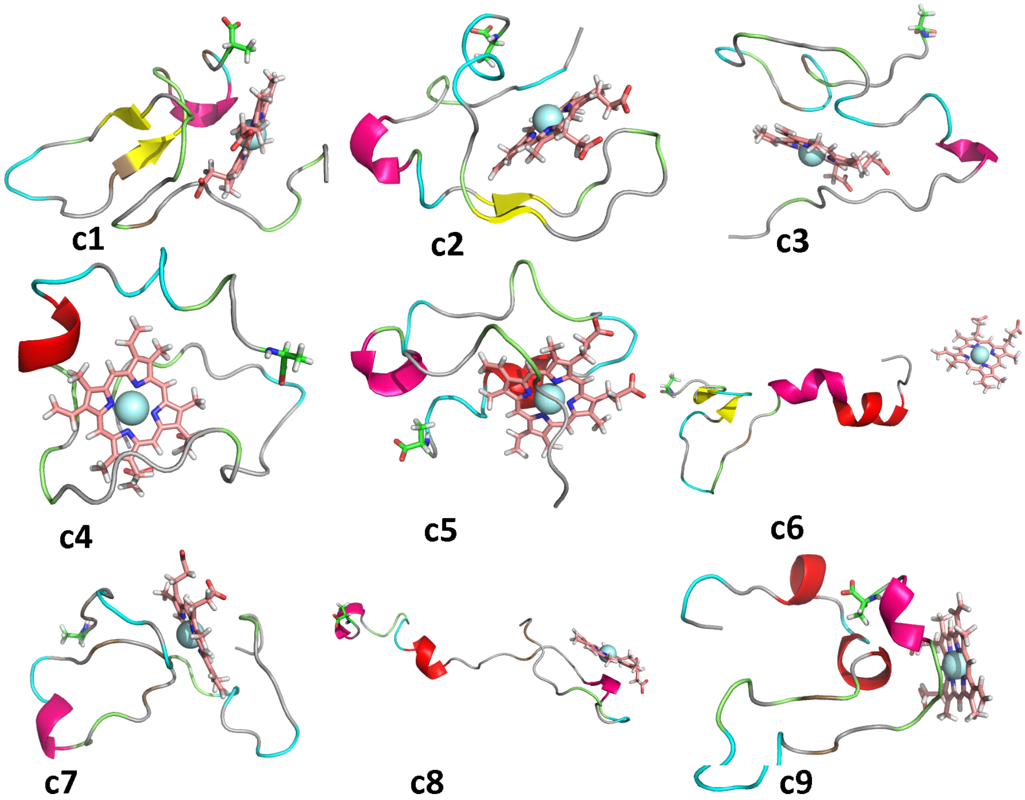

Figure 6.2: Cluster analysis of Aβ-heme complex. The central portion of the first nine most dominant clusters of the 20 trajectories in the last 100 ns are shown in cartoon for protein, sticks for heme and sphere for Fe ion. Note that the C-terminal of the Aβ peptide are indicated as sticks. Note that each structure is the average of all the population of Aβ-heme complex within the cluster.

neighbors. Then, within this cutoff, Aβ-heme structures with similar configurations are identified as one cluster and their frequency of occurrence counted.[329] More precisely, a total of 10,001 conformations were generated from each trajectory, from which 2,814 clusters were identified from the 20 trajectories. The central portion of the 9 most dominant clusters are shown in Figure 6.2. The next 9 most populated clusters are given in Figure 6.3. The population percentage of the 9 most dominant clusters and the residues that surround the Fe ion are given in Table 6.1.

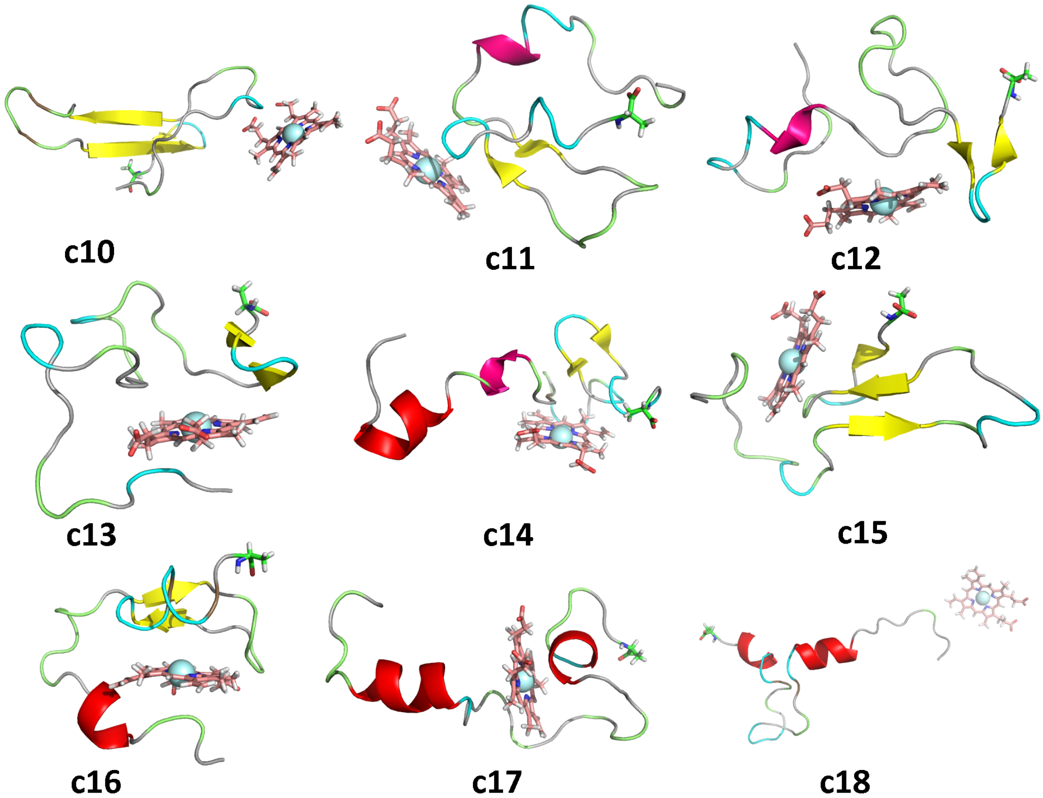

Figure 6.3: Cluster analysis of Aβ-heme complex. The central portion of the 10 $\sim$ 18 most dominant clusters of the 20 trajectories in the last 100 *ns* are shown in cartoon for protein, sticks for heme and sphere for Fe ion. The C-terminal of Aβ are distinguished by sticks. Note that each structure is the average of all the population of Aβ-heme complex within the cluster.

Clusters	Population (%)	Trajectory	Surrounding Residues*
c1	62.27	traj4	Phe-4 Leu-17 Ile-32 Ile-41
c2	58.02	traj9	Phe-4 Phe-20 Val-24 Ile-31 Leu-34 Met-35
c3	54.79	traj15	Phe-4 Arg-5 His-6 Phe-19 Phe-20
c4	54.37	traj14	Arg-5 Leu-17 Phe-19 Val-24
c5	51.85	traj16	Phe-4 Arg-5 Ile-31 Leu-34 Met-35
c6	45.91	traj13	
c7	39.25	traj3	Phe-4 His-6 Ile-32 Gly-33 Met-35
c8	38.57	traj2	Gln-15 Lys-16 Val-18
c9	36.60	traj17	Met-35

Table 6.1: The population of the first 9 most dominant clusters in the last 100 *ns*. $*$ indicates the residues within 5 $\mathring{A}$ of Fe ion.

Aβ-Fe ion		0 ∼ 500 *ns*		last 100*ns*	
Residues	Vicinity affinity (%)	Residues	Vicinity affinity (%)	Residues	Vicinity affinity (%)
PHE	22.86	PHE	19.99	PHE	21.56
VAL	13.93	VAL	16.11	VAL	14.00
ILE	11.77	ILE	10.69	MET	11.74
LEU	10.60	MET	10.66	ILE	11.23
MET	10.22	ARG	8.26	ARG	10.01
ARG	8.68	LEU	7.78	LEU	9.97
HIS	6.11	HIS	6.35	HIS	6.15
GLY	5.52	ALA	5.58	ALA	4.28
ALA	4.71	GLY	4.61	LYS	3.28
GLN	3.05	GLU	2.89	GLY	3.19
LYS	2.39	LYS	1.83	GLN	3.03
GLU	1.74	GLN	1.74	GLU	1.03
ASP	0.23	SER	1.58	ASP	0.30
SER	0.17	TYR	1.01	SER	0.25
ASN	0.06	ASP	0.81	ASN	0.00

Table 6.2: Aβ residues vicinity affinity.

In order to identify the residues that surround heme, wrappers were introduced to define the residues within 0.5 *nm* from the center of mass (COM) of the heme or the Fe ion. From Figure 6.4, we observe that there are three possible sets of wrappers. The first set consists of residues Ala-2−His-6, the second set is made up of Gln-15−Phe-20, while the third set is Ala-30−Val-36. By ranking the residues according to their propensity to locate near to heme, we detect the following order: Phe having the highest affinity, followed by Val, Ile, Leu, Met, Arg, His, ... (see Table 6.2). Remarkably, we observe that the set of residues that have the greatest tendency to lie in the neighborhood of heme are mainly hydrophobic residues. This has led us to surmise that the hydrophobic interaction plays a dominant role in the Aβ-heme complex formation.

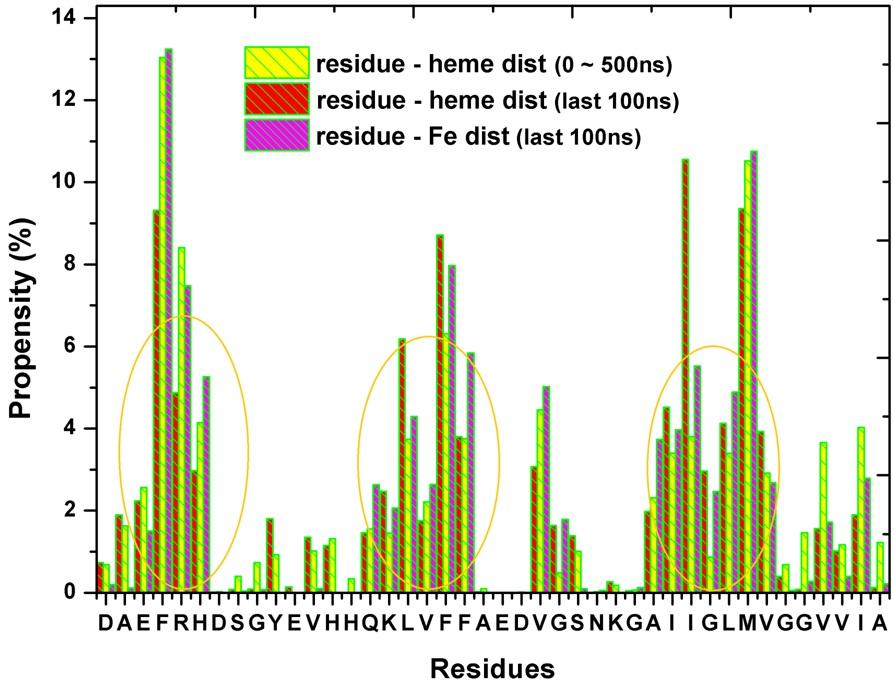

Figure 6.4: The occurrence of the residues appeared within heme/Fe 0.5 *nm* distance of the 1st 9 most dominant clusters were plotted. The red and yellow bars are calculated based on the whole simulation time and the last 100 *ns*, respectively. The purple bar indicates the distance between occurrence of the residues appeared within 0.5 *nm* distance away from Fe in the last 100 *ns*.

6.3.2 Potential of mean forces

In order to provide a more comprehensive view on how the set of high propensity residues situate near to (or interact with) the heme molecule, we plot the potential of mean forces (PMF) between these residues and heme. This is performed through the extensive Aβ-heme configurations that we have obtained from our simulations.[330]

Figure 6.5 shows the PMFs for the residues His, Phe, Leu, Ile, Val, Arg and Met of Aβ with respect to the Fe ion. The PMF shows that the His-6 has a basin of attraction located around the His-6 - Fe minimum distance of 5 $\mathring{A}$, which is absent in the case

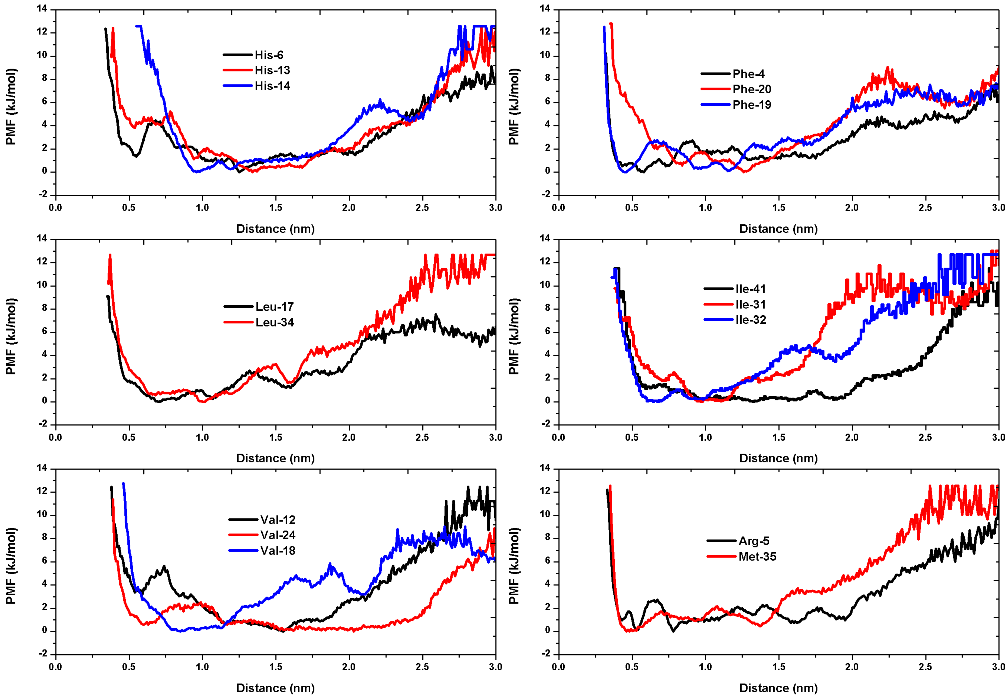

Figure 6.5: Potential of mean force (in kJ/mol).

of the His-13 and His-14 residues. For the three histidines, the global minimum is located within the range of $10-17\,\AA$. On the other hand, the global minimum of Phe-4 is located around $5.8\,\AA$; Phe-19 is located around $4.5\,\AA$; and Phe-20 is around $12.6\,\AA$. We observe that Leu-17 and Leu-34 share a similar basin in the range of $7-10\,\AA$. For Ile-32, the global minimum is located around $6.7\,\AA$. As for Ile-31, it is located around $9.7\,\AA$. But for the residue Ile-41, we observe a wide basin of attraction. In the case of Val-24, the first minimum appears around $6\,\AA$, with another basin appearing in the range $11\,\AA$ to $23\,\AA$. Note that the first potential barrier of Val-24 corresponds to the basin of Val-18. Arg-5 is observed to have a jagged PMF curve while Met-35 has several minima with its global minimum located around $4.6\,\AA$. In conclusion, we observe that hydrophobic residues such as Phe, Val, Leu, IIe of Aβ tend to situate close to heme through the PMF curves. In particular, Phe-19, Met-35 and His-6 are found to have a high possibility of interacting with the heme group at close distance.

6.3.3 Hydrogen bond forming information between Aβ and heme

We have also obtained information on the hydrogen bond formation between heme and Aβ through the 20 trajectories. We observe that the four N atoms of heme have equal probability of being the hydrogen bond acceptor, while the O atoms of heme -COOH groups have a much higher chance (more than 3 times) as the hydrogen bond acceptor (See Table 6.3). In addition, Aβ residues hydrogen bond forming propensity can be seen from Table 6.4.

Atoms	hydrogen bond forming propensity (%)
NC	5.80
ND	6.36
O1A	19.01
O2A	19.09
O1D	19.09
O2D	19.09

Table 6.3: The heme hydrogen bond forming propensity.

A ranking of Aβ residues in terms of hydrogen bonding affinity from highest to lowest is as follows: Arg-5, Asp-1, His-14, His-6, Lys-16 (see Figure 6.6). Interestingly, the highly ranked residues are observed to be neighbours to the identified residues which locate in close vicinity to heme. For example, Arg-5 is situated next to Phe-4 and we know that Phe-4 has a stronger propensity to form Aβ-heme complex than Arg-5. Thus, our results show that hydrophobic interaction is the main force that drives the formation of the Aβ-heme complex, while the hydrogen bond interaction serves as an auxiliary force to stabilize the complex. Finally, we notice through our simulation that the Aβ N-terminus has a slight preference to form hydrogen bonds with heme than the C-terminus.

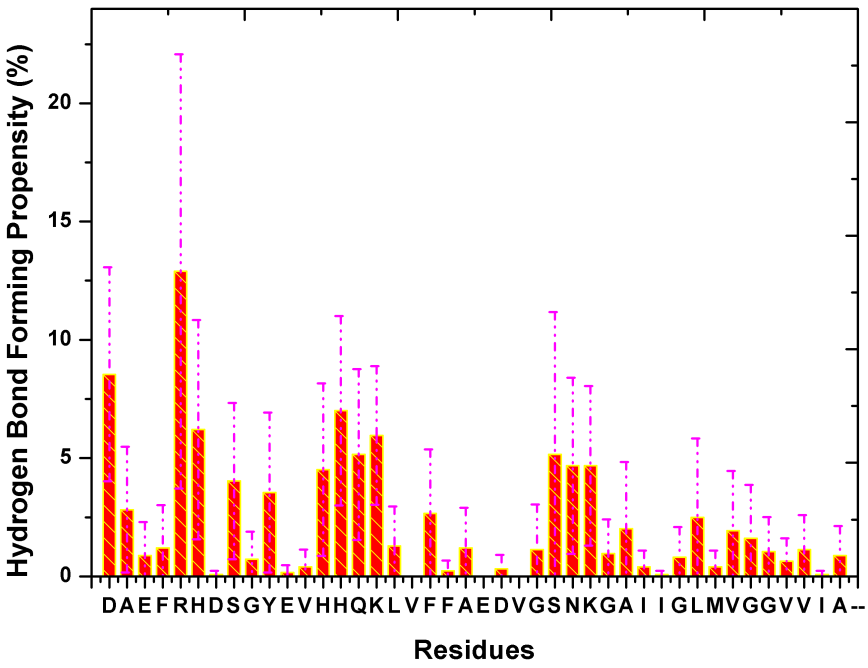

Figure 6.6: The binding propensity of heme towards Aβ residues.

6.3.4 Aβ secondary structure propensity in the presence/absence of heme

The secondary structure propensity of each residue was examined from the 20 "heme-present" trajectories and the 2 "heme-absent" trajectories (see Figure 6.7 and 6.8). Four types of secondary structures: β-structure (β-bridge and β-sheet); helix (α-helix and 3-helix); bend & turn; and coil, are used to categorize the secondary structure propensity. From Figure 6.7, we can see that the residues His-6, Asp-7, Tyr-10, Glu-11, Val-12, Ala-21, Glu-22 and Asp-23 have a high probability of being involved in the β-structure conformations. On the other hand, the residues Ser-26, Asn-27, Lys-28, Gly-29 and Ala-30 show a strong preference in participating in the helical

Residues	hydrogen bond forming propensity (%)
ARG-5	12.89
ASP-1	8.54
HIS-14	7.01
HIS-6	6.20
LYS-16	5.96
SER-26	5.16
GLN-15	5.16
LYS-28	4.67
ASN-27	4.67
HIS-13	4.51
SER-8	4.03
TYR-10	3.55
ALA-2	2.82
PHE-19	2.66
LEU-34	2.50
ALA-30	2.01
VAL-36	1.93
GLY-37	1.61
LEU-17	1.29
PHE-4	1.21
ALA-21	1.21
VAL-40	1.13
GLY-25	1.13
GLY-38	1.05
GLY-29	0.97
ALA-42	0.89
GLU-3	0.89
GLY-33	0.81
GLY-9	0.73
VAL-39	0.64
MET-35	0.40
ILE-31	0.40
VAL-12	0.40
ASP-23	0.32
PHE-20	0.24
GLU-11	0.16
ASP-7	0.08
ILE-41	0.08
ILE-32	0.08
VAL-24	0.00
GLU-22	0.00
VAL-18	0.00

Table 6.4: The Aβ residues hydrogen bond forming propensity.

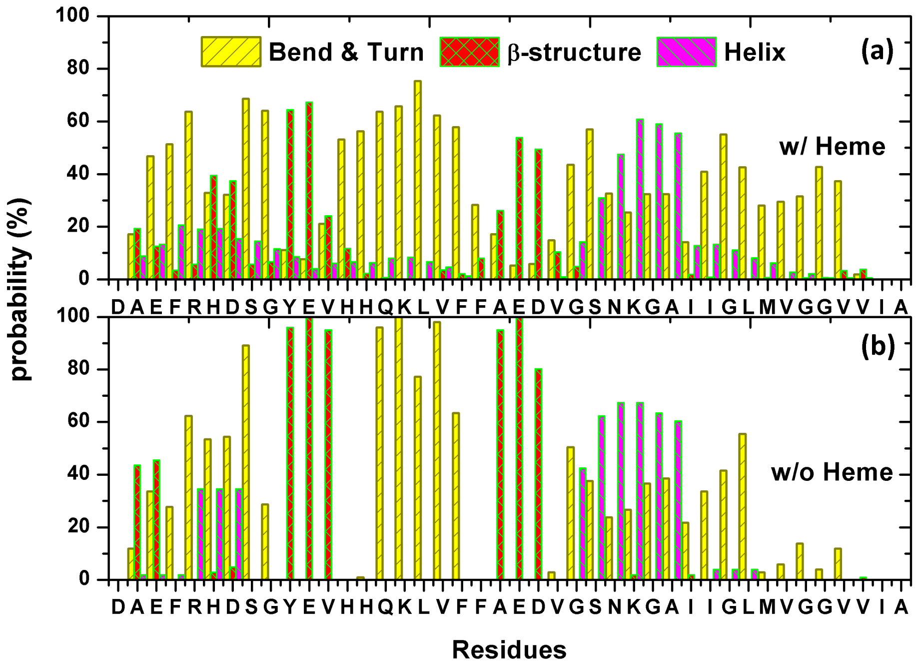

Figure 6.7: Aβ secondary structure propensity with heme (a) and without heme (b) was examined by averaging over all trajectories every 5 *fs*. The statistical error is found to be less than 0.18.

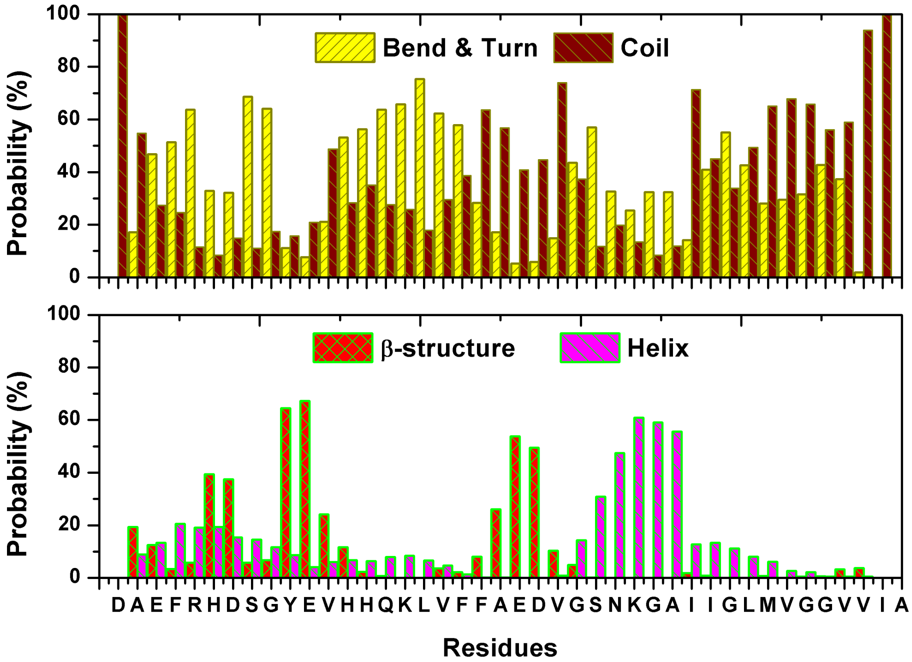

Figure 6.8: Aβ secondary structure propensity in the presence of heme was examined by averaging over 20 trajectories every 5 *fs*. The average statistical error is found to be 0.18.

conformations. By examining the number of residues that adopt the β-structure and the helical structures in our simulation, we see that the presence of heme has the effect of reducing the β-content and increasing the helical-content by 22.1% and 33.6% respectively (See Figure 6.9).

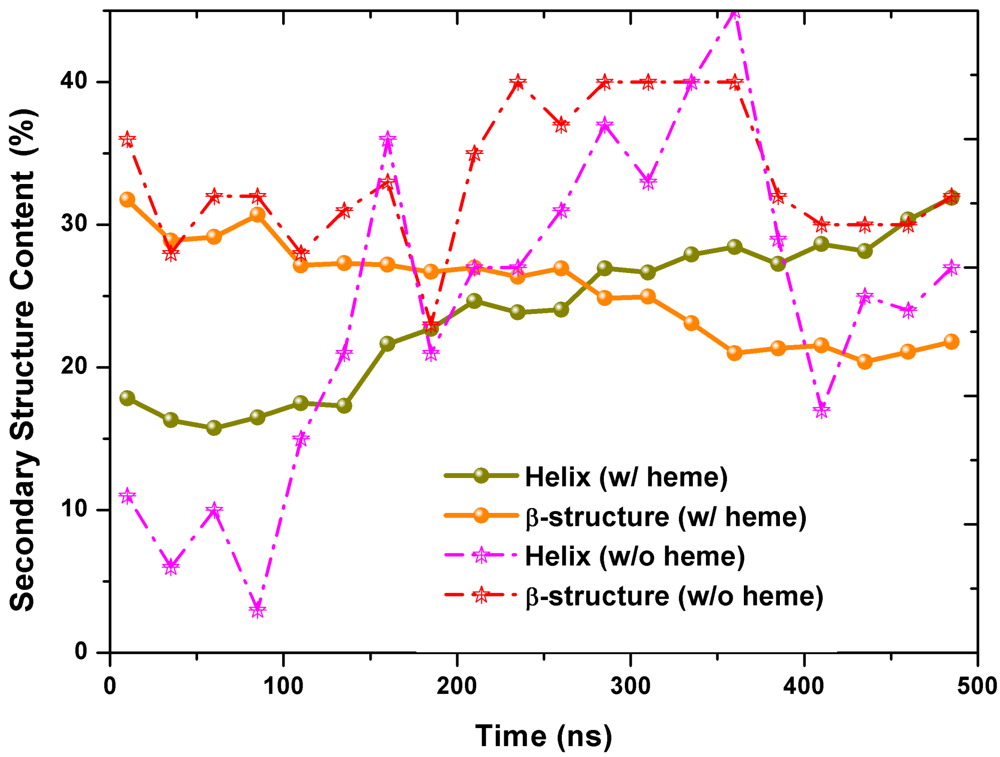

Figure 6.9: The number of residues adopting β-structure and helical content in the presence/absence of heme were examined by averaging over 20 trajectories every 50 *ns*. The statistical error is found to be less than 2.

6.3.5 Aβs-hemes complex

In order to examine the possible heme-binding Aβ motifs during the process of Aβ oligomerization for the 2 Aβ+ 4 hemes system, clustering analysis was carried out on the 16 trajectories with a C_α-rmsd cutoff of 3 $\mathring{A}$. The central portion of the first

9 dominant clusters are shown in Figure 6.10 as well as the population of these 9 dominant clusters. The Aβ residues that surround the Fe ion from heme is given in Table 6.5.

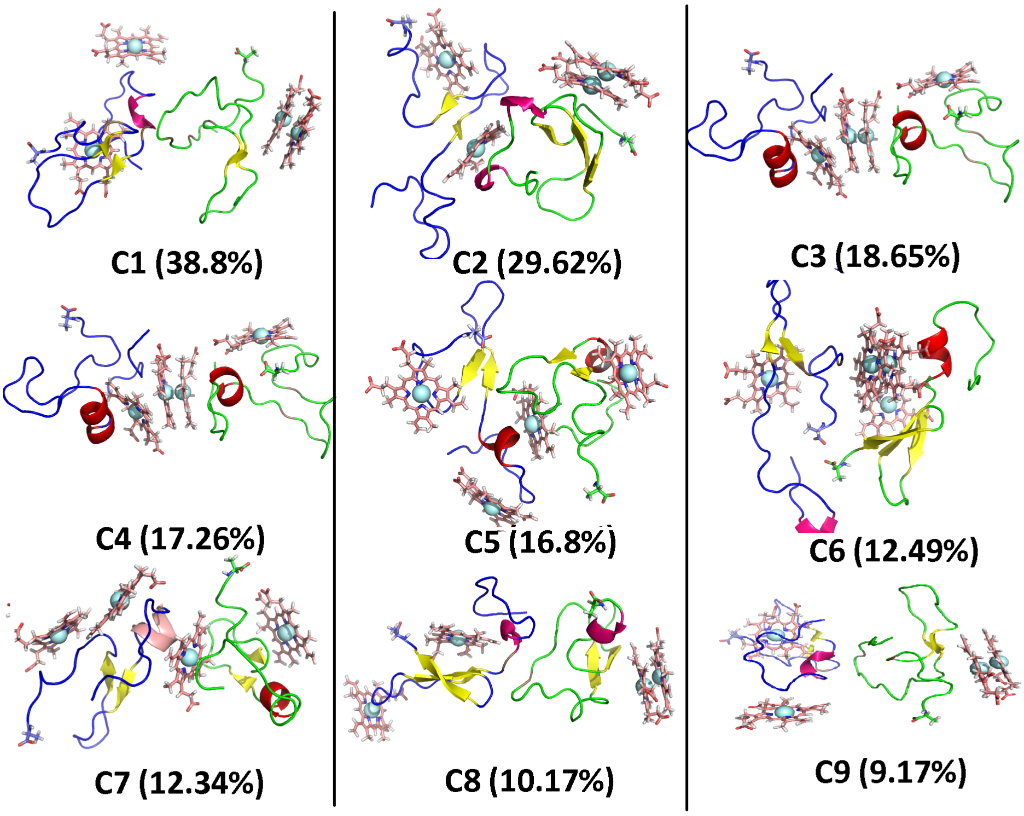

Figure 6.10: Cluster analysis of Aβ-hemes complex at 315 K. The central portion of the first six most dominant clusters are shown in cartoon for protein (Blue: Peptide A; Green: Peptide B), sticks for heme and sphere for the Fe ion. The C-terminal of Aβ are distinguished by sticks. Note that each structure is the average of all the population of Aβ-heme complex within the cluster.

Our results show that the residues, which are 0.5 *nm* away from the COM of heme as shown in Figure 6.11, display the following affinity to reside in the neighbourhood of heme from highest to lowest: Phe, Tyr, Arg, His, Ser, Leu, Met .... On the other hand, the Aβ residues that tend to lie within 0.5 *nm* of the Fe ions of heme has the

Clusters	Trajectory	Surrounding Residues*
C1	11	Peptide A: Phe-4 Tyr-10 Phe-19 Val-39 ILE-41 Peptide B: Val-39
C2	11	Peptide A: Val-18 Asn-27 Gly-37 Gly-38 Ile-41 Peptide B: His-6 Asp-7 Gly-9 Ile-31 Met-35 Val-39
C3	8	Peptide A: Phe-4 Arg-5 Glu-11 His-14 Peptide B: Phe-4 Val-12 Leu-17 Met-35 Val-39
C4	15	Peptide A: Ala-2 Phe-4 Tyr-10 Leu-17 Phe-19 Leu-34 Met-35 Val-36 Peptide B: His-13 Leu-17 Phe-19 Ile-31
C5	13	Peptide A: Arg-5 His-6 Tyr-10 His-14 Gln-15 Ile-32 Met-35 Val-39 Peptide B: Glu-3 Phe-4 Ile-32 Leu-34 Met-35
C6	15	Peptide A: Leu-17 Phe-19 Leu-34 Met-35 Peptide B: His-13 Leu-17 Phe-19 Val-39
C7	13	Peptide A: Arg-5 His-6 Asp-7 Ser-8 Gly-9 Tyr-10 His-14 Gln-15 Met-35 Val-36 Val-39 Peptide B: Ala-2 Glu-3 Phe-4 Ile-31 Ile-32 Met-35
C8	6	Peptide A: Phe-4 Phe-19 Val-24 Gly-25 Ser-26 Val-39 Peptide B: Leu-17 Phe-19 Ile-32
C9	6	Peptide A: Phe-4 Tyr-10 Phe-19 Val-39 Ile-40 Peptide B: Val-39

Table 6.5: The population of the first 9 dominant Aβ-hemes clusters in the last 50 *ns*. $*$ indicates the residues that are within 5 $\AA$ of Fe ion.

following affinity ranking: Phe, Tyr, Arg, His, Met, Leu, Ser ... We see that the Aβ residues that occur in the vicinity of heme and the Fe ions are slightly different for the 2 Aβ+ 4 hemes system and the 1 Aβ+1 heme system. The differences result from interactions between Aβ peptides which affect the Aβ-heme complex motifs. Remarkably, we observe that the residue Phe shows the highest interaction affinity with hemes in both systems.

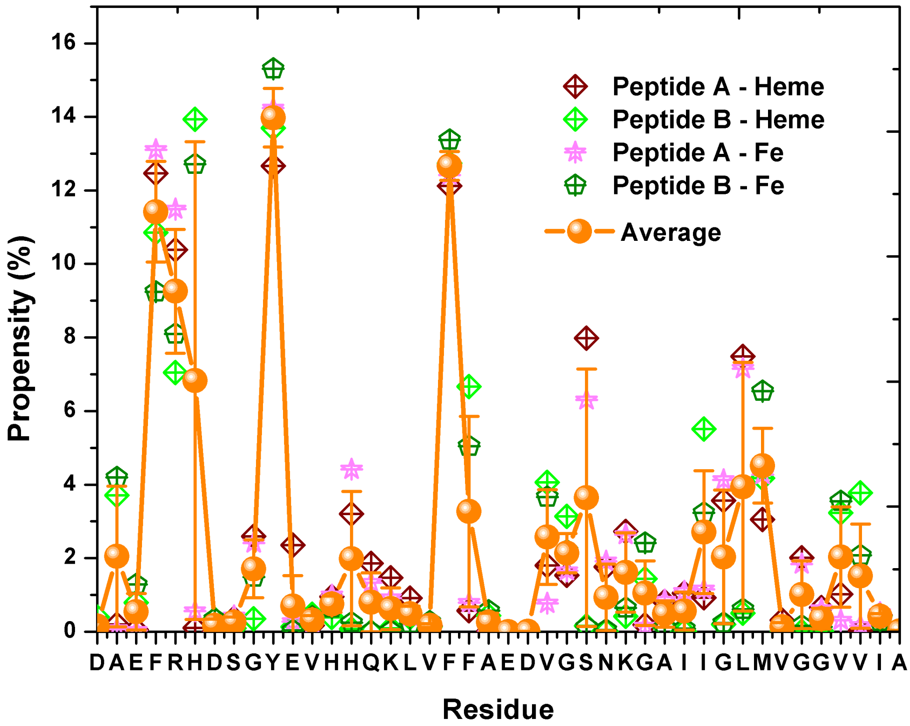

Figure 6.11: The occurrence of Aβ residues within 0.5 *nm* heme/Fe. The average propensity of each residue towards all the 4 hemes/Fe ions are indicated by the orange balls and connected via the orange lines.

Furthermore, the hydrogen bond forming propensity of the Aβ residues towards heme were also examined (see Figure 6.12). Our results show that the Aβ residues share similar propensity in hydrogen bond formation in the 2 Aβ+ 4 hemes and the $1A\beta + 1$ heme simulations, albeit with the ranking Lys-16, Ser-26, Arg-5, Lys-28, His-6....

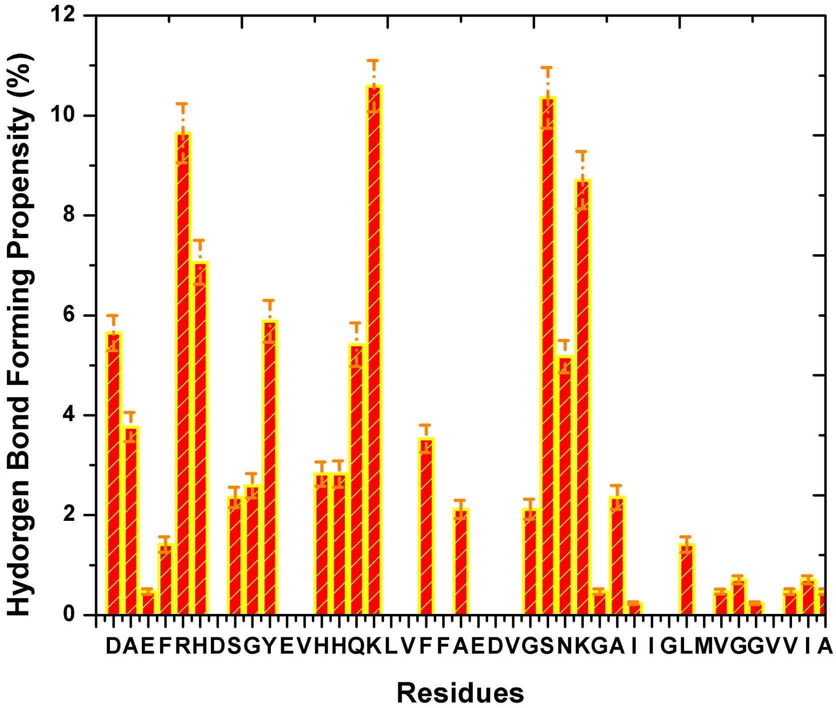

Figure 6.12: The binding propensity of hemes towards Aβ residues.

6.3.6 Heme physically prevents Aβ aggregation

The secondary structure propensity of each residue of the 2 Aβ+ 4 hemes system can be determined from Figure 6.13. As before, four types of secondary structures are considered to categorize the secondary structure propensity of the system. The four types are: β-structure (β-bridge and β-sheet); helix (α-helix and 3-helix); bend & turn; and coil. For the sake of clarity, Figure 6.13 only displays three of the four types, i.e., the β-structure, bend & turn, and the helix structure. By comparing Figure 6.13 with Figure 6.7(a), we observe the similar α-structure propensity for the 2 Aβ+ 4 hemes system with the 1 Aβ + 1 heme system. For example, the sequence ${}_{26}$SNKGAI$_{31}$ is found to be one common helical segment in both systems. By averaging the number of residues adopting the helical-structure and the β-structure every 50 *ns* (see Figure 6.14), one finds that the presence of heme has not led to a significant difference in the secondary structure content of the 2 Aβ+ 4 hemes system in comparison to the situation when heme is absent.

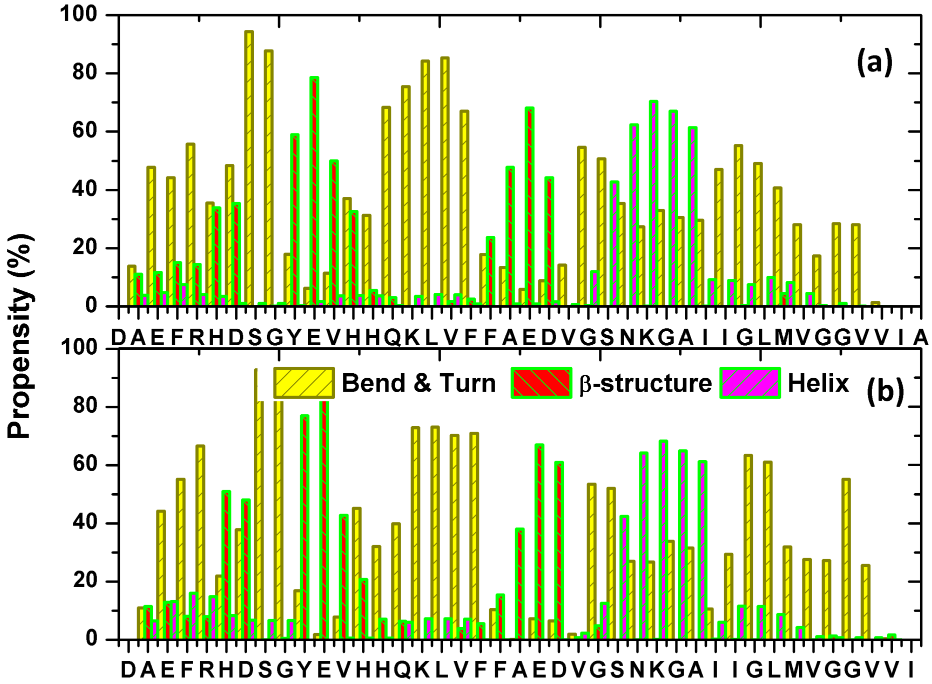

Figure 6.13: The secondary structure propensity of Aβ peptide A (a) and peptide B (b). Note that the yellow bars are for the bend & turn, the red bars are for the β-structure, while the purple bars are for the helical structure. The propensity for the coil structure is, however, not shown.

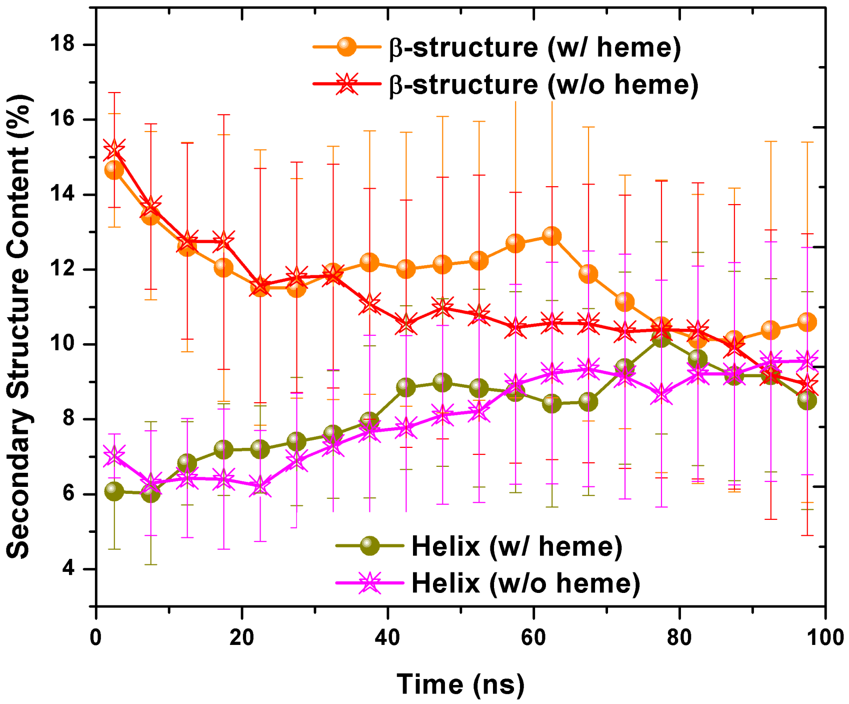

Figure 6.14: The number of residues adopting β-structure and helical content in the presence/absence of heme was plotted after averaging over 16 trajectories every 50 *ns*. The statistical errors are indicated by error bars.

The number of contacts between peptide A and peptide B are calculated for all the 32 trajectories. By averaging the number of contacts every 20 *ns* for the 16 "heme-present" trajectories and "heme-absent" trajectories, we found a lower contact number for the trajectories with the presence of heme in comparison with our group of controls (see Figure 6.15(d)). This reduction in contact implies that the presence of heme has prevented the aggregation of Aβ. By extracting the last 10 *ns* of the 32 trajectories and plotting the averaged contact map (see Figure 6.15(a) and (c)), we see that more contacts are formed in the Aβ peptides without heme than that with heme.

In addition, we have plotted in Figure 6.15(b) a representative Aβs-hemes complex to illustrate its secondary structure.

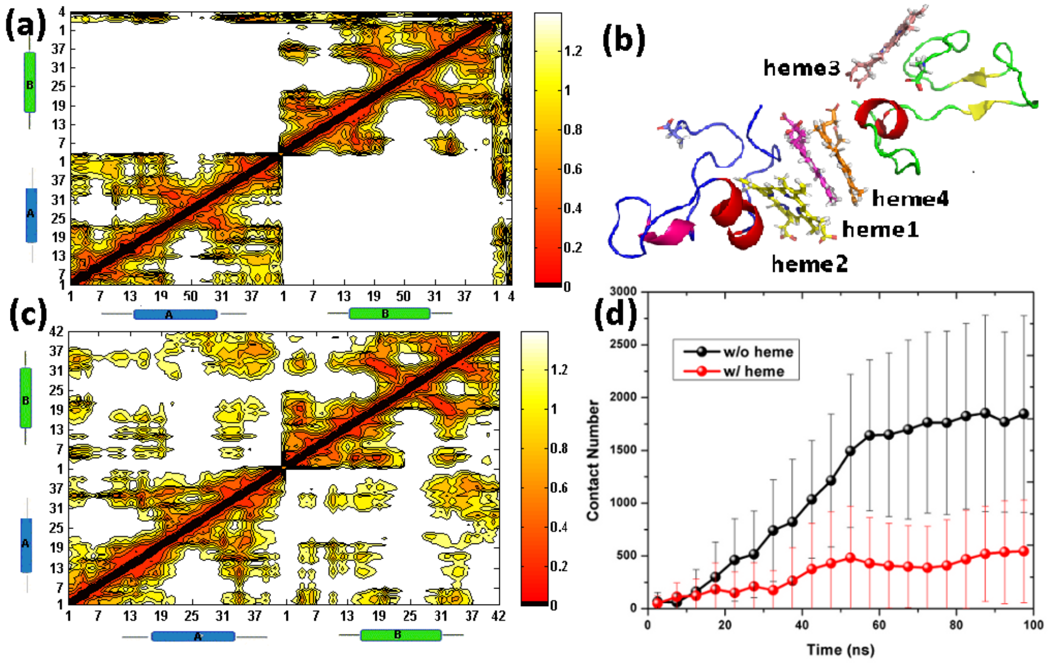

Figure 6.15: The contact map for peptide A, peptide B and heme (a). A representative structure of the Aβs-hemes complex with the four hemes being distinguished through different colors. Note that the loop of peptide A and peptide B are colored as blue and green respectively with the C-terminal Ala-42 being indicated as sticks (b). The contact map between peptide A and peptide B (c). A plot of the average number of contacts between peptide A and peptide B in the presence/absence of heme every 5 *ns*. Note that the error bars indicate the average derivation (d).

6.4 Summary and discussion

The formation of dimer, trimer and higher order oligomers during the process of amyloid β aggregation is believed to be toxic to the neurons. In order to avert the resulting neuronal apoptosis, there is great interest in the study of Aβ-heme complex which plays different roles in the intracellular and extracellular space. While intracellular Aβ-heme complex is proposed to decrease heme bioavailability which leads to a deficiency of the functional heme, extracellular Aβ-heme is reported to inhibit Aβ aggregation and alleviate Aβ oligomer's toxicity.

Past research has uncovered several Aβ-heme motifs which mainly involve the histindine residues, without any analysis on the detailed secondary structure conformations within the configuration. By means of extensive conventional molecular dynamics simulations, we have identified several binding motifs which indicate that hydrophobic residues have a high tendency to interact with heme. Thus, an Aβ-heme complex may not be histindine-focusing, with the hydrophobic interactions between the heme and Aβ hydrophobic residues play a dominant role in the Aβ-heme complex formation as shown in our MD simulations study. However, further experimental as well as QM/MM study is required to provide a more accurate assessment to elucidate whether Aβ-heme complex formation is driven via the interaction with histindine or by hydrophobic interaction. It is important to note that past experiment[331] on Aβ-heme complex involved peptides such as the Aβ_{1-40}, Aβ_{1-16}, Aβ_{17-40} and Aβ_{10-20}, which are mainly non-amyloidgenic, while the toxic Aβ_{1-42} has yet to be tested experimentally. On the other hand, recent QM/MM studies[332] on the Aβ-heme complex had only explored a limited number of configurations. Thus, we expect more work to be performed on QM/MM, experiments and MD simulations that aim to fully grasp the detailed interactions between heme and Aβ in the not too distant future.

Through the PMF, we observe that the position of the Aβ hydrophobic residues has an implicit effect on the binding affinity of heme towards certain residues. In addition, heme physically prevents the Aβ aggregation and it is also found to have an influence on the underlying secondary structure of Aβ during the formation of Aβ-heme complex, which may explains its inhibitory role in neuronal cell death.

The latter conclusion is supported by the simulation of the 2 Aβ+ 4 hemes system, which demonstrates explicitly how heme physically prevents Aβ aggregation with an increase in the α-content within the peptides.

Chapter 7 S100A9 induces Abeta peptides oligomerization revealed by replica exchange molecular dynamics simulation

Inflammation is one of the prominent pathological features in Alzheimer's disease (AD). Recently, there are various proposed roles of neuro-inflammation, such as the driving forces, bystander, byproduct or the neuroprotective response. Notwithstanding these diverse possible mechanisms, experiments have found that S100A9 is one of the pro-inflammatory protein abundant and over-expressed in the inflammation sites of AD. In this paper, we examine the role of S100A9 in the oligomerization process of Aβ peptides by means of replica exchange molecular dynamics simulation. The pro-inflammatory S100A9 protein interacts with the Aβ peptides directly, mainly through strong hydrophobic interactions with the Aβ central hydrophobic core region. In addition, the formation of hydrogen bond between the residues of the S100A9 homodimer which are exposed to the solvent and the two ends of the Aβ peptides are found to cause a lengthening of the Aβ_{12-24} peptides. The longer Aβ_{12-24} peptide with a higher β-content then may function as a template to induce the folding of new incoming Aβ peptides, which leads to the formation of aggregation-prone oligomer. Once such oligomer is formed, it may further serve as a seed to accelerate the aggregation to amyloid fibrils. Furthermore, our results show that amyloid oligomerization is mainly induced by S100A9 rather than Aβ peptides.

7.1 Introduction

The deposition of the Aβ peptides and the accumulation of the tau protein filamentary tangles are suggested to be directly associated with prominent neuroinflammations.[28,29,333,334] Moreover, the neuroinflammations are significantly correlated with the impairment of cognitive abilities.[335]

Aβ oligomers are believed to be the most toxic agent in AD and the aggregation of Aβ peptides forming oligomers turns out to be an important pathological pathways.[3,142,336] Aβ oligomers accompany with deposits may provoke the activation of astro- and microglia, and initiate a series of chronic inflammation process in AD brains. Clinical studies have revealed that anti-inflammation drugs can delay the early-onset and progression of AD, but however weakly ameliorate the impact of cognitive impairment.[29,30] On the other hand, the neuroprotective effect of inflammation has been considered to be a beneficial response in AD.[31–34]

Phagocytic S100 are proteins that belong to the class of EF-hand Ca^{2+}-binding protein family. These proteins regulate a plethora of extracellular and intracellular processes such as cell growth, cell differentiation, calcium homeostasis and inflammation response.[337] S100A8 (myeloid-related protein, MR8), S100A9 (calgranulin B; MRP14) and S100A12, are three inflammation-associated proteins in the S100 family. They are over-expressed and actively secreated by non-traditional Golgi-route pathway at the inflammation sites.[35] S100A8 and S100A9 are normally coexpressed. They exist as heterotetramer complex which are highly stabilized, and are able to confer certain indispensable functional roles such as the regulation of cellular motility.[338,339]

S100A9 can also be expressed and function independently without forming heterodimer with S100A8. The enhanced expression of S100A9 is observed in the AD brains. Interestingly, by knocking out the S100A9 gene, the AD brain of Tg2576 is found to recover from cognitive impairment with a concomitant reduction in the amounts of Aβ.[36] The pro-inflammatory effect of S100A9 partially relies on its binding to receptors such as the Toll-like receptors (TLRs).[340] In addition, the binding of calcium to S100A9 exposes its broad hydrophobic surface to interact with other proteins and further modulate the activities of its target. On the other hand, it can also induce S100A9 to self-interact to form homodimer or to combine with S100A8 to assemble into heterodimers or even high order oligomers. Recent experimental study shows that the binding of S100A9 towards the Aβ peptide promotes the formation of Aβ plaques, which reduces the toxic Aβ oligomers and hence plays a further protective response in the AD brains.[34]

In this chapter, we perform replica exchange molecular dynamic (REMD) simulation to study the effect of the interaction of S100A9 with Aβ peptide and to examine its consequence on Aβ aggregation. We have taken the chain Aβ_{12-24} to represent the full-length Aβ peptide. It has been reported that Aβ_{12-24} is able to assist in the exploration of many fundamental aspects of the thermodynamics and kinetics of the Aβ oligomerization processes.[258,278,341] Furthermore, Aβ_{12-24} contains one of the central hydrophobic region, whose inter-chain interaction, hydrogen bond matching pattern and dimerization process in the presence of S100A9 will shed light on how S100A9 affect the mechanism of full-length Aβ oligomerization.

7.2 Methods and simulation setup

S100A9 has a dimeric structure consisting of two tightly packed EF-hand motifs. It is composed of a helix-loop-helix region, which is connected by a linker (also dubbed as "hinge") region. The homodimeric structure of S100A9 was obtained from the Protein Data Bank (PDB) ID: 1IRJ.[338] We had represented this S100A9 with 4 calcium and the 2 extended $_{12}$VHHQKLVFFAEDV$_{24}$ Aβ peptides by the AMBER99SB force field. We then solvated these molecules in a cubic box of dimensions $92.574\,\AA \times 71.590\,\AA \times 105.702\,\AA$. Note that the two peptides are labeled as peptide A and peptide B, respectively. 42 Na^+ and 44 Cl^- were added to the $22,235$ water molecules to reach a concentration of $0.1\ mol/L$.

The peptides were capped by a N-terminal acetyl group and a C-terminal amide group. The protonation state of HIS, LYS, ARG and ASP are listed as follow:

Aβ_{12-24} protonation state		
Residue ID	pKa Value	Charge States
HIS-13	5.5	-1^{ε}
HIS-14	7.6	$+1^{\varepsilon,\delta}$
LYS-16	9.7	$+1$
GLU-22	4.5	-1
ASP-23	4.4	-1

Table 7.1: The protonation state of Aβ_{12-24} titratable residues at pH$=7$. ε - H on C (epsilon-1). ε,δ - H on C (epsilon-1) and C (delta-2).

S100A9 and the calcium were restrained in the center of the cubic box with a constant applied force of 2000 $kJmol^{-1}nm^{-2}$ and 1000 $kJmol^{-1}nm^{-2}$ respectively. The two Aβ peptides were then placed randomly around the S100A9. 108 different conformations were taken as starting structures to minimize bias and to accelerate the REMD convergence.

All bonds were constrained using the linear constraint solver (LINCS)[161] algorithm with a leap-frog molecular dynamics simulation using an integration time step of 2 *ps*. The Van der Waals cutoff was set to 1.2 *nm*, while the cut-off for electrostatic interactions was set within the range of 0.9 *nm*. The S100A9, calcium, two Aβ peptides and solvent were then separately coupled to an external heat bath with a relaxation time of 0.1 *ps*. The temperatures of the 108 replicas in our REMD simulations are listed as following: 315.00 *K*, 315.97 *K*, 316.94 *K*, 317.92 *K*, 318.91 *K*, 319.89 *K*, 320.88 *K*, 321.88 *K*, 322.88 *K*, 323.89 *K*, 324.90 *K*, 325.91 *K*, 326.93 *K*, 327.96 *K*, 328.99 *K*, 330.02 *K*, 331.06 *K*, 332.11 *K*, 333.15 *K*, 334.21 *K*, 335.27 *K*, 336.33 *K*, 337.40 *K*, 338.47 *K*, 339.55 *K*, 340.64 *K*, 341.73 *K*, 342.82 *K*, 343.92 *K*, 345.03 *K*, 346.14 *K*, 347.26 *K*, 348.38 *K*, 349.51 *K*, 350.64 *K*, 351.78 *K*, 352.92 *K*, 354.07 *K*, 355.23 *K*, 356.39 *K*, 357.56 *K*, 358.73 *K*, 359.91 *K*, 361.10 *K*, 362.29 *K*, 363.49 *K*, 364.69 *K*, 365.90 *K*, 367.12 *K*, 368.34 *K*, 369.57 *K*, 370.80 *K*, 372.04 *K*, 373.29 *K*, 374.54 *K*, 375.81 *K*, 377.07 *K*, 378.35 *K*, 379.63 *K*, 380.92 *K*, 382.21 *K*, 383.51 *K*, 384.82 *K*, 386.14 *K*, 387.46 *K*, 388.79 *K*, 390.13 *K*, 391.47 *K*, 392.82 *K*, 394.18 *K*, 395.55 *K*, 396.92 *K*, 398.31 *K*, 399.69 *K*, 401.09 *K*, 402.50 *K*, 403.91 *K*, 405.33 *K*, 406.76 *K*, 408.20 *K*, 409.64 *K*, 411.10 *K*, 412.56 *K*, 414.03 *K*, 415.51 *K*, 417.00 *K*, 418.49 *K*, 420.00 *K*, 421.51 *K*, 423.04 *K*, 424.57 *K*, 426.11 *K*, 427.66 *K*, 429.22 *K*, 430.79 *K*, 432.36 *K*, 433.95 *K*, 435.55 *K*, 437.16 *K*, 438.77 *K*, 440.40 *K*, 442.04 *K*, 443.68 *K*, 445.34 *K*, 447.01 *K*, 448.69 *K*, 450.38 *K* and 452.07 *K*. The averaged acceptance ratio is around 30% and the neighboring replicas exchanged at every 2 *ps* is achived. The cumulative simulation time was 22.14 μs with a total of $22,140,000$ structures generated.

To check the influence of the S100A9 on the Aβ peptides, another REMD simulations were done on the Aβ peptides alone, without the S100A9. The temperatures of the 64 replicas are as follow: 315.00 K, 316.88 K, 318.77 K, 320.67 K, 322.57 K, 324.49 K, 326.42 K, 328.35 K, 330.29 K, 332.26 K, 334.22 K, 336.19 K, 338.17 K, 340.16 K, 342.16 K, 344.17 K, 346.19 K, 348.22 K, 350.26 K, 352.31 K, 354.37 K, 356.44 K, 358.52 K, 360.61 K, 362.71 K, 364.83 K, 366.95 K, 369.07 K, 371.21 K, 373.37 K, 375.53 K, 377.70 K, 379.88 K, 382.07 K, 384.27 K, 386.48 K, 388.71 K, 390.94 K, 393.18 K, 395.44 K, 397.71 K, 399.99 K, 402.28 K, 404.58 K, 406.89 K, 409.21 K, 411.55 K, 413.89 K, 416.25 K, 418.62 K, 421.00 K, 423.39 K, 425.79 K, 428.21 K, 430.64 K, 433.11 K, 435.56 K, 438.02 K, 440.49 K, 442.98 K, 445.48 K, 447.99 K, 450.51 K and 453.04 K..

Note that each replica was completed with the same simulation time, and a total of $13,120,000$ structures were generated through the process. Note that the REMD simulations and analysis were carried out using the GROMACS package.[326–328] PyMOL[271] and VMD[272] were used to visualize the structure. Additional analysis and visualization were assisted by plotmtv, MATLAB, originPro and some in-house scripts.

7.3 Characterization of the interaction between Aβ and S100A9 as well as kinetics of amyloid oligomerization

7.3.1 Hydrogen bond

It has been reported that amyloid oligomerization is mainly induced by Aβ rather than by S100A9 from our experimental study and previous research.[34] To better examine the role of S100A9 in the dimerization process, we had calculated the number of hydrogen bonds between Aβ peptides and S100A9, and the number of hydrogen bonds and contact numbers between the two peptides. We found that the number of hydrogen bonds formed between Aβ peptides and S100A9 has a high positive correlation with the number of contacts between the two peptides (with a Pearson correlation coefficient of 0.88). On the other hand, the number of hydrogen bonds formed between the two peptides shows a negative correlation with the number of contacts between the peptides (with a Pearson correlation coefficient of -0.22). This had led us to conclude that S100A9 plays a major role in the oligomerization process.

We have examined hydrogen bond formation at 315 K. We have identified a total of 980 hydrogen bonds between Aβ and S100A9 within our 205 *ns* simulation, with 492 between peptide A and S100A9, and 488 between peptide B and S100A9. The propensity of hydrogen bond formation for each residue is illustrated in Figure 7.1. We observe that residues from both peptides A and B have similar hydrogen bond forming propensity, with the central hydrophobic core (CHC) residues weakly involve in the hydrogen bond formation.

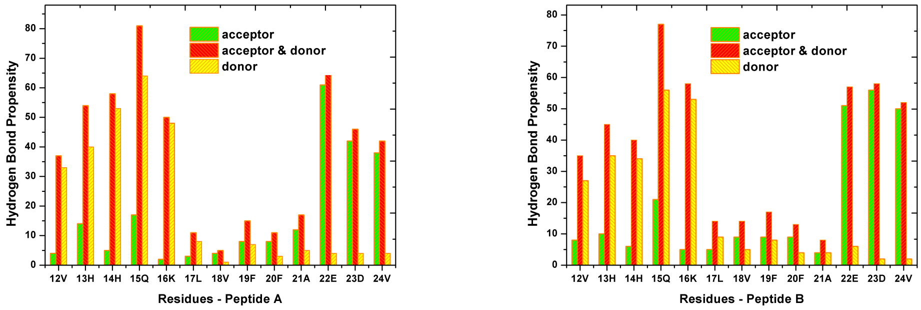

(a) (b)

Figure 7.1: The hydrogen bond propensity of peptide A (a) and the hydrogen bond propensity of peptide B (b). Note that the green bar indicates that the residue acts as an acceptor towards S100A9, while the yellow bar indicates the residue acts as donor. On the other hand, the red bar shows the strength of the residues involved in hydrogen bond formation with S100A9.

Recall that S100A9 comprises two EF-hand domains which are connected via a linker region,[342] with each EF-hand domain consisting of a helix-loop-helix conformation. The direct binding of Aβ peptides to S100A9 protein has been reported by Zhang et al. experimentally.[34] Based on the amino acid composition and structure of S100A9, Zhang et al. had proposed a putative binding pattern composing of hinge region of S100A9 (Leu-45-Asn-55) and the hydrophobic core of Aβ peptides (Leu-17-Ala-21). In order to verify this result, we again examined hydrogen bond formation at 315 K. Overall, we found that each region of S100A9 (as defined in Table 7.2) shares nearly the same tendency to interact with Aβ via hydrogen bonds (see Table 7.2 and Figure 7.2). In particular, the hydrogen bond forming affinity of S100A9 towards Aβ residues is observed to rank as follows: Asn > Lys > Arg > Asp ...

	region name	residues	percentage
	helix I	7 – 23	13.3%
EF-hand I	Ca^{2+}-binding loop I	24 – 33	13.0%
	helix II	34 – 44	10.1%
linker region		45 – 55	16.0%
	helix III	56 – 66	19.1%
EF-hand II	Ca^{2+}-binding loop II	67 – 75	13.9%
	helix IV	76 – 94	-

Table 7.2: The hydrogen bond binding propensity of each part of S100A9.

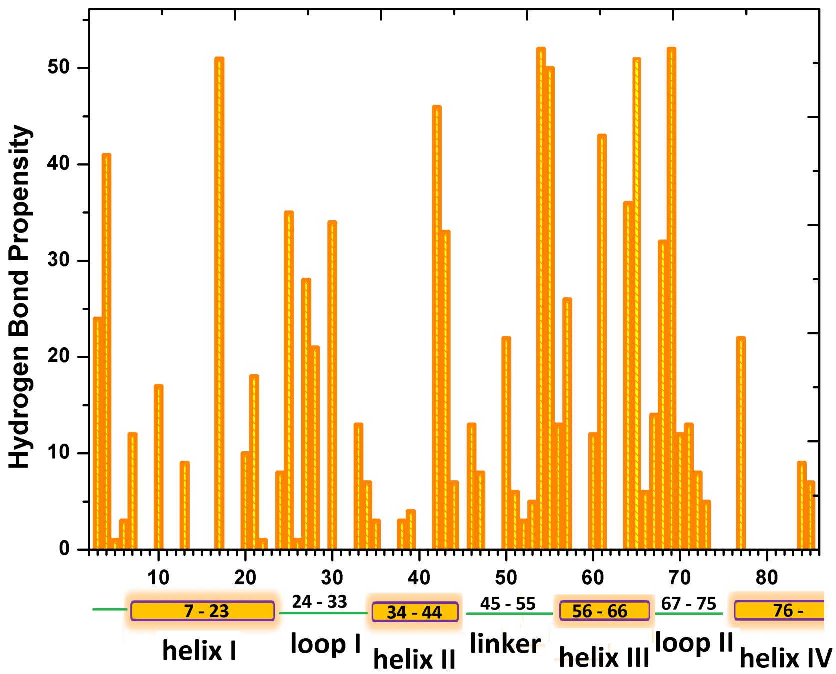

Figure 7.2: A plot of hydrogen bonding propensity of S100A9 towards the Aβ peptides.

7.3.2 Contact numbers

Furthermore, we have calculated the number of contacts between the amino-acid residues of $A\beta_{12-24}$ peptides and those of S100A9. As shown in Figure 7.3, the amino acids from the hydrophobic cores of $A\beta_{12-24}$ peptides (Leu-17-Ala-21) form more contacts with S100A9 than the other amino acids. In particular, the residues Phe-19 and Phe-20 form 3 times more contacts than the rest. The result here re-emphasizes the strong binding of the hydrophobic cores of $A\beta_{12-24}$ peptides with S100A9. On the other hand, the regions of S100A9 with more contacts to the $A\beta_{12-24}$ peptides occur at the C-terminal of Helix I, the hinge region connecting Helix II and Helix III, Helix III, and the calcium-binding loop II connecting Helix III and Helix IV (see Figure 7.3(b)). Notably, while the hinge region did form quite a number of contacts with the $A\beta_{12-24}$ peptides, it is not the region with the highest number of contacts.

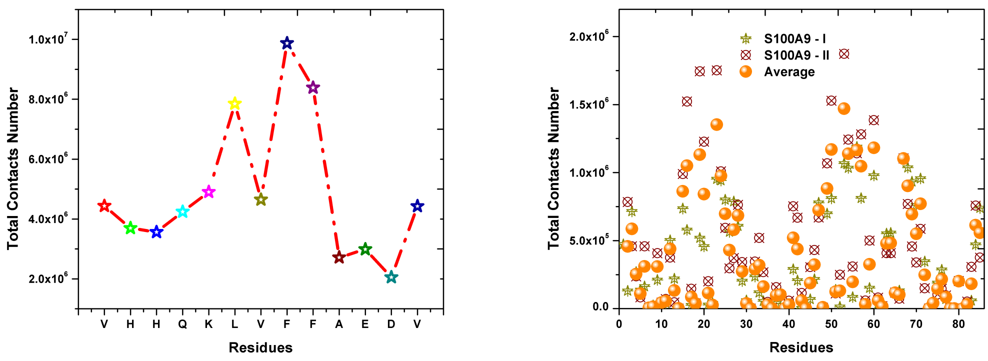

(a) (b)

Figure 7.3: A plot of the contact between S100A9 and Aβ_{12-24} peptides at the level of amino acids. The contacts were defined as atom pairs within a cut-off distance of 5 $\AA$. The analysis was based on an ensemble of trajectories at 315 K. (a) The cumulative number of contacts of amino acids of Aβ_{12-24} peptides with S100A9 protein. (b) The average cumulative number of contacts of amino acids of S100A9 homodimer towards Aβ_{12-24} peptides. Note that S100A9-1 indicates the first S100A9 constitutes the homodimer and S100A9-2 indicates the second one.

7.3.3 Cluster analysis

The cluster analysis was performed by extracting trajectories where the distance between S100A9 and Aβ was within 0.5 nm. We had extracted $5,364$ frames with 149 clusters identified, and the RMSD cutoff was 0.2 nm. The first 30 most populated clusters were selected with the C_α shown as dots (see Figure 7.4). We observed that those Aβ close to S100A9 were mainly distributed around the exterior of S100A9. No single Aβ was found to penetrate into the S100A9. The first 7 most populated clusters are given in Figure 7.5(a) and the largest cluster (with a population of 22.12%) is shown in Figure 7.5(b). In addition, we notice that Helix II and Helix IV form very little contact with Aβ. This is because Helix II is rich in charged residues, while Helix IV is buried in the hydrophobic core of the S100A9 homodimer.

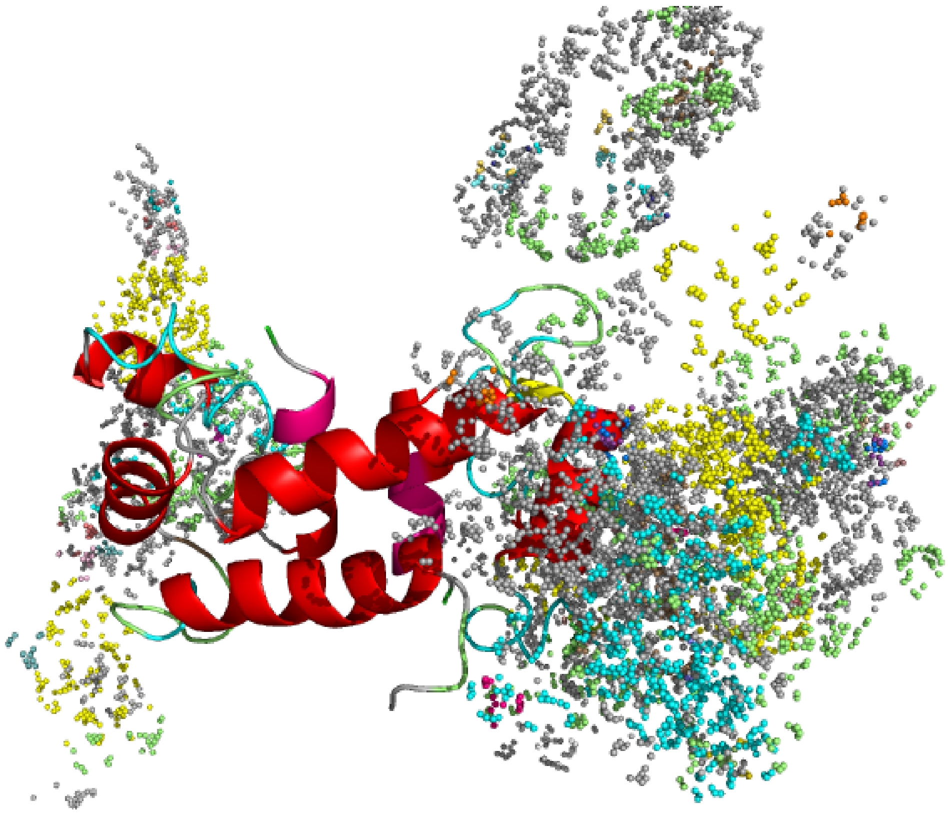

Figure 7.4: The representative spatial distribution of Aβ_{12-24} (shown as dots and colored by its secondary structure) around S100A9 (shown in red).

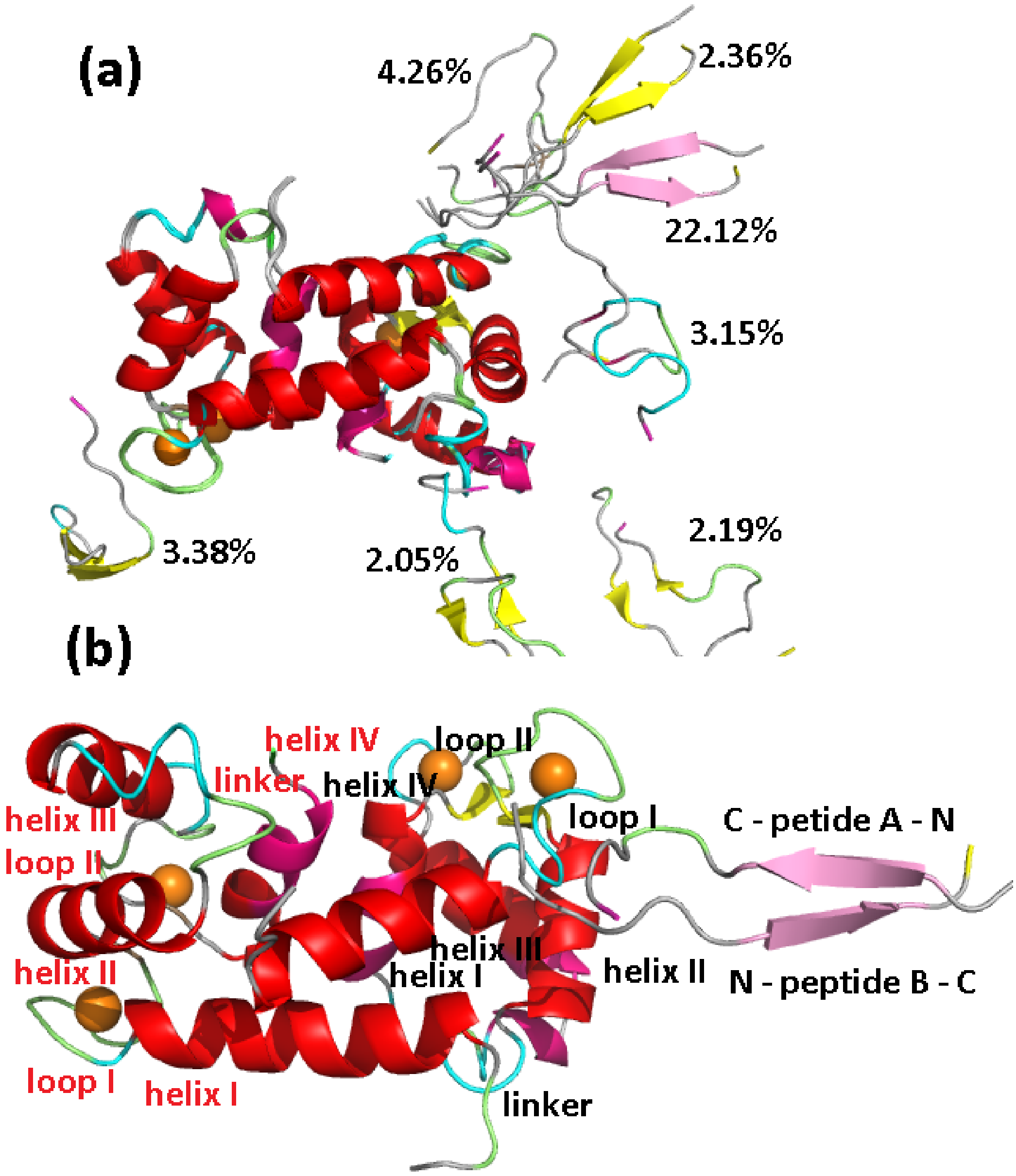

Figure 7.5: The first 7 most populated clusters are shown in (a). The largest cluster is shown in (b).

7.3.4 Potential of mean force

The ensemble of extensive configurations generated from our REMD simulation results provide an alternative channel for the calculation of the potential of mean force (PMF) during Aβ dimerization. In order to examine the potential of mean force in the presence of S100A9, a 1-dimensional grid was constructed with respect to (i) the distance between the center of mass of the two central hydrophobic cluster (CHC) (namely from 17-21) heavy atom; (ii) the minimum distance between CHCs and S100A9 and (iii) the distance between the centre of mass of CHCs and the four calcium atoms respectively to count the number of sampled conformations in each bin, denoted as N_i. The potential of mean force V_{pmf} is then given by:

$$V_{pmf} = -k_B T log(N_i/N_{max}). \tag{7.1}$$

Here k_B is the Boltzmann constant, T is the absolute temperature and N_{max} is the maximum number of sampled conformations counted in each bin.

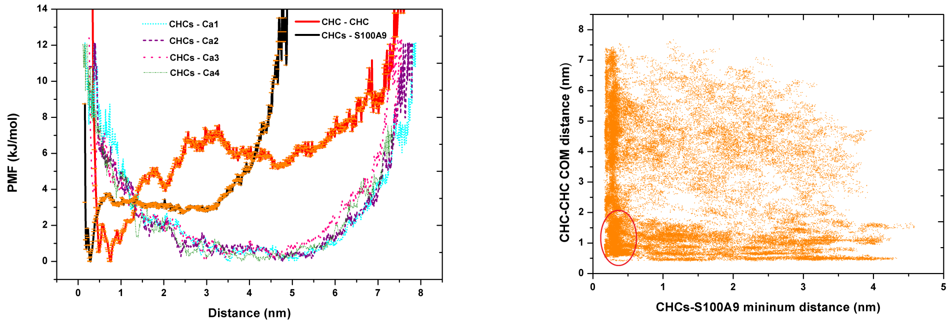

(a) (b)

Figure 7.6: (a) A plot of the potential of mean force at 315 K. Note that the four Calcium atoms are labeled as Ca1-Ca4. The error bars in the figure are shown as orange dash for CHC-CHC and CHCs-S100A9. (b) The density distribution of CHC-CHC COM distance with respect to the minimal distance towards S100A9 at 315 K. x-label indicates the minimum distance between CHCs and S100A9, y-label represents the COM distance between the two CHC. The red circle indicated the densest distribution area.

From Figure 7.6, we can see that the basin of the CHC-CHC PMF curve is located in the range of inter-chain distance $5-10\ \mathring{A}$ with a global minimum around $7.6\ \mathring{A}$, which corresponds to the Aβ dimerization distance. We can see that Aβ possesses the lowest free energy as a dimer. To further investigate the influence of S100A9 in the Aβ dimerization, we plot the density distribution of CHC-CHC COM distance with respect to the minimal distance towards S100A9 (see Figure 7.6(b)). First the CHCs-S100A9 PMF curve indicates presence of a basin in the range $2.5-3.3\ \mathring{A}$ with global minimum at $2.9\ \mathring{A}$. Second, we observe that this global minimum corresponds to the densest Aβ dimer distribution (indicated by the red circle in Figure 7.6(b)). These results again imply that S100A9 may facilitate the Aβ dimerization. This can result from S100A9 binding one peptide at a time. In other words, the interaction of S100A9 with one Aβ peptide may provide a more energy favorable situation for the attachment of another Aβ peptide.

7.4 Characterization of the Aβ dimer conformations

7.4.1 Dimer distribution against temperature changes

The self-assembly of Aβ_{12-24} forming into dimers was observed in this study. We took the last 10 *ns* of our simulation data to characterize the dimer distribution and structure diversity. We found the maximum density of dimers to occur between 315 *K* and 342 *K* with an average proportion of 20.7% in the presence of S100A9. On the other hand, we observed that single monomers are dominant at a higher temperature (> 402 *K*). Meanwhile, the number of residues adopting β-structure was noticed to decrease with an increase in temperature. We have also examined dimer formation without S100A9 during the last 10 *ns*. In this case, the maximum density of dimers is found between 315 *K* and 369 *K* with an average proportion of 25.78%. Again, single monomers were observed to be dominant at a higher temperature (> 425 *K*).

In comparison to dimer formation without S100A9, the presence of S100A9 seems to reduces the chances of the two peptides coming together by simply presenting itself between the two peptides in some of our simulations. Another underlying reason may involve the interaction of the monomer Aβ with S100A9.

7.4.2 Parallel and antiparallel β-sheet patterns

The formation of parallel and anti-parallel β-sheet pattern between two Aβ peptides in the presence of S100A9 were examined using all the REMD sampled configurations at 315 *K*. We have identified $146,097$ first bridge pattern, which consists of $3,068$ parallel and $143,029$ anti-parallel patterns. We shall employ a pair of residue numbers i and j to denote these patterns: $i-j$ to indicate the parallel patterns, while $i+j$ to indicate the anti-parallel patterns. For the parallel β-sheets (see Figure 7.7(a)), the highly populated patterns include: (1) $i-j=\pm3$ (35.5%); (2) $i-j=\pm5$ (18.9%); (3) $i-j=\pm7$ (15.6%) and (4) $i-j=\pm9$ (13.3%). For the anti-parallel β-sheets (see Figure 7.7(b)), the highly populated patterns are: (1) $i+j=39$ (30.12%); (2) $i+j=35$ (29.28%); (3) $i+j=36$ (19.74%); (4) $i+j=37$ (8.06%); (5) $i+j=34$ (4.5%) and (6) $i+j=33$ (3.8%).

The diversity of the populated β-sheet configurations were also reported on the same[330,343] or other Aβ fragments such as Aβ_{16-22}, Aβ_{16-35}, Aβ_{10-35},[278,344,345] and even the mutated Aβ_{29-42} fragments.[346] In comparison to the study of dimer formation of the same fragment (namely Aβ_{12-24}) at different pH levels,[330] our studies have revealed new patterns which may be related to factors such as different pH, different replicas and most importantly, the presence of S100A9. Next, we examine the parallel and anti-parallel β-sheet patterns in Aβ without the presence of S100A9 using all sampled REMD configurations at 315 K. We have identified $58,482$ first bridge patterns, which consist of $1,579$ parallel and $56,903$ anti-parallel patterns. For the parallel β-sheets, we observe the following highly populated patterns: (1) $i-j=0$ (68.22%); (2) $i-j=\pm1$ (28.13%); (3) $i-j=\pm2$ (3.3%). On the other hand, we observe the following highly populated patterns for the anti-parallel β-sheets: (1) $i+j=38$ (11.74%); (2) $i+j=40$ (10.48%); (3) $i+j=36$ (10.43%); (4) $i+j=34$ (10.25%); (5) $i+j=42$ (9.33%) and (6) $i+j=32$ (9.29%).

In summary, we can see that the presence of S100A9 has not only increased the parallel and anti-parallel patterns, it has also given rise to some new patterns such as the $i-j=\pm3$, $i-j=\pm5$ and $i-j=\pm7$.

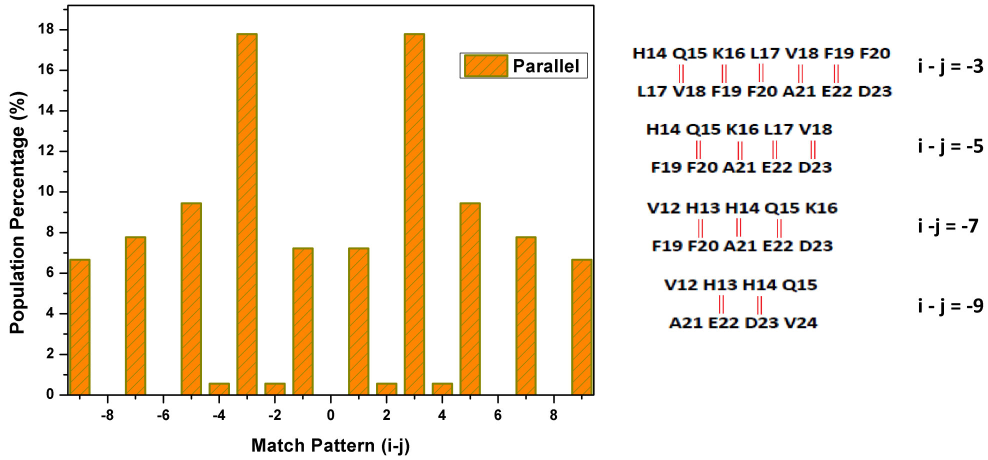

(a)

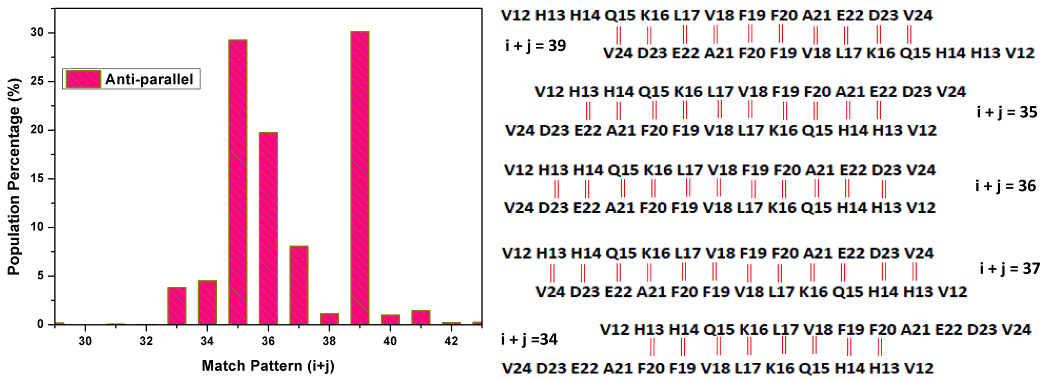

(b)

Figure 7.7: (a) A plot of the population percentage of various matching patterns (i-j) for the parallel alignments. (b) A plot of the population percentage of various matching patterns (i+j) for the antiparallel alignments. Note that the configurations of the highly populated parallel and anti-parallel Aβ_{12-24} dimerization pattern are given to the right of the plots with the vertical lines (in red) indicate the hydrogen bond formed between two residues.

7.4.3 Aβ secondary structure propensity

We have obtained the average secondary structure propensity of each residue of the Aβ through the last 50 *ns* of our simulation data (see Figure 7.8(a)) with and without S100A9. We have categorized the secondary structure propensity into four classes: bend and turn; coil; β-structure (β bridge and β-sheet), and helix (α-helix and 3-helix). Our results have indicated a very low helical conformational propensity for each residues. Note that similar results were obtained for Aβ_{12-24} dimer under different pH values.[330] We found that residues from HIS-14 to GLU-22 have the same preference of adopting coil, then bend & turn, and then the β-structure. Another interesting observation is that without the S100A9 the CHCs have a high propensity to adopt the β structure. It also corresponds to an increase in the number of dimers. Both are mainly due to the presence of S100A9 which reduces the chances of the two peptides coming together by simply presenting itself in the middle of our simulations. Furthermore, the β-structure of each residue is found to decrease with an increase in temperature.

7.4.4 Free energy landscape

Dihedral angle principal component analysis (dPCA) method[347] based on the transformation of the peptide dihedral angles was employed to construct the free energy landscape. Our results clearly show the presence of several free energy minima. For each local minima, we had performed the clustering analysis based on the pair-wise RMSD. We had uncovered several characteristic β-rich secondary structures as a result, and they were shown as snapshots in Figure 7.9. We had also provided the contact map of one representative structure for the purpose of illustration. We found that

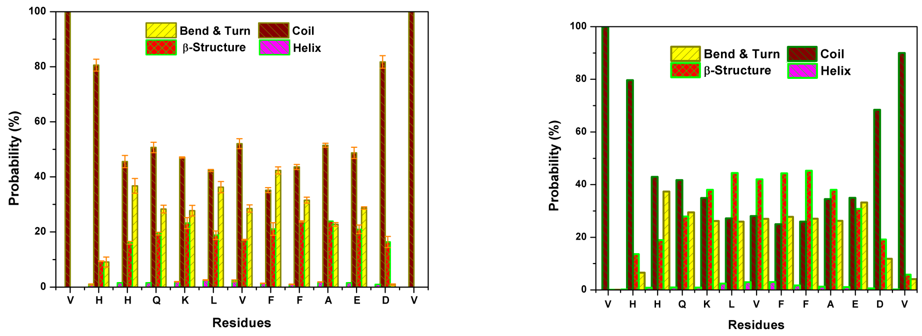

(a)

(b)

Figure 7.8: The secondary structure propensity of each residues at $T = 315\ K$ in the last 50 *ns* of the simulation data in the presence of S100A9 (a) and in the absence of S100A9 (b).

the structures in the local minimum have a high propensity to be rich in β-structure, followed by random-coil structure (not plotted in Figure 7.9). Most importantly, in those local minima, Aβ exists as dimer.

7.5 Conclusions and discussion

An extensive REMD simulation had been performed to examine the role of S100A9 in the process of Aβ_{12-24} peptides oligomerization and the secondary structure evolution propensity of each Aβ_{12-24} residues. We have found that the presence of S100A9 facilitate the formation of Aβ secondary structure such as the parallel and anti-parallel β-sheets.

In comparison to the simulation results of Aβ in water without the presence of S100A9, we found that the presence of S100A9 can affect the number of Aβ dimers and Aβ secondary structure propensity. The main reason being that in simulation without S100A9, the Aβ has a higher chance to meet. On the other hand, with

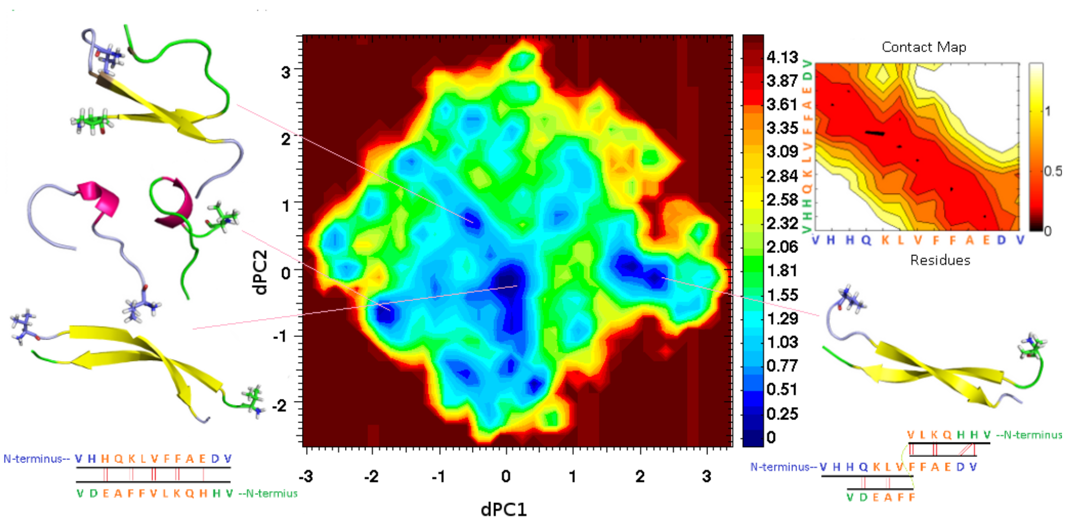

Figure 7.9: A plot of the free energy landscape of the Aβ_{12-24} in the presence of S100A9 computed from the last 50 *ns*. Four representative structures at the local minima are shown in cartoon (β-sheet: Yellow; 3-10-Helix: Purple; Coil: Lightblue for peptide A, green for peptide B). The N-terminus of peptide A and B are shown as stick and colored by element (N: blue; H: grey; O: red). The details of the hydrogen bond of two anti-parallel-β-sheet structures are illustrated at the bottom (Blue residues are from peptide A, green from peptide B, the orange residues are located on the β structure). A contact map is also plotted to show the detailed contact information. Note that the figures were generated by Plotmtv, PyMol[271] and Matlab.

S100A9, the Aβ may not encounter each other due to the large size of S100A9 which prevents their interaction. By further scrutinizing the number of hydrogen bonds formed between Aβ peptides and S100A9, and the number of hydrogen bonds and contact numbers between the two peptides, we found that the number of hydrogen bonds formed between Aβ peptides and S100A9 has a high positive correlation with the number of contacts between the two peptides. On the other hand, the number of hydrogen bonds formed between the two peptides shows a negative correlation with the number of contacts. We conclude that S100A9 promotes the process of Aβ oligomerization, although it has been reported that amyloid oligomerization is mainly induced by Aβ rather than by S100A9.

Furthermore, we have also found that the CHCs of Aβ form less hydrogen bond with S100A9 but have more contact with S100A9 than the other residues. We believe that the strong hydrophobic interaction between the CHC of Aβ_{12-24} peptides towards S100A9, as well as the hydrogen bond formed between the two ends of Aβ_{12-24} with the residues exposed to the solvent from S100A9, play an important role in the induction of the amyloid oligomerization. In addition, the potential of mean force between the two CHC-CHC heavy atom, and the minimum distance between CHCs and S100A9 and the free energy landscape, reveal that the Aβ peptides have the lowest free energy as a dimer.

Chapter 8 Conclusions and future directions

8.1 Introduction

There is as yet no cure for Alzheimer's disease (AD), which is the sixth-leading cause of death in the world. In the last few decades, many research groups have endeavoured to work on the unresolved problems in the field as well as to look for potential and safe therapeutics that can overcome AD. Aβ toxicity is a very intricate process which involves so many aspects that fundamental questions such as how Aβ is being released from APP and where does the intracellular Aβ come from remain unanswered. In addition, there are many problems one would classify as elusive and whose answers are currently under heavy speculations.

By using computational methods, we attempt to advance the research by elucidating the underlying mechanisms of Aβ aggregation and to examine several possible candidates which have the potential of inhibiting its self-assembly. In consequence, we have examined the detailed interaction scenario of Aβ with lipids, small molecules and macromolecules.

8.2 Summary of work and contribution to the field

Experimental demonstration has indicated that Aβ_{1-28} prefers to interact with the hydrophilic headgroup of lipids while Aβ_{25-40} tends to bury itself inside the hydrophobic core of the membrane.[152] Our computational modelling of Aβ peptides in membrane environment has revealed the same tendency with residues 1-27 of Aβ prone to interact with the lipid-aqueous hydrophilic interface region while residues 28-42 incline remain inside the hydrophobic core region.[142] Our simulations have confirmed experimental observations. In addition, we found that the short segment of Aβ from 14-23 (namely, HQKLVFFAED) maintain a well-preserved α-helical structure. Nevertheless, the secondary structure of Aβ can transform from α helices to β sheets.

The complex interaction network among the Aβ peptides, cholesterol and DPPC lipids we uncovered show that the presence of Aβ peptides has led to severe defects on the membrane surface. The presence of Aβ peptides has caused the membrane surface to sink and form a hydrophilic well filled with water. Furthermore, it has also disturbed the order of the cholesterol. The binding of the lipids with Aβ_{1-42} peptides has shown the possibility of enhancing the already-formed hydrogen bonds between the peptides residues. The interaction between cholesterol and Aβ peptides is found to compete with the intra-peptides interaction which leads to a negative correlation between the cholesterol-peptide interaction and the peptide-peptide interaction.

The aggregation of Aβ in membrane which consists of DPPC and cholesterol is a very slow process compared to the aggregation in aqueous environment. In our study, GLN-15 as well as ALA-42 at the C-terminus is observed to play a noticeable role during the oligomerization process in the membrane environment.

The therapeutic potential and intrinsic non-toxicity of curcumin endow it the power to be one of the best candidate to prevent AD and the most easily accessible food therapy for AD patient. In our study, we have examined the mechanisms behind the therapeutic potential of curcumin with respect to AD via its effect on the stability of the Aβ dimers. Our all-atom explicit solvent simulations have indicated that curcumin plays the role of an efficient β-sheet breaker by reducing the number of residues adopting the β-sheet secondary structure. We have proposed two possible mechanisms for its effectiveness. One is the intrinsic hydrophobicity of curcumin. The presence of curcumin near Aβ peptides has obviously perturbed and deformed the β-sheet secondary structure. The other relates to the π-π stacking interactions. The π-stackings between the curcumin keto-ring or enol-ring with the Aβ aromatic rings exist throughout our whole simulations. Thus, we propose that π-stacking interaction, as well as the hydrophobic effects, may play a non-negligible role in the inhibiting effects of curcumin on the stability and aggregation of Aβ peptides. Furthermore, as curcumin approaches the Aβ dimer, the polar groups of curcumin may form hydrogen bonds with Aβ, with the π-π stacking interaction between curcumin and the dimer partially immobilizes the aromatic arms of the curcumin. The result is a strengthening of the hydrogen bond network between the two species. The curcumin is observed to visit the residue LEU-34 regularly and this residue is found to serve as a hub among the common routes travel by curcumin around the dimer.

Heme, which is abundant in the hemoglobin and many other hemoproteins, is presents in the intracellular as well as the extracellular space. In fact, the presence of heme leads to the formation of Aβ-heme complex which plays different roles in the two spaces. While the intracellular Aβ-heme complex is proposed to decrease heme bioavailability which leads to a deficiency of the functional heme, extracellular

Aβ-heme is reported to be capable of inhibiting Aβ aggregation and thus alleviating Aβ oligomer's toxicity.

Past research has uncovered several Aβ-heme motifs which mainly involve the histindine residues, but lack in the provision of detailed secondary structure conformations within the configuration. By means of extensive conventional molecular dynamics and replica exchange molecular dynamics simulations, we have identified several binding motifs which indicate that hydrophobic residues have a high affinity to interact with heme. Thus, an Aβ-heme complex turns out not to be histindine-focusing. We conclude that hydrophobic interactions between the heme and Aβ hydrophobic residues play a dominant role in the Aβ-heme complex formation. In addition, heme is found to have a strong influence on the underlying secondary structure of Aβ during the formation of Aβ-heme complex, which explains its inhibitory role in neuronal cell death. The simulation of the 2 A$\beta+$ 4 hemes system demonstrates explicitly how heme prevents Aβ aggregation through increasing the α-content within the peptides. Meanwhile, our simulation studies show that heme and heme have a strong tendency to self-assemble into dimers and trimers.

S100A9 is observed to over-expressed in the inflammation sites of AD brains. There are various proposed roles of S100A9 in AD brains, such as the driving forces, bystander, byproduct or the neuroprotective response. Despite the controversy of those roles, it is crucial to understand the interaction between S100A9 and Aβ. In our studies, we examine the interaction between Aβ_{12-24} and S100A9 homodimer by replica exchange molecular dynamics simulations. Our result shows that S100A9 induces Aβ to adopt a prone-aggregation conformation. Furthermore, we found that the pro-inflammatory S100A9 protein interacts with the Aβ peptides directly, mainly through strong hydrophobic interactions with the Aβ central hydrophobic core region, and the formation of hydrogen bond between the residues of the S100A9 homodimer which are exposed to the solvent and the two ends of the Aβ peptides are found to cause a lengthening of the Aβ_{12-24} peptides. Interestingly, the longer Aβ_{12-24} peptide with a higher β-content then may function as a template to induce the folding of new incoming Aβ peptides, which leads to the formation of aggregation-prone oligomer. Once such oligomer is formed, it may further serve as a seed to accelerate the aggregation to amyloid fibrils. Overall, our results have shed new light on the influence of the inflammation protein on the Aβ oligomerization process.

8.3 Future directions

The general methods and simulation protocols that was employed in this dissertation can be applied to examine problems relating to Aβ peptides, DNA and other small moleclules. Here we list two projects we are interested:

8.3.1 The relationship between DNA and Aβ

Under physiological conditions, "naked" double-stranded DNA exists in three general helical forms, namely, A-DNA, B-DNA and Z-DNA. The right-handed double helical B-form structure with Watson-Crick base pairing and global repetitive features is the most ubiquitous DNA form within a variety of genome. Compared to the B-DNA, A-DNA has a shorter and more compact helical structure, which makes interconversion between the two forms to be relatively easy. In contrast, the conversion from A- or B- to the left-handed Z-form requires drastic conformational changes.

With the higher level of gene expression in the brain, cumulative DNA damage may have a cascading effect on the transcriptional effectivity and fidelity. Indeed, alteration of DNA conformation in the hippocampus region has been observed in the brain of AD patient.[348]

Negatively charged DNA is found to readily associate with Aβ oligomers at a PH of $4-9$.[349] Surface plasma resonance reveals that DNA binds to all forms of Aβ oligomers regardless the stage of aggregation.[350] The supercoiled DNA (scDNA) has also been reported to uncoil to a relatively relaxed form by Aβ via helicity and superhelicity modulation. It is also proposed that Aβ can alter the structure of DNA.[351] Further experiments have revealed that Aβ is able to nick open the circular and linear configurations of scDNA to form the Aβ-DNA complex.[352] Time-dependent DNA condensation in the presence of Aβ has also been observed with the β-sheet structure being suggested as the condensational nuclei for the DNA condensation.[353] Recent experiments have shown that the Aβ oligomers can convert the left-handed Z-DNA back to the right-handed B-DNA.[354] It has also been reported that the binding of nucleic acid to Aβ may facilitate the conversion of Aβ to insoluble amyloid fibrills.[355]

The initial structures of A-DNA and B-DNA are generated via the 3DNA-Driven DNA Analysis and Rebuilding Tool (3D-DART)[356] with the nucleic acid sequence (5'→3') of AGGGGCCCCT and CATGGCCATG respectively. The Z-DNA is obtained from PDB ID: 3P4J,[357] while the Aβ peptide is determined from PDB ID: 1IYT, with a sequence of *DAEFRHDSGYEVHHQKLVFFAEDVGSNKGAIIGLMVG-GVVIA*.

Four Aβ peptides were aligned in parallel in a cubic box of dimensions $100\,\mathring{A} \times 100\,\mathring{A} \times 100\,\mathring{A}$ with the DNA placed in the center. $30,325$ water molecules as well as 57 CL^- and 77 NA^+ were added in the 4 A$\beta + 1$ A-DNA system; $30,311$ water molecules as well as 57 CL^- and 77 NA^+ were added in the 4 A$\beta + 1$ B-DNA system.

Both systems are represented by CHARMM27 all-atom force field (with CMAP) - version 2.0.[325] The Van der Waals cutoff and short-range electrostatic forces were set to $7 \sim 8\,\AA$. Particle Mesh Ewald method[270] was used for electrostatic interaction with a Fourier grid spacing of 0.15 *nm*. 500 *ns* MD simulations were performed on both systems using NAMD[358] with a multiple timestepping of 2 *fs*.

The objectivity of this project is examination of the DNA on the effects of the Aβ oligomerization as well as the effect of the Aβ on the structure of the DNA.

8.3.2 The possible role of serotonin

Serotonin, [$C_{10}H_{12}N_2O$; 5-hydroxytryptamine], is a hormone present in the digestive tract, pineal gland and nervous system. In the human body, about four-fifths of the serotonin is in the gut's enterochromaffin cells, while the rest is in the central nervous system. It is one of the well-known neurotransmitters, which transmit signals across synapses. Serotonin plays an important role in learning, emotion (anxiety and migraine), sleep, appetite and vomiting. In particular, the alteration of serotonin levels in the brain can directly affect the mood of a person. In fact, during the treatment of depression, antidepressants work by affecting the action of serotonin. The chemical structure of serotonin is illustrated in Figure 8.1.

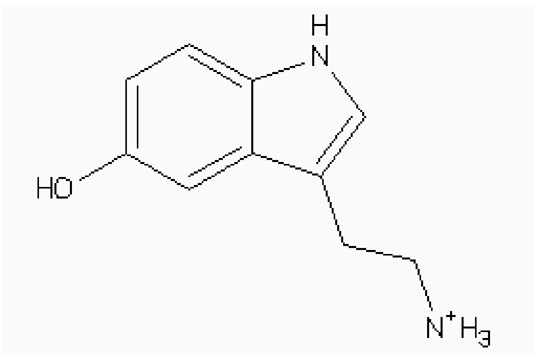

Figure 8.1: The chemical structure of serotonin.

Recent study on dogs with advanced age has uncovered Aβ deposits that indicate a significant loss of the serotonergic neurons.[359] On the other hand, the infusion of serotonin into the mice hippocampus and treating it with selective selective serotonin reuptake inhibitor (SSRI) have led to a reduction in the Aβ levels.[360] In the near future, a comprehensive simulation study would be carried out to examine the relationship between Aβ and serotonin.

Appendices

pKa value for titratable residues

Residues	pKa values
N-terminus	7.9
AspNT	2.4
Glu-3	4.2
Arg-5	12.2
His-6	6.0
Asp-7	4.2
Tyr-10	11.0
Glu-11	4.6
His-13	5.5
His-14	7.6
Lys-16	9.7
Glu-22	4.5
Asp-23	4.4
Lys-28	10.3
C-terminus	4.4

Table A1: Calculated pKa value for titratable residues.

The curcumin topology

```
[ moleculetype ]
; Name nrexcl
CUR    3

[ atoms ]
;   nr   type   resnr resid   atom   cgnr   charge      mass
1      CH3      1    CUR      C21      1    0.200    15.0350
2      OA       1    CUR    O4       1    -0.400    15.9994
3      C      1    CUR      C19      1    0.200    12.0110
4      CR1      1    CUR      C20      1    -0.060    12.0110
5      HC       1    CUR      H20      1    0.060    1.0080
6      C      1    CUR      C18      1    0.265    12.0110
7      OA       1    CUR    O5       1    -0.683    15.9994
8      H      1    CUR      H52      1    0.418    1.0080
9      CR1      1    CUR      C17      2    -0.060    12.0110
10      HC      1    CUR      H17      2    0.060    1.0080
11      CR1      1    CUR      C16      2    -0.060    12.0110
12      HC      1    CUR      H16      2    0.060    1.0080
13      C      1    CUR      C15      2    -0.000    12.0110
14      C      1    CUR      C14      3    0.000    13.0190
15      C      1    CUR      C13      3    0.000    13.0190
```

16 C 1 CUR C12 3 0.265 12.0110

17 OA 1 CUR O3 3 -0.683 15.9994

18 H 1 CUR H32 3 0.418 1.0080

19 C 1 CUR C11 3 0.000 13.0190

20 C 1 CUR C10 3 0.265 12.0110

21 O 1 CUR O6 3 -0.265 15.9994

22 C 1 CUR C9 4 0.000 13.0190

23 C 1 CUR C8 4 0.000 13.0190

24 C 1 CUR C4 4 -0.000 12.0110

25 CR1 1 CUR C3 4 -0.060 12.0110

26 HC 1 CUR H31 4 0.060 1.0080

27 CR1 1 CUR C5 5 -0.060 12.0110

28 HC 1 CUR H51 5 0.060 1.0080

29 CR1 1 CUR C6 6 -0.060 12.0110

30 HC 1 CUR H6 6 0.060 1.0080

31 C 1 CUR C7 6 0.265 12.0110

32 OA 1 CUR O2 6 -0.683 15.9994

33 H 1 CUR H22 6 0.418 1.0080

34 C 1 CUR C2 6 0.200 12.0110

35 OA 1 CUR O1 6 -0.400 15.9994

36 CH3 1 CUR C1 6 0.200 15.0350

[bonds]

; ai aj fu c0, c1, ...

2 1 2 0.143 8180000.0 0.143 8180000.0 ; O4 C21

3	2	2	0.136	10200000.0	0.136	10200000.0	;	C19	O4
3	4	2	0.139	10800000.0	0.139	10800000.0	;	C19	C20
3	6	2	0.139	10800000.0	0.139	10800000.0	;	C19	C18
4	5	2	0.109	12300000.0	0.109	12300000.0	;	C20	H20
13	4	2	0.139	10800000.0	0.139	10800000.0	;	C15	C20
6	7	2	0.136	10200000.0	0.136	10200000.0	;	C18	O5
6	9	2	0.139	10800000.0	0.139	10800000.0	;	C18	C17
7	8	2	0.100	15700000.0	0.100	15700000.0	;	O5	H52
9	10	2	0.109	12300000.0	0.109	12300000.0	;	C17	H17
9	11	2	0.139	10800000.0	0.139	10800000.0	;	C17	C16
11	12	2	0.109	12300000.0	0.109	12300000.0	;	C16	H16
13	11	2	0.139	10800000.0	0.139	10800000.0	;	C15	C16
13	14	2	0.139	10800000.0	0.139	10800000.0	;	C15	C14
14	15	2	0.153	7150000.0	0.153	7150000.0	;	C14	C13
16	15	2	0.153	7150000.0	0.153	7150000.0	;	C12	C13
16	17	2	0.136	10200000.0	0.136	10200000.0	;	C12	O3
16	19	2	0.153	7150000.0	0.153	7150000.0	;	C12	C11
17	18	2	0.100	15700000.0	0.100	15700000.0	;	O3	H32
20	19	2	0.153	7150000.0	0.153	7150000.0	;	C10	C11
20	21	2	0.123	16600000.0	0.123	16600000.0	;	C10	O6
20	22	2	0.153	7150000.0	0.153	7150000.0	;	C10	C9
22	23	2	0.153	7150000.0	0.153	7150000.0	;	C9	C8
24	23	2	0.139	10800000.0	0.139	10800000.0	;	C4	C8
24	25	2	0.139	10800000.0	0.139	10800000.0	;	C4	C3
24	27	2	0.139	10800000.0	0.139	10800000.0	;	C4	C5

```
25    26    2    0.109    12300000.0    0.109    12300000.0 ;    C3    H31
34    25    2    0.139    10800000.0    0.139    10800000.0 ;    C2    C3
27    28    2    0.109    12300000.0    0.109    12300000.0 ;    C5    H51
27    29    2    0.139    10800000.0    0.139    10800000.0 ;    C5    C6
29    30    2    0.109    12300000.0    0.109    12300000.0 ;    C6    H6
31    29    2    0.139    10800000.0    0.139    10800000.0 ;    C7    C6
31    32    2    0.136    10200000.0    0.136    10200000.0 ;    C7    O2
31    34    2    0.139    10800000.0    0.139    10800000.0 ;    C7    C2
32    33    2    0.100    15700000.0    0.100    15700000.0 ;    O2    H22
34    35    2    0.136    10200000.0    0.136    10200000.0 ;    C2    O1
35    36    2    0.143    8180000.0    0.143    8180000.0 ;    O1    C1

[ pairs ]
; ai    aj    fu    c0, c1, ...
1    4    1                        ;    C21    C20
1    6    1                        ;    C21    C18
2    5    1                        ;    O4    H20
2    7    1                        ;    O4    O5
2    9    1                        ;    O4    C17
2    13    1                       ;    O4    C15
3    8    1                        ;    C19    H52
3    10    1                       ;    C19    H17
3    11    1                       ;    C19    C16
3    14    1                       ;    C19    C14
4    7    1                        ;    C20    O5
```

4	9	1	;	C20	C17
4	12	1	;	C20	H16
4	15	1	;	C20	C13
5	6	1	;	H20	C18
5	11	1	;	H20	C16
5	14	1	;	H20	C14
6	12	1	;	C18	H16
6	13	1	;	C18	C15
7	10	1	;	O5	H17
7	11	1	;	O5	C16
8	9	1	;	H52	C17
9	14	1	;	C17	C14
10	12	1	;	H17	H16
10	13	1	;	H17	C15
11	15	1	;	C16	C13
12	14	1	;	H16	C14
13	16	1	;	C15	C12
14	17	1	;	C14	O3
14	19	1	;	C14	C11
15	18	1	;	C13	H32
15	20	1	;	C13	C10
16	21	1	;	C12	O6
16	22	1	;	C12	C9
17	20	1	;	O3	C10
18	19	1	;	H32	C11

19 23 1 ; C11 C8
20 24 1 ; C10 C4
21 23 1 ; O6 C8
22 25 1 ; C9 C3
22 27 1 ; C9 C5
23 26 1 ; C8 H31
23 28 1 ; C8 H51
23 29 1 ; C8 C6
23 34 1 ; C8 C2
24 30 1 ; C4 H6
24 31 1 ; C4 C7
24 35 1 ; C4 O1
25 28 1 ; C3 H51
25 29 1 ; C3 C6
25 32 1 ; C3 O2
25 36 1 ; C3 C1
26 27 1 ; H31 C5
26 31 1 ; H31 C7
26 35 1 ; H31 O1
27 32 1 ; C5 O2
27 34 1 ; C5 C2
28 30 1 ; H51 H6
28 31 1 ; H51 C7
29 33 1 ; C6 H22
29 35 1 ; C6 O1

```
30   32   1                    ;   H6   O2
30   34   1                    ;   H6   C2
31   36   1                    ;   C7   C1
32   35   1                    ;   O2   O1
33   34   1                    ;   H22   C2

[ angles ]
; ai   aj   ak   fu   c0, c1, ...
1   2   3   2   109.5      380.0   109.5      380.0 ;   C21   O4   C19
2   3   4   2   120.0      560.0   120.0      560.0 ;   O4   C19   C20
2   3   6   2   115.0      610.0   115.0      610.0 ;   O4   C19   C18
4   3   6   2   120.0      560.0   120.0      560.0 ;   C20   C19   C18
3   4   5   2   120.0      505.0   120.0      505.0 ;   C19   C20   H20
3   4   13   2   120.0      505.0   120.0      505.0 ;   C19   C20   C15
5   4   13   2   120.0      505.0   120.0      505.0 ;   H20   C20   C15
3   6   7   2   115.0      610.0   115.0      610.0 ;   C19   C18   O5
3   6   9   2   120.0      560.0   120.0      560.0 ;   C19   C18   C17
7   6   9   2   120.0      560.0   120.0      560.0 ;   O5   C18   C17
6   7   8   2   109.5      450.0   109.5      450.0 ;   C18   O5   H52
6   9   10   2   120.0      505.0   120.0      505.0 ;   C18   C17   H17
6   9   11   2   120.0      505.0   120.0      505.0 ;   C18   C17   C16
10   9   11   2   120.0      505.0   120.0      505.0 ;   H17   C17   C16
9   11   12   2   120.0      505.0   120.0      505.0 ;   C17   C16   H16
9   11   13   2   120.0      505.0   120.0      505.0 ;   C17   C16   C15
12   11   13   2   120.0      505.0   120.0      505.0 ;   H16   C16   C15
```

4	13	11	2	120.0	560.0	120.0	560.0	;	C20	C15	C16
4	13	14	2	120.0	560.0	120.0	560.0	;	C20	C15	C14
11	13	14	2	120.0	560.0	120.0	560.0	;	C16	C15	C14
13	14	15	2	115.0	610.0	115.0	610.0	;	C15	C14	C13
14	15	16	2	115.0	610.0	115.0	610.0	;	C14	C13	C12
15	16	17	2	115.0	610.0	115.0	610.0	;	C13	C12	O3
15	16	19	2	115.0	610.0	115.0	610.0	;	C13	C12	C11
17	16	19	2	115.0	610.0	115.0	610.0	;	O3	C12	C11
16	17	18	2	109.5	450.0	109.5	450.0	;	C12	O3	H32
16	19	20	2	115.0	610.0	115.0	610.0	;	C12	C11	C10
19	20	21	2	121.0	685.0	121.0	685.0	;	C11	C10	O6
19	20	22	2	115.0	610.0	115.0	610.0	;	C11	C10	C9
21	20	22	2	121.0	685.0	121.0	685.0	;	O6	C10	C9
20	22	23	2	115.0	610.0	115.0	610.0	;	C10	C9	C8
22	23	24	2	115.0	610.0	115.0	610.0	;	C9	C8	C4
23	24	25	2	120.0	560.0	120.0	560.0	;	C8	C4	C3
23	24	27	2	120.0	560.0	120.0	560.0	;	C8	C4	C5
25	24	27	2	120.0	560.0	120.0	560.0	;	C3	C4	C5
24	25	26	2	120.0	505.0	120.0	505.0	;	C4	C3	H31
24	25	34	2	120.0	505.0	120.0	505.0	;	C4	C3	C2
26	25	34	2	120.0	505.0	120.0	505.0	;	H31	C3	C2
24	27	28	2	120.0	505.0	120.0	505.0	;	C4	C5	H51
24	27	29	2	120.0	505.0	120.0	505.0	;	C4	C5	C6
28	27	29	2	120.0	505.0	120.0	505.0	;	H51	C5	C6
27	29	30	2	120.0	505.0	120.0	505.0	;	C5	C6	H6

```
27   29   31   2   120.0      505.0   120.0      505.0 ;   C5    C6    C7
30   29   31   2   120.0      505.0   120.0      505.0 ;   H6    C6    C7
29   31   32   2   120.0      560.0   120.0      560.0 ;   C6    C7    O2
29   31   34   2   120.0      560.0   120.0      560.0 ;   C6    C7    C2
32   31   34   2   115.0      610.0   115.0      610.0 ;   O2    C7    C2
31   32   33   2   109.5      450.0   109.5      450.0 ;   C7    O2    H22
25   34   31   2   120.0      560.0   120.0      560.0 ;   C3    C2    C7
25   34   35   2   120.0      560.0   120.0      560.0 ;   C3    C2    O1
31   34   35   2   115.0      610.0   115.0      610.0 ;   C7    C2    O1
34   35   36   2   109.5      380.0   109.5      380.0 ;   C2    O1    C1

[ dihedrals ]
; ai    aj    ak    al    fu    c0, c1, m, ...
3    2    4    6    2    0.0    167.4    0.0    167.4    ; imp    C19    O4    C20    C18
4    3    13    5    2    0.0    167.4    0.0    167.4    ; imp    C20    C19    C15    H20
6    9    7    3    2    0.0    167.4    0.0    167.4    ; imp    C18    C17    O5    C19
9    6    11    10    2    0.0    167.4    0.0    167.4    ; imp    C17    C18    C16    H17
11    9    13    12    2    0.0    167.4    0.0    167.4    ; imp    C16    C17    C15    H16
13    14    11    4    2    0.0    167.4    0.0    167.4    ; imp    C15    C14    C16    C20
16    19    17    15    2    0.0    167.4    0.0    167.4    ; imp    C12    C11    O3    C13
20    22    21    19    2    0.0    167.4    0.0    167.4    ; imp    C10    C9    O6    C11
24    23    27    25    2    0.0    167.4    0.0    167.4    ; imp    C4    C8    C5    C3
25    24    34    26    2    0.0    167.4    0.0    167.4    ; imp    C3    C4    C2    H31
27    24    29    28    2    0.0    167.4    0.0    167.4    ; imp    C5    C4    C6    H51
29    27    31    30    2    0.0    167.4    0.0    167.4    ; imp    C6    C5    C7    H6
```

31 29 32 34 2 0.0 167.4 0.0 167.4 ; imp C7 C6 O2 C2
34 25 35 31 2 0.0 167.4 0.0 167.4 ; imp C2 C3 O1 C7
3 4 13 11 2 0.0 209.3 0.0 209.3 ; imp C19 C20 C15 C16
4 13 11 9 2 0.0 209.3 0.0 209.3 ; imp C20 C15 C16 C17
13 11 9 6 2 0.0 209.3 0.0 209.3 ; imp C15 C16 C17 C18
11 9 6 3 2 0.0 209.3 0.0 209.3 ; imp C16 C17 C18 C19
9 6 3 4 2 0.0 209.3 0.0 209.3 ; imp C17 C18 C19 C20
6 3 4 13 2 0.0 209.3 0.0 209.3 ; imp C18 C19 C20 C15
24 25 34 31 2 0.0 209.3 0.0 209.3 ; imp C4 C3 C2 C7
25 34 31 29 2 0.0 209.3 0.0 209.3 ; imp C3 C2 C7 C6
34 31 29 27 2 0.0 209.3 0.0 209.3 ; imp C2 C7 C6 C5
31 29 27 24 2 0.0 209.3 0.0 209.3 ; imp C7 C6 C5 C4
29 27 24 25 2 0.0 209.3 0.0 209.3 ; imp C6 C5 C4 C3
27 24 25 34 2 0.0 209.3 0.0 209.3 ; imp C5 C4 C3 C2
6 3 2 1 1 180.0 16.7 2 180.0 16.7 2 ; dih C18 C19 O4 C21
3 6 7 8 1 180.0 7.1 2 180.0 7.1 2 ; dih C19 C18 O5 H52
15 14 13 4 1 180.0 5.9 2 180.0 5.9 2 ; dih C13 C14 C15 C20
16 15 14 13 1 180.0 5.9 2 180.0 5.9 2 ; dih C12 C13 C14 C15
19 16 15 14 1 180.0 5.9 2 180.0 5.9 2 ; dih C11 C12 C13 C14
15 16 17 18 1 180.0 16.7 2 180.0 16.7 2 ; dih C13 C12 O3 H32
20 19 16 15 1 180.0 5.9 2 180.0 5.9 2 ; dih C10 C11 C12 C13
22 20 19 16 1 180.0 5.9 2 180.0 5.9 2 ; dih C9 C10 C11 C12
23 22 20 19 1 180.0 5.9 2 180.0 5.9 2 ; dih C8 C9 C10 C11
24 23 22 20 1 180.0 5.9 2 180.0 5.9 2 ; dih C4 C8 C9 C10

27 24 23 22 1 180.0 5.9 2 180.0 5.9 2 ; dih C5 C4 C8 C9

29 31 32 33 1 180.0 7.1 2 180.0 7.1 2 ; dih C6 C7 O2 H22

25 34 35 36 1 180.0 16.7 2 180.0 16.7 2 ; dih C3 C2 O1 C1

Glossary

Aβ Amyloid β.

AD Alzheimer's disease.

aMCI amnestic mild cognitive impairment.

APOE Apro lipoprotein E.

APP amyloid precursor protein.

CHARMM Chemistry at HARvard using Molecular Mechanics.

CNS centeral nervous sysem.

DOPS dioleylphosphatidylserine.

DPPC dipalmitoylphosphatidylcholine.

FAD familial Alzheimer's disease.

GIMP GNU image manipulation program.

IUP intrinsically unstructured protein.

LINCS linear constraint solver.

LRPAPL low-density lipoprotein receptor-related protein associated protein 1.

MAPT microtubule-associated protein tau.

MCI mild cognitive impairment.

nAChRs nicotinic acetylcholine receptors.

NFT neurofibrillary tangle.

NMDA N-methyl-D-aspartate.

OPLS optimized potentials for liquid simulation.

P75NTR P75 neurotrophin receptor.

PDB Protein Data Bank.

PHF paired helical filaments.

POPG palmitoyloleoylphosphatidylglycerol.

PrP^C prion protein.

RAGE receptor for advanced glycosylation end-products.

REMD replica exchange molecular dynamics.

sAD sporadic Alzheimer's disease.

SEC-R serpin-enzyme complex receptor.

SFs straight filaments.

SSRI selective serotonin reuptake inhibitor.

References

[1] Evin, G.; Weidemann, A. Biogenesis and metabolism of Alzheimer's disease Abeta amyloid peptides. *Peptides* **2002**, *23*, 1285–1297.

[2] Hardy, J.; Selkoe, D. J. The amyloid hypothesis of Alzheimer's disease: progress and problems on the road to therapeutics. *Science* **2002**, *297*, 353–356.

[3] Zhao, L. N.; Long, H.; Mu, Y.; Chew, L. Y. The toxicity of amyloid β oligomers. *Int. J. Mol. Sci.* **2012**, *13*, 7303–7327.

[4] Kirkitadze, M. D.; Bitan, G.; Teplow, D. B. Paradigm shifts in Alzheimer's disease and other neurodegenerative disorders: the emerging role of oligomeric assemblies. *J. Neurosci. Res.* **2002**, *69*, 567–577.

[5] Bucciantini, M.; Giannoni, E.; Chiti, F.; Baroni, F.; Formigli, L.; Zurdo, J.; Taddei, N.; Ramponi, G.; Dobson, C. M.; Stefani, M. Inherent toxicity of aggregates implies a common mechanism for protein misfolding diseases. *Nature* **2002**, *416*, 507–511.

[6] Walsh, D. M.; Klyubin, I.; Fadeeva, J. V.; Cullen, W. K.; Anwyl, R.; Wolfe, M. S.; Rowan, M. J.; Selkoe, D. J. Naturally secreted oligomers of amyloid β protein potentl y inhibit hippocampal long-term potentiation in vivo. *Nature* **2002**, *416*, 535–539.

[7] Resende, R.; Ferreiro, E.; Pereira, C.; de Oliveira, C. R. Neurotoxic effect of oligomeric and fibrillar species of amyloid β peptide 1-42: involvement of endoplasmic reticulum calcium release in oligomer-induced cell death. *Neuroscience* **2008**, *155*, 725–737.

[8] Haass, C.; Selkoe, D. J. Soluble protein oligomers in neurodegeneration: lessons from the Alzheimer's amyloid β-peptide. *Nat. Rev. Mol. Cell Biol.*

2007, *8*, 101–112.

[9] Leoni, V.; Solomon, A.; Kivipelto, M. Links between ApoE brain cholesterol metabolism, tau and amyloid β-peptide in patients with cognitive impairment. *Biochem. Soc. Trans.* **2010**, *38*, 1021–1025.

[10] Liang, G.; Li, X.; Chen, L.; Yang, S.; Wu, X.; Studer, E.; Gurley, E.; Hylemon, P. B.; Ye, F.; Li, Y.; Zhou, H. Synthesis and anti-inflammatory activities of mono-carbonyl analogues of curcumin. *Bioorg. Med. Chem. Lett.* **2008**, *18*, 1525–1529.

[11] Hatcher, H.; Planalp, R.; Cho, J.; Tortia, F. M.; Torti, S. V. Curcumin: From ancient medicine to current clinical trials. *Cellular and Molecular Life Sciences* **2008**, *65*, 1631–1652.

[12] Yoshida, H.; Okumura, N.; Nishimura, Y.; Kitagishi, Y.; Matsuda, S. Turmeric and curcumin suppress presenilin 1 protein expression in Jurkat cells. *Experimental and Therapeutic Medicine* **2011**, *2*, 629–632.

[13] Balasubramanian, K. Molecular orbital basis for yellow curry spice curcumin's prevention of Alzheimer's disease. *J. Agric. Food Chem.* **2006**, *54*, 3512–3520.

[14] Yang, F.; Lim, G. P.; Begum, A. N.; Ubeda, O. J.; Simmons, M. R.; Ambegaokar, S. S.; Chen, P. P.; Kayed, R.; Glabe, C. G.; Frautschy, S. A.; Cole, G. M. Curcumin inhibits formation of amyloid β oligomers and fibrils, binds plaques, and reduces amyloid in vivo. *J. Biol. Chem.* **2005**, *280*, 5892–5901.

[15] Geng, J.; Zhao, C.; Ren, J.; Qu, X. Alzheimer's disease amyloid beta converting left-handed Z-DNAs back to right-handed B-form. *Chem. Commun.* **2010**, *46*, 7187–7189.

[16] Atamna, H.; Boyle, K. Amyloid-β peptide binds with heme to form a peroxidase: Relationship to the cytopathologies of Alzheimer's disease. *Proc. Natl.*

Acad. Sci. U.S.A. **2006**, *103*, 3381–3386.

[17] Garcia-Alloza, M.; Borrelli, L. A.; Rozkalne, A.; Hyman, B. T.; Bacskai, B. J. Curcumin labels amyloid pathology in vivo, disrupts existing plaques, and partially restores distorted neurites in an Alzheimer mouse model. *J. Neurochem.* **2007**, *102*, 1095–1104.

[18] Aggarwal, B. B.; Harikumar, K. B. Potential therapeutic effects of curcumin, the anti-inflammatory agent, against neurodegenerative, cardiovascular, pulmonary, metabolic, autoimmune and neoplastic diseases. *The International Journal of Biochemistry and Cell Biology* **2009**, *41*, 40–59.

[19] Kumar, S.; Bandyopadhyay, U. Free heme toxicity and its detoxification systems in human. *Toxicol. Lett.* **2005**, *157*, 175–188.

[20] Smith, A. G.; Raven, E. L.; Chernova, T. The regulatory role of heme in neurons. *Metallomics* **2011**, *3*, 955–962.

[21] Atamna, H.; II, W. H. F. A role for heme in Alzheimer's disease: Heme binds amyloid β and has altered metabolism. *Proc. Natl. Acad. Sci. U.S.A.* **2004**, *101*, 11153–11158.

[22] Bao, Q.; Luo, Y.; Li, W.; Sun, X.; Zhu, C.; Li, P.; Huang, Z.-X.; Tan, X. The mechanism for heme to prevent Aβ_{1-40} aggregation and its cytotoxicity. *J. Biol. Inorg. Chem* **2011**, *16*, 809–816.

[23] Stevens, J. M.; Uchida, T.; Daltrop, O.; Ferguson, S. J. Covalent cofactor attachment to proteins: cytochrome c biogenesis. *Biochem. Soc. Trans.* **2005**, *33*, 792–795.

[24] Sanders, C.; Turkarslan, S.; Lee, D.-W.; Daldalsend, F. Cytochrome c biogenesis: the Ccm system. *Trends in Microbiology* **2010**, *18*, 266–274.

[25] Aramini, J. M.; Hamilton, K.; Rossi, P.; Ertekin, A.; Lee, H.; Lemak, A.;

Wang, H.; Xiao, R.; Acton, T. B.; Everett, J. K.; Montelione, G. T. Solution NMR structure, backbone dynamics, and heme-binding properties of a novel cytochrome c maturation protein CcmE from desulfovibrio vulgaris. *Biochemistry* **2012**, *51*, 3705–3707.

[26] Atamna, H. Amino acids variations in amyloid-β peptides, mitochondrial dysfunction, and new therapies for Alzheimer's disease. *J. Bioenerg. Biomembr.* **2009**, *41*, 457–464.

[27] Yuan, C.; Yi, L.; Yang, Z.; Deng, Q.; Huang, Y.; Li, H.; Gao, Z. Amyloid beta-heme peroxidase promoted protein nitrotyrosination: relevance to widespread protein nitration in Alzheimer's disease. *J. Biol. Inorg. Chem* **2012**, *17*, 197–207.

[28] Akiyama, H. et al. Inflammation and Alzheimer's disease. *Neurobiology of Aging* **2000**, *21*, 383–421.

[29] Heneka, M. T.; O'Banion, M. K. Inflammatory processes in Alzheimer's disease. *J. of Neuroimmunol.* **2007**, *184*, 69–91.

[30] Cameron, B.; Landreth, G. E. Inflammation, microglia, and Alzheimer's disease. *Neurobiology of Disease* **2010**, *37*, 503–509.

[31] Wyss-Coray, T. Inflammation in Alzheimer disease: driving force, bystander or beneficial response? *Nature Med.* **2006**, *12*, 1005–1015.

[32] Salminen, A.; Ojala, J.; Kauppinen, A.; Kaarniranta, K.; Suuronen, T. Inflammation in Alzheimer's disease: Amyloid-β oligomers trigger innate immunity defence via pattern recognition receptors. *Progress in Neurobiology* **2009**, *87*, 181–194.

[33] Tripathy, D.; Thirumangalakudi, L.; Grammas, P. RANTES upregulation in the Alzheimer's disease brain: A possible neuroprotective role. *Neurobiology*

of Aging **2010**, *31*, 8–16.

[34] Zhang, C.; Liu, Y.; Gilthorpe, J.; van der Maarel, J. R. C. MRP14 (S100A9) protein interacts with Alzheimer beta-amyloid peptide and induces its fibrillization. *PLoS One* **2012**, *7*, e32953.

[35] Rammes, A.; Roth, J.; Goebeler, M.; Klempt, M.; Hartmann, M.; Sorg, C. Myeloid-related protein (MRP) 8 and MRP14, calcium-binding proteins of the S100 family, are secreted by activated monocytes via a novel, tubulin-dependent pathway. *J. Biol. Chem.* **1997**, *272*, 9496–9502.

[36] Chang, K.-A.; Kim, H. J.; Suh, Y.-H. The role of S100a9 in the pathogenesis of Alzheimer's disease: the therapeutic effects of S100a9 knockdown or knockout. *Neurodegenerative Disease* **2012**, *10*, 27–29.

[37] Gould, H.; Tobochnik, J.; Christian, W. *An Introduction to Computer Simulation Methods: Applications to Physical System*, 3rd ed.; Addison-Wesley, 2006.

[38] Charalambous, C.; Conn, A. R. An efficient method to solve the minimax problem directly. *SIAM J. Numer. Anal.* **1978**, *15*, 162–178.

[39] Hjorteland, T. The action variational principle in cosmology. M.Sc. thesis, University of Oslo, 1999.

[40] Press, W. H.; Teukolsky, S. A.; Vetterling, W. T.; Flannery, B. P. *Numerical Recipes in C: The Art of Scientific Computing*, 2nd ed.; Cambridge University Press: Cambridge, 1992.

[41] Kabsch, W.; Sander, C. Dictionary of protein secondary structure: pattern recognition of hydrogen-bonded and geometrical features. *Biopolymers* **1983**, *22*, 2577–637.

[42] Ritchie, K.; Kildea, D.; Robine, J.-M. The relationship between age and the

prevalence of senile dementia: A meta-analysis of recent data. *Int. J. Epidemiol.* **1992**, *21*, 763–769.

[43] Bird, T. D. In *GeneReviews^{TM} [Internet]*; Pagon, R. A., Bird, T. D., Dolan, C. R., et al.,, Eds.; 1998.

[44] Duara, R.; Alberola, R. F.; Barker, W. W.; Loewenstein, D. A.; Zatinsky, M.; Eisdorfer, C. E.; Weinberg, G. B. A comparison of familial and sporadic Alzheimer's disease. *Neurobiology* **1993**, *43*, 1377–1384.

[45] Bird, T. D. Genetic aspects of Alzheimer disease. *Genet. Med.* **2008**, *10*, 231–239.

[46] Gatz, M.; Reynolds, C. A.; Fratiglioni, L.; Johansson, B.; Mortimer, J. A.; Berg, S.; Fiske, A.; Pedersen, N. L. Role of genes and environments for explaining Alzheimer disease. *Arch. Gen. Psychiatry* **2006**, *63*, 168–174.

[47] Minati, L.; Edginton, T.; Bruzzone, M. G.; Giaccone, G. Current concepts in Alzheimer's disease: a multidisciplinary review. *Am. J. Aszheimers Dis. Other Demen.* **2009**, *24*, 95–121.

[48] Combarros, O.; Arcaya, A.; Guerra, M.; Infante, J.; Berciano, J. Candidate gene association studies in sporadic Alzheimer's disease. *Dement. Geriatr. Cogn. Disord.* **2002**, *14*, 41–54.

[49] Mucke, L. Neuroscience: Alzheimer's disease. *Nature* **2009**, *461*, 895–897.

[50] Arriagada, P. V.; Growdon, J. H.; Hedley-Whyte, E. T.; Hyman, B. T. Neurofibrillary tangles but not senile plaques parallel duration and severity of Alzheimer's disease. *Neurology* **1992**, *42*, 631.

[51] Chen, F.; David, D.; Ferrari, A.; Gotz, J. Posttranslational modifications of tau - role in human tauopathies and modeling in transgenic animals. *Current Drug Targets* **2004**, *13*, 503–515.

[52] Flaherty, D. B.; Soria, J. P.; Tomasiewicz, H. G.; Wood, J. G. Phosphorylation of human tau protein by microtubule-associated kinases: GSK3b and cdk5 are key participants. *J. Neurosci. Res.* **2000**, *62*, 463–472.

[53] Avila, J.; Lucas, J. J.; pérez, M.; Herández, F. Role of tau protein in both physiological and pathological conditions. **2004**, *84*, 361–384.

[54] Hoover, B. R.; Reed, M. N.; Su, J.; Penrod, R. D.; Kotilinek, L. A.; Grant, M. K.; Pitstick, R.; Carlson, G. A.; Lanier, L. M.; Yuan, L.-L.; Ashe, K. H.; Liao, D. Tau mislocalization to dendritic spines mediates synaptic dysfunction independently of neurodegeneration. *Neuron* **2010**, *68*, 1067–1081.

[55] Crowther, R. A.; Wischik, C. M. Image reconstruction of the Alzheimer paired helical filament. *The EMBO journal* **1985**, *4*, 3661–3665.

[56] Friedhoff, P.; von Bergen, M.; Mandelkow, E.-M.; Mandelkow, E. Structure of tau protein and assembly into paired helical filaments. *BBA - Protein Proteom.* **2000**, *1502*, 122–132.

[57] Hoe, H.-S.; Lee, K. J.; Rosalind S.E. Carney, Jiyeon Lee, Alexandra Markova, Ji-Yun Lee, Brian W. Howell, Bradley T. Hyman, Daniel T.S. Pak, Guojun Bu,; Rebeck, G. W. Interaction of reelin with amyloid precursor protein promotes neurite outgrowth. *J. Neurosci.* **2009**, *29*, 7459–7473.

[58] Bellingham, S. A.; Ciccotosto, G. D.; Needham, B. E.; Fodero, L. R.; White, A. R.; Masters, C. L.; Cappai, R.; Camakaris, J. Gene knockout of amyloid precursor protein and amyloid precursor-like protein-2 increases cellular copper levels in primary mouse cortical neurons and embryonic fibroblasts. *J. Neurochem.* **2004**, *91*, 423–428.

[59] Priller, C.; Bauer, T.; Mitteregger, G.; Krebs, B.; Kretzschmar, H. A.; Herms, J. Synapse formation and function is modulated by the amyloid precursor protein.

Neurobiology of Disease **2006**, *26*, 7212–7221.

[60] H'erard, A. S.; Besret, L.; Dubois, A.; Dauguet, J.; Delzescaux, T.; Hantraye, P.; Bonvento, G.; Moya, K. L. siRNA targeted against amyloid precursor protein impairs synaptic activity in vivo. *Neurobiology of Aging* **2006**, *27*, 1740–1750.

[61] Zheng, H.; Jiang, M.; Trumbauer, M. E.; Sirinathsinghji, D. J. S.; Hopkins, R.; Smith, D. W.; Heavens, R. P.; Dawson, G. R.; Boyce, S.; Conner, M. W.; Stevens, K. A.; Slunt, H. H.; Sisodia, S. S.; Chen, H. Y.; der Ploeg, L. H. T. V. β-amyloid precursor protein-deficient mice show reactive gliosis and decreased locomotor activity. *Cell* **1995**, *81*, 525–531.

[62] Donald, J. M. M.; Savva, G. M.; Brayne, C.; Welzel, A. T.; Forster, G.; Shankar, G. M.; Selkoe, D. J.; Ince, P. G.; Walsh, D. M. The presence of sodium dodecyl sulphate-stable Aβ dimers is strongly associated with Alzheimer-type dementia. *Brain* **2010**, *133*, 1328–1341.

[63] Talafous, J.; Marcinowski, K. J.; Klopman, G.; Zagorski, M. G. Solution structure of residues 1-28 of the amyloid beta-peptide. *Biochemistry* **1994**, *33*, 7796.

[64] Talafous, J.; Marcinowski, K. J.; Klopman, G.; Zagorski, M. G. Solution structure of residues 1-28 of the amyloid beta-peptide. *Biochemistry* **1994**, *33*, 7796.

[65] Sticht, H.; Bayer, P.; Willbold, D.; Dames, S.; Hilbich, C.; Beyreuther, K.; Frank, R. W.; Rosch, P. Structure of amyloid A4-(1-40)-peptide of Alzheimer's disease. *Eur. J. Biochem.* **1995**, *233*, 298.

[66] Coles, M.; Bicknell, W.; Watson, A. A.; Fairlie, D. P.; Craik, D. J. Solution structure of amyloid beta-peptide(1-40) in a water-micelle environment. Is the membrane-spanning domain where we think it is? *Biochemistry* **1998**, *37*,

11077.

[67] Watson, A. A.; Fairlie, D. P.; Craik, D. J. Solution structure of methionine-oxidized amyloid beta-peptide (1-40). Does oxidation affect conformational switching? *Biochemistry* **1998**, *37*, 12706.

[68] Poulsen, S.-A.; Watson, A. A.; Craik, D. J. Solution structures in aqueous SDS micelles of two amyloid beta peptides of A β(1-28) mutated at the α-secretase cleavage site (K16E, K16F). *J. Struct. Biol.* **2000**, *130*, 152.

[69] Zhang, S.; Iwata, K.; Lachenmann, M. J.; Peng, J. W.; Li, S.; Stimson, E. R.; Lu, Y.; Felix, A. M.; Maggio, J. E.; Lee, J. P. The Alzheimer's peptide a beta adopts a collapsed coil structure in water. *J. Struct. Biol.* **2000**, *130*, 141.

[70] Crescenzi, O.; Tomaselli, S.; Guerrini, R.; Salvadori, S.; D'Ursi, A. M.; Temussi, P. A.; Picone, D. Solution structure of the Alzheimer amyloid beta-peptide (1-42) in an apolar microenvironment. Similarity with a virus fusion domain. *Eur. J. Biochem.* **2002**, *269*, 5648.

[71] Huang, J.; Yao, Y.; Lin, J.; Ye, Y. H.; Sun, W. Y.; Tang, W. X. The solution structure of rat Abeta-(1-28) and its interaction with zinc ion: insights into the scarcity of amyloid deposition in aged rat brain. *J. Biol. Inorg. Chem.* **2004**, *9*, 635.

[72] D'Ursi, A. M.; Armenante, M. R.; Guerrini, R.; Salvadori, S.; Sorrentino, G.; Picone, D. Solution structure of amyloid beta-peptide (25-35) in different media. *J. Med. Chem.* **2004**, *47*, 4238.

[73] Zirah, S.; Kozin, S. A.; Mazur, A. K.; Blond, A.; Cheminant, M.; Segalas-Milazzo, I.; Debey, P.; Rebuffat, S. Structural changes of region 1-16 of the Alzheimer disease amyloid beta-peptide upon zinc binding and in vitro aging. *J. Biol. Chem.* **2006**, *281*, 2161.

[74] Istrate, A. N.; Tsvetkov, P. O.; Mantsyzov, A. B.; Kulikova, A. A.; Kozin, S. A.; Makarov, A. A.; Polshakov, V. I. NMR solution structure of rat Abeta(1-16): toward understanding the mechanism of rats' resistance to Alzheimer's disease. *Biophys.J.* **2012**, *102*, 143.

[75] Richard, T.; Papastamoulis, Y.; Pierre, W. T.; Monti, J. P. 3D NMR structure of a complex between the amyloid beta peptide (1-40) and the polyphenol epsilon-viniferin glucoside: Implications in Alzheimer's disease. *Biochim.Biophys.Acta* **2013**, *1830*, 5074.

[76] Colletier, J.; Laganowsky, A.; Landau, M.; Zhao, M.; Soriaga, A. B.; Goldschmidt, L.; Flot, D.; Cascio, D.; Sawaya, M. R.; Eisenberg, D. Molecular basis for Amyloid-β polymorphism. *Proc. Natl. Acad. Sci. U.S.A.* **2011**, *108*.

[77] Landau, M.; Sawaya, M. R.; Faull, K. F.; Laganowsky, A.; Jiang, L.; Sievers, S. A.; Liu, J.; Barrio, J. R.; Eisenberg, D. Towards a pharmacophore for amyloid. *Plos Biol.* **2011**, *9*, e1001080.

[78] Hoyer, W.; Gronwall, C.; Jonsson, A.; Stahl, S.; Hard, T. Stabilization of a beta-hairpin in monomeric Alzheimer's amyloid-beta peptide inhibits amyloid formation. *Proc. Natl. Acad. Sci. U.S.A.* **2008**, *105*, 5104.

[79] Hynes, T. R.; Randal, M.; Kennedy, L. A.; Eigenbrot, C.; Kossiakoff, A. A. X-ray crystal structure of the protease inhibitor domain of Alzheimer's amyloid beta-protein precursor. *Biochemistry* **1990**, *29*, 10022.

[80] Perona, J. J.; Tsu, C. A.; McGrath, M. E.; Craik, C. S.; Fletterick, R. J. Relocating a negative charge in the binding pocket of trypsin. *J. Mol. Biol.* **1993**, *230*, 949.

[81] Scheidig, A. J.; Hynes, T. R.; Pelletier, L. A.; Wells, J. A.; Kossiakoff, A. A. Crystal structures of bovine chymotrypsin and trypsin complexed to the in-

hibitor domain of Alzheimer's amyloid beta-protein precursor (APPI) and basic pancreatic trypsin inhibitor (BPTI): engineering of inhibitors with altered specificities. *Protein Sci.* **1997**, *6*, 1824.

[82] Zhang, Z.; Lee, C. H.; Mandiyan, V.; Borg, J. P.; Margolis, B.; Schlessinger, J.; Kuriyan, J. Sequence-specific recognition of the internalization motif of the Alzheimer's amyloid precursor protein by the X11 PTB domain. *EMBO J.* **1997**, *16*, 6150.

[83] Rossjohn, J.; Cappai, R.; Feil, S. C.; Henry, A.; McKinstry, W. J.; Galatis, D.; Hesse, L.; Multhaup, G.; Beyreuther, K.; Masters, C. L.; Parker, M. W. Crystal structure of the N-terminal, growth factor-like domain of Alzheimer amyloid precursor protein. *Nat.Struct.Mol.Biol.* **1999**, *6*, 331.

[84] Yun, M.; Keshvara, L.; Park, C.-G.; Zhang, Y.-M.; Dickerson, J. B.; Zheng, J.; Rock, C. O.; Curran, T.; Park, H.-W. Crystal structures of the Dab homology domains of mouse disabled 1 and 2. *J. Biol. Chem.* **2003**, *278*, 36581.

[85] Barnham, K. J.; McKinstry, W. J.; Multhaup, G.; Galatis, D.; Morton, C. J.; Curtain, C. C.; Williamson, N. A.; White, A. R.; Hinds, M. G.; Norton, R. S.; Beyreuther, K.; Masters, C. L.; Parker, M. W.; Cappai, R. Structure of the Alzheimer's disease amyloid precursor protein copper binding Domain: A regulator of neuronal copper homeostasis. *J. Biol. Chem.* **2003**, *278*, 17407.

[86] Dulubova, I.; Ho, A.; Huryeva, I.; Sudhof, T. C.; Rizo, J. Three-dimensional structure of an independently folded extracellular domain of human amyloid-beta precursor protein. *Biochemistry* **2004**, *43*, 9588.

[87] Navaneetham, D.; Jin, L.; Pandey, P.; Strickler, J. E.; Babine, R. E.; Abdel-Meguid, S. S.; Walsh, P. N. Structural and mutational analyses of the molecular interactions between the catalytic domain of factor XIa and the kunitz protease

inhibitor domain of protease nexin 2. *J. Biol. Chem.* **2005**, *280*, 36175.

[88] Luhrs, T.; Ritter, C.; Adrian, M.; Riek-Loher, D.; Bohrmann, B.; Dobeli, H.; Schubert, D.; Riek, R. 3D structure of Alzheimer's amyloid-beta(1-42) fibrils. *Proc. Natl. Acad. Sci. U.S.A.* **2005**, *102*, 17347.

[89] Shen, Y.; Joachimiak, A.; Rosner, M. R.; Tang, W. J. Structures of human insulin-degrading enzyme reveal a new substrate recognition mechanism. *Nature* **2006**, *443*, 874.

[90] Kong, G. K.; Adams, J. J.; Harris, H. H.; Boas, J. F.; Curtain, C. C.; Galatis, D.; Masters, C. L.; Barnham, K. J.; McKinstry, W. J.; Cappai, R.; Parker, M. W. Structural studies of the Alzheimer's amyloid precursor protein copper-binding domain reveal how it binds copper ions. *J. Mol. Biol.* **2007**, *367*, 161.

[91] Kong, G. K.; Adams, J. J.; Cappai, R.; Parker, M. W. Structure of Alzheimer's disease amyloid precursor protein copper-binding domain at atomic resolution. *Acta Crystallogr., Sect. F* **2007**, *63*, 824.

[92] Gardberg, A. S.; Dice, L. T.; Ou, S.; Rich, R. L.; Helmbrecht, E.; Ko, J.; Wetzel, R.; Myszka, D. G.; Patterson, P. H.; Dealwis, C. Molecular basis for passive immunotherapy of Alzheimer's disease. *Proc. Natl. Acad. Sci. U.S.A.* **2007**, *104*, 15664.

[93] Li, H.; Koshiba, S.; Hayashi, F.; Tochio, N.; Tomizawa, T.; Kasai, T.; Yabuki, T.; Motoda, Y.; Harada, T.; Watanabe, S.; Inoue, M.; Hayashizaki, Y.; Tanaka, A.; Kigawa, T.; Yokoyama, S. Structure of the C-terminal phosphotyrosine interaction domain of Fe65L1 complexed with the cytoplasmic tail of amyloid precursor protein reveals a novel peptide binding mode. *J. Biol. Chem.* **2008**, *283*, 27178.

[94] Miles, L. A.; Wun, K. S.; Crespi, G. A.; Fodero-Tavoletti, M. T.; Galatis, D.;

Bagley, C. J.; Beyreuther, K.; Masters, C. L.; Cappai, R.; McKinstry, W. J.; Barnham, K. J.; Parker, M. W. Amyloid-beta-anti-amyloid-beta complex structure reveals an extended conformation in the immunodominant B-cell epitope. *J. Mol. Biol.* **2008**, *377*, 192.

[95] Radzimanowski, J.; Simon, B.; Sattler, M.; Beyreuther, K.; Sinning, I.; Wild, K. Structure of the intracellular domain of the amyloid precursor protein in complex with Fe65-PTB2. *Embo Rep.* **2008**, *9*, 1140.

[96] Mirza, Z.; Vikram, G.; Singh, N.; Sinha, M.; Bhushan, A.; Sharma, S.; Srinivasan, A.; Kaur, P.; Singh, T. P. Phospholipase A2 prevents the aggregation of Amyloid beta peptides: Crystal structure of the complex of phospholipase A2 with octapeptide fragment of Amyloid beta peptide, Asp-Ala-Glu-Phe-Arg-His-Asp-Ser at 2 Å resolution. *To be Published.*

[97] Basi, G. S. et al. Structural correlates of antibodies associated with acute reversal of amyloid beta-related behavioral deficits in a mouse model of Alzheimer disease. *J. Biol. Chem.* **2010**, *285*, 3427.

[98] Guo, Q.; Manolopoulou, M.; Bian, Y.; Schilling, A. B.; Tang, W. J. Molecular basis for the recognition and cleavages of Igf-II, Tgf-Alpha, and amylin by human insulin degrading enzyme. *J. Mol. Biol.* **2010**, *395*, 443.

[99] Dahms, S. O.; Hoefgen, S.; Roeser, D.; Schlott, B.; Guhrs, K. H.; Than, M. E. Structure and biochemical analysis of the heparin-induced E1 dimer of the amyloid precursor protein. *Proc. Natl. Acad. Sci. U.S.A.* **2010**, *107*, 5386.

[100] Burgos, P. V.; Mardones, G. A.; Rojas, A. L.; daSilva, L. L.; Prabhu, Y.; Hurley, J. H.; Bonifacino, J. S. Sorting of the Alzheimer's disease amyloid precursor protein mediated by the AP-4 complex. *Dev. Cell* **2010**, *18*, 436.

[101] Pandey, N.; Mirza, Z.; Vikram, G.; Singh, N.; Bhushan, A.; Kaur, P.; Srini-

vasan, A.; Sharma, S.; Singh, T. P. Crystal structure of the complex formed between Phospholipase A2 with beta-amyloid fragment, Lys-Gly-Ala-Ile-Ile-Gly-Leu-Met at 1.8 Å resolution. *To be Published.*

[102] Salameh, M. A.; Soares, A. S.; Navaneetham, D.; Sinha, D.; Walsh, P. N.; Radisky, E. S. Determinants of affinity and proteolytic stability in interactions of Kunitz family protease inhibitors with mesotrypsin. *J. Biol. Chem.* **2010**, *285*, 36896.

[103] Streltsov, V. A.; Varghese, J. N.; Masters, C. L.; Nuttall, S. D. Crystal Structure of the Amyloid-beta p3 Fragment Provides a Model for Oligomer Formation in Alzheimer's Disease. *J. Neurosci.* **2011**, *31*, 1426.

[104] Das, S.; Raychaudhuri, M.; Sen, U.; Mukhopadhyay, D. Functional implications of the conformational switch in AICD peptide upon binding to Grb2-SH2 domain. *J. Mol. Biol.* **2011**, *414*, 230.

[105] Lee, S.; Xue, Y.; Hu, J.; Wang, Y.; Liu, X.; Demeler, B.; Ha, Y. The E2 domains of APP and APLP1 share a conserved mode of dimerization. *Biochemistry* **2011**, *50*, 5464.

[106] Wang, Y.; Ha, Y. The X-ray structure of an antiparallel dimer of the human amyloid precursor protein E2 domain. *Mol. Cell* **2004**, *15*, 353.

[107] Colletier, J.; Laganowsky, A.; Landau, M.; Zhao, M.; Soriaga, A. B.; Goldschmidt, L.; Flot, D.; Cascio, D.; Sawaya, M. R.; Eisenberg, D. Molecular Basis for Amyloid-Beta Polymorphism. *Proc. Natl. Acad. Sci. U.S.A.* **2011**, *108*.

[108] Hashimoto, H.; Takeuchi, T.; Komatsu, K.; Miyazaki, K.; Sato, M.; Higashi, S. Structural basis for matrix metalloproteinase-2 (MMP-2)-selective inhibitory action of beta-amyloid precursor protein-derived inhibitor. *J. Biol. Chem.* **2011**,

[109] Petkova, A.; Yau, W.; Tycko, R. Experimental constraints on quaternary structure in Alzheimer's beta-amyloid fibrils. *Biochemistry* **2006**, *45*, 512.

[110] Paravastu, A.; Leapman, R.; Yau, W.; Tycko, R. Molecular structural basis for polymorphism in Alzheimer's beta-amyloid fibrils. *Proc. Natl. Acad. Sci. U.S.A.* **2008**, *105*, 18354.

[111] Qiang, W.; Yau, W. M.; Luo, Y.; Mattson, M. P.; Tycko, R. Antiparallel beta-sheet architecture in Iowa-mutant beta-amyloid fibrils. *Proc. Natl. Acad. Sci. U.S.A.* **2012**, *109*, 4448.

[112] Nadezhdin, K. D.; Bocharova, O. V.; Bocharov, E. V.; Arseniev, A. S. Dimeric structure of transmembrane domain of amyloid precursor protein in micellar environment. *Febs Lett.* **2012**, *586*, 1692.

[113] Barrett, P. J.; Song, Y.; Horn, W. D. V.; Hustedt, E. J.; Schafer, J. M.; Hadziselimovic, A.; Beel, A. J.; Sanders, C. R. The amyloid precursor protein has a flexible transmembrane domain and binds cholesterol. *Science* **2012**, *336*, 1171.

[114] Nadezhdin, K. D.; Bocharova, O. V.; Bocharov, E. V.; Arseniev, A. S. Structural and dynamic study of the transmembrane domain of the amyloid precursor protein. *Acta Nature* **2011**, *3*, 76.

[115] Porte, S. L. L.; Bollini, S. S.; Lanz, T. A.; Abdiche, Y. N.; Rusnak, A. S.; Ho, W. H.; Kobayashi, D.; Harrabi, O.; Pappas, D.; Mina, E. W.; Milici, A. J.; Kawabe, T. T.; Bales, K.; Lin, J. C.; Pons, J. Structural basis of C-terminal beta-Amyloid peptide binding by the antibody ponezumab for the treatment of Alzheimer's disease. *J. Mol. Biol.* **2012**, *421*, 536.

[116] Dahms, S. O.; Konnig, I.; Roeser, D.; Guhrs, K. H.; Mayer, M. C.; Kaden, D.; Multhaup, G.; Than, M. E. Metal binding dictates conformation and function

of the amyloid precursor protein (APP) E2 domain. *J. Mol. Biol.* **2012**, *416*, 452.

[117] Xie, X.; Yan, X.; Wang, Z.; Zhou, H.; Diao, W.; Zhou, W.; Long, J.; Shen, Y. Open-closed motion of Mint2 regulates APP metabolism. *J. Mol. Cell Biol.* **2013**, *5*, 56.

[118] Miles, L. A.; Crespi, G. A.; Doughty, L.; Parker, M. W. Bapineuzumab captures the N-terminus of the Alzheimer's disease amyloid-beta peptide in a helical conformation. *Sci Rep* **2013**, *3*, 1302.

[119] Lu, J. X.; Qiang, W.; Yau, W. M.; Schwieters, C. D.; Meredith, S. C.; Tycko, R. Molecular structure of beta-Amyloid fibrils in Alzheimer's disease brain tissue. *Cell* **2013**, *154*, 1268.

[120] Chen, W.; Lopez, M.; Gamache, E.; Li, Y.; Wang, C. Familial Alzheimer's mutation V44M promotes helical unwinding at the ε-cleavage site for Abeta42 production. *To be Published.*

[121] Jang, S.; Shin, S. Amyloid β-peptide oligomerization in silico: dimer and trimer. *J. Phys. Chem. B* **2006**, *110*, 1955–1958.

[122] Urbanc, B.; Cruz, L.; Ding, F.; Sammond, D.; Khare, S.; Buldyrev, S. V.; Stanley, H. E.; Dokholyan, N. V. Molecular dynamics simulation of amyloid β dimer formation. *Biophys. J.* **2004**, *87*, 2310–2321.

[123] Xu, Y.; Shen, J.; Luo, X.; Zhu, W.; Chen, K.; Ma, J.; Jiang, H. Conformational transition of amyloid β-peptide. *Proc. Natl. Acad. Sci. U.S.A.* **2005**, *102*, 5403–5407.

[124] Lemkul, J. A.; Bevan, D. R. A comparative molecular dynamics analysis of the amyloid β-peptide in a lipid bilayer. *Arch. Biochem. Biophys.* **2008**, *470*, 54–63.

[125] Bitan, G.; Kirkitadze, M. D.; Lomakin, A.; Vollers, S. S.; Benedek, G. B.; Teplow, D. B. Amyloid β-protein (Aβ) assembly: Aβ40 and Aβ42 oligomerize through distinct pathways. *Proc. Natl. Acad. Sci. U.S.A.* **2003**, *100*, 330–335.

[126] LaFerla, F. M. Pathways linking Aβ and tau pathologies. *Biochem. Soc. Trans.* **2010**, *38*, 993–995.

[127] Gouras, G. K.; Tsai, J.; Naslund, J.; Vincent, B.; Edgar, M.; Checler, F.; Greenfield, J. P.; Haroutunian, V.; Buxbaum, J. D.; Xu, H.; Greengard, P.; Relkin, N. R. Intraneuronal Abeta42 accumulation in human brain. *Am. J. Pathol.* **2000**, *156*, 15–20.

[128] Rissman, R.; Poon, W. W.; Blurton, M.; Oddo, S.; Torp, R.; Vitek, M.; LaFerla, F.; Rohn, T. T. Caspase-cleavage of tau is an early event in Alzheimer disease tangle pathology. *J. Clin. Invest.* **2004**, *114*, 121–130.

[129] Blurton-Jones, M.; LaFerla, F. M. Pathways by which Abeta facilitates tau pathology. *Curr. Alzheimer Res.* **2006**, *3*, 437–448.

[130] Jang, H.; Zheng, J.; Lal, R.; Nussinov, R. New structures help the modeling of toxic amyloidβ ion channels. *Trends Biochem. Sci.* **2008**, *33*, 91–100.

[131] Jang, H.; Arce, F. T.; Ramachandran, S.; Capone, R.; Lal, R.; Nussinov, R. Structural convergence among diverse, toxic beta-sheet ion channels. *J. Phys. Chem. B* **2010**, *114*, 9445–9451.

[132] Jang, H.; Arce, F. T.; Ramachandran, S.; Capone, R.; Azimova, R.; Kagan, B. L.; Nussinov, R.; Lal, R. Truncated β-amyloid peptide channels provide an alternative mechanism for Alzheimer's disease and Down syndrome. *Proc. Natl. Acad. Sci. U.S.A.* **2010**, *107*, 6538–6543.

[133] Jang, H.; Arce, F. T.; Ramachandran, S.; Capone, R.; Lal, R.; low asterisk,;

Nussinov, R. β-Barrel Topology of Alzheimer's β-Amyloid Ion Channels. *J. Mol. Biol.* **2010**, *404*, 917–934.

[134] Shafrir, Y.; Durell, S.; Arispe, N.; Guy, H. R. Models of membrane-bound Alzheimer's Abeta peptide assemblies. *Proteins: Structure, Function, and Bioinformatics.* **2010**, *78*, 3473–3487.

[135] Sepulveda, F. J.; Parodi, J.; Peoples, R. W.; Opazo, C.; Aguayo, L. G. Synaptotoxicity of Alzheimer beta amyloid can be explained by its membrane perforating property. *PLoS One* **2010**, *5*, e11820.

[136] Wang, Q.; Walsh, D. M.; Rowan, M. J.; Selkoe, D. J.; Anwyl, R. Block of long-term potentiation by naturally secreted and synthetic amyloid beta-peptide in hippocampal slices is mediated via activation of the kinases c-Jun N-terminal kinase, cyclin-dependent kinase 5, and p38 mitogen-activated protein kinase as well as metabotropic glutamate receptor type 5. *J. Neurosci.* **2004**, *24*, 3370–8.

[137] Mutisya, E. M.; Bowling, A. C.; Beal, M. F. Cortical cytochrome oxidase activity is reduced in Alzheimer's disease. *J. Neurochem.* **1994**, *63*, 2179–2184.

[138] Huang, H.-C.; Lin, C.-J.; Liu, W.-J.; Jiang, R.-R.; Jiang, Z.-F. Dual effects of curcumin on neuronal oxidative stress in the presence of Cu(II). *Food and Chemical Toxicology* **2011**, *49*, 1578–1583.

[139] Verdier, Y.; Penke, B. Binding sites of amyloid beta-peptide in cell plasma membrane and implications for Alzheimer's disease. *Curr. Protein Pept. Sci.* **2004**, *5*, 19–31.

[140] Takahashi, T.; Mihara, H. Peptide and protein mimetics inhibiting amyloid beta-peptide aggregation. *Acc. Chem. Res.* **2008**, *41*, 1309–1318.

[141] Kirkitadze, M. D.; Kowalska, A. Molecular mechanisms initiating amyloid

beta-fibril formation in Alzheimer's disease. *Acta Biochim. Pol.* **2005**, *52*, 417–423.

[142] Zhao, L. N.; Chiu, S.-W.; Benoit, J.; Chew, L. Y.; Mu, Y. Amyloid β peptide aggregation in a mixed membrane bilayer: A molecule dynamic study. *J. Phys. Chem. B* **2011**, *115*, 12247–12256.

[143] Zhao, L. N.; Chiu, S.-W.; Benoit, J.; Chew, L. Y.; Mu, Y. The effect of curcumin on the stability of Aβ dimers. *J. Phys. Chem. B* **2012**, *116*, 7428–7435.

[144] Barz, B.; Urbanc, B. Dimer formation enhances structural differences between amyloid β-protein (1-40) and (1-42): an explicit-solvent molecular dynamics study. *PLoS One* **2012**, *7*, e34345.

[145] Côté, S.; Laghaei, R.; Derreumaux, P.; Mousseau, N. Distinct dimerization for various alloforms of the amyloid-beta protein: Aβ_{1-40}, Aβ_{1-42}, and Aβ_{1-40}(D23N). *J. Phys. Chem. B* **2012**, *116*, 4043–4055.

[146] Mitternacht, S.; Staneva, I.; Hard, T.; Irback, A. Monte Carlo study of the formation and conformational properties of dimers of Aβ42 variants. *J. Mol. Biol.* **2011**, *410*, 357–367.

[147] Williams, T. L.; Serpell, L. C. Membrane and surface interactions of Alzheimer's Aβ peptide-insights into the mechanism of cytotoxicity. *FEBS J.* **2011**, *278*, 3905–3917.

[148] Zhao, J.; Wang, Q. M.; Liang, G. Z.; Zheng, J. Molecular dynamics simulations of low-ordered Alzheimer beta-amyloid oligomers from dimer to hexamer on self-assembled monolayers. *Langmuir* **2011**, *27*, 14876–14887.

[149] Wang, Q.; Zhao, J.; Yu, X.; Zhao, C.; Li, L.; Zheng, J. Alzheimer Abeta(1-42) monomer adsorbed on the self-assembled monolayers. *Langmuir* **2010**, *26*, 12722–12732.

[150] Tsai, H. H.; Lee, J. B.; Tseng, S. S.; Pan, X. A.; Shih, Y. C. Folding and membrane insertion of amyloid-beta (25-35) peptide and its mutants: implications for aggregation and neurotoxicity. *Protein* **2010**, *78*, 1909–1925.

[151] Maltseva, E.; Brezesinski, G. Adsorption of amyloid beta (1-40) peptide to phosphatidylethanolamine monolayers. *ChemPhysChem* **2004**, *5*, 1185–1190.

[152] Ionov, M.; Klajnert, B.; Gardikis, K.; Hatziantoniou, S.; Palecz, B.; Salakhutdinov, B.; Cladera, J.; Zamaraeva, M.; Demetzos, C.; Bryszewska, M. Effect of amyloid beta peptides A β_{1-28} and Aβ_{25-40} on model lipid membranes. *J. Therm. Anal. Calorim.* **2010**, *99*, 741–747.

[153] Sgourakis, N. G.; Yan, Y.; McCallum, S. A.; Wang, C.; Garcia, A. E. The Alzheimer's peptides aβ40 and 42 adopt distinct conformations in water: a combined MD/NMR study. *J. Mol. Biol.* **2007**, *368*, 1448–1457.

[154] Krone, M. G.; Hua, L.; Soto, P.; Zhou, R.; B. J. Berne,,; Shea, J.-E. Role of water in mediating the assembly of Alzheimer amyloid A$\beta 16-22$ protofilaments. *J. Am. Chem. Soc.* **2008**, *130*, 11066–11072.

[155] Glabe, C. C. In *Alzheimer's Disease*; Harris, J. R., Fahrenholz, F., Eds.; Subcellular Biochemistry; Springer US, 2005; Vol. 38; pp 167–177.

[156] Chiu, S.; Pandti, S.; Scott, H. L.; Jakobsson, E. An improved united atom force field for simulation of mixed lipid bilayers. *J. Phys. Chem. B* **2009**, *113*, 2748–2763.

[157] Pandit, S. A.; Chiu, S.-W.; Jakobsson, E.; Grama, A.; Scott, H. L. Cholesterol packing around lipids with saturated and unsaturated chains: A simulation study. *Langmuir* **2008**, *24*, 6858–6865.

[158] Pandit, S. A.; Chiu, S.-W.; Jakobsson, E.; Grama, A.; Scott, H. L. Cholesterol surrogates: A comparison of cholesterol and 16:0 ceramide in POPC bilayers.

Biophys. J. **2007**, *92*, 920–927.

[159] Pandit, S. A.; Vasudevan, S.; Chiu, S. W.; Jakobsson, E.; Scott, H. L. Sphingomyelin-cholesterol domains in phospholipid membranes: atomistic simulation. *Biophys. J.* **2004**, *87*, 1092–1100.

[160] Chiu, S. W.; Vasudevan, S.; Jakobsson, E.; Mashl, R. J.; Scott, H. L. Structure of sphingomyelin bilayers: A simulation study. *Biophys. J.* **2003**, *85*, 3624–3635.

[161] Hess, B.; Bekker, H.; Berendsen, H. J. C.; Fraaije, J. G. E. M. LINCS: A linear constraint solver for molecular simulations. *J. Comput. Chem.* **1997**, *113*, 1463–1472.

[162] Nosé, S. A molecular dynamics method for simulations in the canonical ensemble. *Mol. Phys.* **1984**, *55*, 255–268.

[163] Hoover, W. G. Canonical dynamics: Equilibrium phase space distributions. *Phys. Rev. A* **1985**, *31*, 1695–1697.

[164] Miyashita, N.; Straub, J. E.; Thirumalai, D.; Sugita, Y. Transmembrane structures of amyloid precursor protein dimer predicted by replica-exchange molecular dynamics simulations. *J. Am. Chem. Soc.* **2009**, *131*, 3438–3439.

[165] Okada, T.; Wakabayashi, M.; Ikeda, K.; Matsuzaki, K. Formation of toxic fibrils of Alzheimer's amyloid beta-protein-(1-40) by monosialoganglioside GM1, a neuronal membrane component. *J. Mol. Biol.* **2007**, *371*, 481–489.

[166] Molander-Melin, M.; Blennow, K.; Bogdanovic, N.; Dellheden, B.; Månsson, J. E.; Fredman, P. Structural membrane alterations in Alzheimer brains found to be associated with regional disease development: increased density of gangliosides GM1 and GM2 and loss of cholesterol in detergent-resistant membrane domains. *J. Neurochem.* **2005**, *92*, 171–182.

[167] Wakabayashi, M.; Matsuzaki, K. Ganglioside-induced amyloid formation by human islet amyloid polypeptide in lipid rafts. *FEBS Letters* **2009**, *583*, 2854–2858.

[168] Kakio, A.; Nishimoto, S. I.; Kozotsumi, Y.; Matsuzaki, K. Formation of a membrane-active form of amyloid β-protein in raft-like model membranes. *Biochem. Biophys. Res. Commun.* **2003**, *303*, 514–518.

[169] Yu, X.; Zheng, J. Cholesterol promotes the interaction of Alzheimer β-amyloid monomer with lipid bilayer. *J. Mol. Biol.* **2011**, *421*, 561–571.

[170] Yahi, N.; Aulas, A.; Fantini, J. How cholesterol constrains glycolipid conformation for optimal recognition of Alzheimer's β amyloid peptide (Aβ1-40). *PLoS One* **2010**, *5*, e9079.

[171] Wakabayashi, M.; Okada, T.; Kozutsumi, Y.; Matsuzaki, K. GM1 ganglioside-mediated accumulation of amyloid beta-protein on cell membranes. *Biochem. Biophys. Res. Commun.* **2005**, *328*, 1019–1023.

[172] Kakio, A.; ichi Nishimoto, S.; Yanagisawa, K.; Kozutsumi, Y.; Matsuzaki, K. Interactions of amyloid β-protein with various gangliosides in raft-like membranes: Importance of GM1 ganglioside-bound form as an endogenous seed for Alzheimer amyloid? *Biochemistry* **2002**, *41*, 7385–7390.

[173] Abramov, A. Y.; Ionov, M.; Pavlov, E.; Duchen, M. R. Membrane cholesterol content plays a key role in the neurotoxicity of β-amyloid: implications for Alzheimer's disease. *Aging Cell* **2011**, *10*, 595–603.

[174] Fantini, J.; Yahi, N. Molecular insights into amyloid regulation by membrane cholesterol and sphingolipids: common mechanisms in neurodegenerative diseases. *Expert Reviews in Molecular Medicine.* **2010**, *12*, e27.

[175] Wegiel, J. et al. Intraneuronal Aβ immunoreactivity is not a predictor of brain

amyloidosis-β or neurofibrillary degeneration. *Acta Neuropathol.* **2007**, *113*, 389–420.

[176] Bayer, T. A.; Wirths, O. Intracellular accumulation of amyloid-beta - A predictor for synaptic dysfunction and neuron loss in Alzheimer's disease. *Frontiers in Aging Neurosci.* **2010**, *2*, 1–9.

[177] Cuello, A. C. Intracellular and extracellular Abeta, a tale of two neuropathologies. *Brain Pathol.* **2005**, *15*, 66–71.

[178] Nagele, R. G.; DÁndrea, M. R.; Anderson, W. J.; Wang, H. Y. Intracellular accumulation of beta-amyloid (1-42) in neurons is facilitated by the alpha 7 nicotinic acetylcholine receptor in Alzheimer's disease. *Neuroscience* **2002**, *110*, 199–211.

[179] DÁndrea, M. R.; Nagele, R. G. Targeting the alpha 7 nicotinic acetylcholine receptor to reduce amyloid accumulation in Alzheimer's disease pyramidal neurons. *Current Pharmaceutical Design* **2006**, *12*, 677–684.

[180] Fuentealba, R. A.; Liu, Q.; Zhang, J.; Kanekiyo, T.; Hu, X.; Lee, J.-M.; LaDu, M.; Bu, G. Low-density lipoprotein receptor-related protein 1 (LRP1) mediates neuronal Aβ42 uptake and lysosomal trafficking. *PLoS One* **2010**, *5*, e11884.

[181] Takuma, K. et al. RAGE-mediated signaling contributes to intraneuronal transport of amyloid-β and neuronal dysfunction. *Proc. Natl. Acad. Sci. U.S.A.* **2009**, *106*, 20021–20026.

[182] LaFerla1, F. M.; Green1, K. N.; Oddo, S. Intracellular amyloid-β in Alzheimer's disease. *Nature Reviews Neuroscience* **2007**, *8*, 499–509.

[183] Lai, A. Y.; McLaurin, J. Mechanisms of amyloid-beta peptide uptake by neurons: The role of lipid rafts and lipid raft-associated proteins. *International*

Journal of Alzheimer's Disease **2011**, *2011*, 548380.

[184] Pigino, G.; Morfini, G.; Atagi, Y.; Deshpande, A.; Yu, C.; Jungbauer, L.; LaDu, M.; Busciglio, J.; Brady, S. Disruption of fast axonal transport is a pathogenic mechanism for intraneuronal amyloid beta. *Proc. Natl. Acad. Sci. U.S.A.* **2009**, *106*, 5907–5912.

[185] Christensen, D. Z.; Schneider-Axmann, T.; Lucassen, P. J.; Bayer, T. A.; Wirths, O. Accumulation of intraneuronal Aβ correlates with ApoE4 genotype. *Acta Neuropathol.* **2010**, *119*, 555–566.

[186] Christensen, D. Z.; Bayer, T. A.; Wirths, O. Intracellular Aβ triggers neuron loss in the cholinergic system of the APP/PS1KI mouse model of Alzheimer's disease. *Neurobiology of Aging* **2010**, *31*, 1153–1163.

[187] Christensen, D. Z.; Kraus, S. L.; Flohr, A.; Cotel, M.-C.; Wirths, O.; Bayer, T. A. Transient intraneuronal Aβ rather than extracellular plaque pathology correlates with neuron loss in the frontal cortex of APP/PS1KI mice. *Acta Neuropathol.* **2008**, *116*, 647–655.

[188] Bayer, T. A.; Wirths, O. Review on the APP/PS1KI mouse model: intraneuronal Aβ accumulation triggers axonopathy, neuron loss and working memory impairment. *Genes, Brain and Behavior* **2008**, *7*, 6–11.

[189] Breyhan, H.; Wirths, O.; Duan, K.; Marcello, A.; Rettig, J.; Bayer, T. A. APP/PS1KI bigenic mice develop early synaptic deficits and hippocampus atrophy. *Acta Neuropathol.* **2009**, *117*, 677–685.

[190] Gouras, G. K.; Tampellini, D.; Takahashi, R. H.; Capetillo-Zarate, E. Intraneuronal β-amyloid accumulation and synapse pathology in Alzheimer's disease. *Acta Neuropathol.* **2010**, *119*, 523–541.

[191] Lashuel, H. A.; Hartley, D.; Petre, B. M.; Walz, T.; Lansbury, P. T. Neurode-

generative disease: Amyloid pores from pathogenic mutations. *Nature* **2002**, *418*, 291.

[192] Nelson Arispe, Eduardo Rojas,; Pollard, H. B. Alzheimer disease amyloid β protein forms calcium channels in bilayer membranes: Blockade by tromethamine and aluminum. *Proc. Natl. Acad. Sci. U.S.A.* **1993**, *90*, 567–571.

[193] Wong, P. T.; Schauerte, J. A.; Wisser, K. C.; Ding, H.; Lee, E. L.; Steel, D. G.; Gafni, A. Amyloid-beta membrane binding and permeabilization are distinct processes influenced separately by membrane charge and fluidity. *J. Mol. Biol.* **2009**, *386*, 81–96.

[194] Strodel, B.; Lee, J. W. L.; Whittleston, C. S.; Wales, D. J. Transmembrane structures for Alzheimer's Aβ_{1-42} oligomers. *J. Am. Chem. Soc.* **2010**, *132*, 13300–13312.

[195] Lin, H.; Bhatia, R.; Lal, R. Amyloid beta protein forms ion channels: implications for Alzheimer's disease pathophysiology. *FASEB J.* **2001**, *15*, 2433–2444.

[196] Lin, H.; Zhu, Y. J.; Lal, R. Amyloid β protein (1-40) forms calcium-permeable, Zn^{2+}-sensitive channel in reconstituted lipid vesicles. *Biochemistry* **1999**, *38*, 11189–11196.

[197] Kagan, B. L.; Hirakura, Y.; Azimov, R.; Azimova, R.; Lin, M.-C. The channel hypothesis of Alzheimer's disease: current status. *Peptides* **2002**, *23*, 1311–1315.

[198] Diaz, J. C.; Simakova, O.; Jacobson, K. A.; Arispe, N.; Pollard, H. B. Small molecule blockers of the Alzheimer Aβ calcium channel potently protect neurons from Aβ cytotoxicity. *Proc. Natl. Acad. Sci. U.S.A.* **2009**, *106*, 3348–3353.

[199] Felice, F. G. D.; Vieira, M. N. N.; Bomfim, T. R.; Decker, H.; Velasco, P. T.;

Lambert, M. P.; Viola, K. L.; Zhao, W.-Q.; Ferreira, S. T.; Klein, W. L. Protection of synapses against Alzheimer's-linked toxins: Insulin signaling prevents the pathogenic binding of Aβ oligomers. *Neuroscience* **2009**, *106*, 1971–1976.

[200] Lacor, P. N.; Buniel, M. C.; Furlow, P. W.; Clemente, A. S.; Velasco, P. T.; Wood, M.; Viola, K. L.; Kleinaalina, W. L. Aβ oligomer-induced aberrations in synapse composition, shape, and density provide a molecular basis for loss of connectivity in Alzheimer's disease. *J. Neurosci.* **2007**, *27*, 796–807.

[201] Zhao, W.-Q.; Felice, F. G. D.; Fernandez, S.; Chen, H.; Lambert, M. P.; Quon, M. J.; Krafft, G. A.; Klein, W. L. Amyloid beta oligomers induce impairment of neuronal insulin receptors. *FASEB J.* **2008**, *22*, 246–260.

[202] Snyder, E. M.; Nong, Y.; Almeida, C. G.; Paul, S.; Moran, T.; Choi, E. Y.; Nairn, A. C.; Salter, M. W.; Lombroso, P. J.; Greengard, G. K. G. P. Regulation of NMDA receptor trafficking by amyloid-β. *Nature Neuroscience* **2005**, *8*, 1051–1058.

[203] Yan, S. D.; Chen, X.; Fu, J.; Chen, M.; Zhu, H.; Roher, A.; Slattery, T.; Zhao, L.; Nagashima, M.; Morser, J.; Migheli, A.; Nawroth, P.; Stern, D.; Schmidt, A. M. RAGE and amyloid-beta peptide neurotoxicity in Alzheimer's disease. *Nature* **1996**, *382*, 685–691.

[204] Parri, R. H.; Dineley, T. K. Nicotinic acetylcholine receptor interaction with beta-amyloid: molecular, cellular, and physiological consequences. *Curr. Alzheimer Res.* **2010**, *7*, 27–39.

[205] Diarra, A.; Geetha, T.; Potter, P.; Babu, J. R. Signaling of the neurotrophin receptor p75 in relation to Alzheimer's disease. *Biochem. Biophys. Res. Commun.* **2009**, *390*, 352–356.

[206] Alberdi, E.; Sánchez-Gómez, M. V.; Cavaliere, F.; Pérez-Samartín, A.;

Zugaza, J. L.; Trullas, R.; Domercq, M.; Matute, C. Amyloid β oligomers induce Ca^{2+} dysregulation and neuronal death through activation of ionotropic glutamate receptors. *Cell Calcium* **2010**, *47*, 264–272.

[207] Ma, Q.; Yang, F.; Rosario, E. R.; Ubeda, O. J.; Beech, W.; Gant, D. J.; Chen, P. P.; Hudspeth, B.; Chen, C.; Zhao, Y.; Vinters, H. V.; Frautschy, S. A.; Cole, G. M. β-amyloid oligomers induce phosphorylation of Tau and inactivation of insulin receptor substrate via c-Jun N-Terminal kinase signaling: suppression by omega-3 fatty acids and curcumin. *J. Neurosci.* **2009**, *29*, 9078–9089.

[208] Malinow, R. New developments on the role of NMDA receptors in Alzheimer's disease. *Current Opinion in Neurobiology* **2012**, *22*, 559–563, In press.

[209] Li, S.; Jin, M.; Koeglsperger, T.; Shepardson, N. E.; Shankar, G. M.; Selkoe, D. J. Soluble Aβ oligomers inhibit long-term potentiation through a mechanism involving excessive activation of extrasynaptic NR2B-containing NMDA receptors. *J. Neurosci.* **2011**, *31*, 6627–6638.

[210] Texido, L.; Martin-Satue, M.; Alberdi, E.; Solsona, C.; Matute, C. Amyloid β peptide oligomers directly activate NMDA receptors. *Cell Calcium* **2011**, *49*, 184–190.

[211] Verges, D. K.; Restivo, J. L.; Goebel, W. D.; Holtzman, D. M.; Cirrito, J. R. Opposing synaptic regulation of amyloid-β metabolism by NMDA receptors in Vivo. *J. Neurosci.* **2011**, *31*, 11328–11337.

[212] Bordji, K.; Becerril-Ortega, J.; Nicole, O.; Buisson, A. Activation of extrasynaptic, but not synaptic, NMDA receptors modifies amyloid precursor protein expression pattern and increases amyloid-β production. *J. Neurosci.* **2010**, *30*, 15927–15942.

[213] Rönicke, R.; Mikhaylova, M.; Rönicke, S.; Meinhardt, J.; Schröder, U. H.; Fändrich, M.; Reiser, G.; Kreutz, M. R.; Reymann, K. G. Early neuronal dysfunction by amyloid β oligomers depends on activation of NR2B-containing NMDA receptors. *Neurobiology of Aging* **2011**, *32*, 2219–2228.

[214] Bicca, M. A.; Figueiredo, C. P.; Piermartiri, T. C.; Meotti, F. C.; Bouzon, Z. L.; Tasca, C. I.; Medeiros, R.; Calixto, J. B. The selective and competitive N-methyl-D-aspartate receptor antagonist, (-)-6-phosphonomethyl-decahydroisoquinoline-3-carboxylic acid, prevents synaptic toxicity induced by amyloid-β in mice. *Neuroscience* **2011**, *192*, 631–641.

[215] Maglio, L. E.; Martins, V. R.; Izquierdo, I.; Ramirez, O. A. Role of cellular prion protein on LTP expression in aged mice. *Brain Research* **2006**, *1097*, 11–18.

[216] Criado, J. R.; S anchez-Alavez, M.; Conti, B.; Giacchino, J. L.; Wills, D. N.; Henriksen, S. J.; Race, R.; Manson, J. C.; Chesebro, B.; Oldstone, M. B. A. Mice devoid of prion protein have cognitive deficits that are rescued by reconstitution of PrP in neurons. *Neurobiology of Disease* **2005**, *19*, 255–265.

[217] Khosravani, H.; Zhang, Y.; Tsutsui, S.; Hameed, S.; Altier, C.; Hamid, J.; Chen, L.; Villemaire, M.; Ali, Z.; Jirik, F. R.; Zamponi, G. W. Prion protein attenuates excitotoxicity by inhibiting NMDA receptors. *J. Cell Biol.* **2008**, *181*, 551–565.

[218] Vassallo, N.; Herms., J. Cellular prion protein function in copper homeostasis and redox signalling at the synapse. *J. Neurochem.* **2003**, *86*, 538–544.

[219] McLennan, N. F.; Brennan, P. M.; McNeill, A.; Davies, I.; Fotheringham, A.; Rennison, K. A.; Ritchie, D.; Brannan, F.; Head, M. W.; Ironside, J. W.; Williams, A.; Bell, J. E. Prion protein accumulation and neuroprotection in

hypoxic brain damage. *Am. J. Pathol.* **2004**, *165*, 227–235.

[220] Shyu, W.-C.; Lin, S.-Z.; Chiang, M.-F.; Ding, D.-C.; Li, K.-W.; Chen, S.-F.; Yang, H.-I.; Li, H. Overexpression of PrP^{C} by adenovirus-mediated gene targeting reduces ischemic injury in a stroke rat model. *J. Neurosci.* **2005**, *25*, 8967–8977.

[221] Santuccione, A.; Sytnyk, V.; Leshchyns'ka, I.; Schachner, M. Prion protein recruits its neuronal receptor NCAM to lipid rafts to activate $p59^{fyn}$ and to enhance neurite outgrowth. *J. Cell Biol.* **2005**, *169*, 341–354.

[222] Laurén, J.; Gimbel, D. A.; Nygaard, H. B.; Gilbert, J. W.; Strittmatter, S. M. Cellular prion protein mediates impairment of synaptic plasticity by amyloid-β oligomers. *Nature* **2009**, *457*, 1128–1132.

[223] Kessels, H. W.; Nguyen, L. N.; Nabavi, S.; Malinow, R. The prion protein as a receptor for amyloid-β. *Nature* **2010**, *466*, E3–E4.

[224] Calella, A. M.; Farinelli, M.; Nuvolone, M.; Mirante, O.; Moos, R.; Falsig, J.; Mansuy, I. M.; Aguzzi, A. Prion protein and Aβ-related synaptic toxicity impairment. *EMBO Mol. Med.* **2010**, *2*, 306–314.

[225] Wang, H. Y.; Lee, D. H. S.; D'Andrea, M. R.; Peterson, P. A.; Shank, R. P.; Reitz, A. B. β-Amyloid(1-42) binds to α7 nicotinic acetylcholine receptor with high affinity: Implications for Alzheimer's disease pathology. *J. Biol. Chem.* **2000**, *275*, 5626–5632.

[226] Pettit, D. L.; Shao, Z.; Yakel, J. L. β-amyloid 1-42 peptide directly modulates nicotinic receptors in the rat hippocampal slice. *J. Neurosci.* **2001**, *21*, RC120–RC125.

[227] Liu, Q. S.; Kawai, H.; Berg, D. K. Beta-amyloid peptide blocks the response of alpha7-containing nicotinic receptors on hippocampal neurons. *Proc. Natl.*

Acad. Sci. U.S.A. **2001**, *48*, 4734–4739.

[228] Dougherty, J. J.; Wu, J.; Nichols, R. A. β-amyloid regulation of presynaptic nicotinic receptors in rat hippocampus and neocortex. *J. Neurosci.* **2003**, *23*, 6740–6747.

[229] Hernandez, C. M.; Kayed, R.; Zheng, H.; Sweatt, J. D.; Dineley, K. T. Loss of α7 nicotinic receptors enhances β-amyloid oligomer accumulation, exacerbating early-stage cognitive decline and septohippocampal pathology in a mouse model of Alzheimer's disease. *J. Neurosci.* **2010**, *30*, 2442–2453.

[230] Wang, H.-Y.; Bakshi, K.; Shen, C.; Frankfurt, M.; Trocmé-Thibíerge, C.; Morain, P. S24795 limits β-amyloid-α7 nicotinic receptor interaction and reduces Alzheimer's disease-like pathologies. *Biological Psychiatry* **2010**, *67*, 522–530.

[231] Lagostena, L.; Trocme-Thibierge, C.; Morain, P.; Cherubini, E. The partial α7 nicotine acetylcholine receptor agonist S 24795 enhances long-term potentiation at CA3-CA1 synapses in the adult mouse hippocampus. *Neuropharmacology* **2008**, *54*, 676–685.

[232] Beracochea, D.; Boucard, A.; Trocme-Thibierge, C.; Morain, P. Improvement of contextual memory by S24795 in aged mice: comparison with memantine. *Psychopharmacology* **2008**, *196*, 555–564.

[233] Small, D. H.; Maksel, D.; Kerr, M. L.; Ng, J.; Hou, X.; Chu, C.; Mehrani, H.; Unabia, S.; Azari, M. F.; Loiacono, R.; Aguilar, M.; Chebib, M. The beta-amyloid protein of Alzheimer's disease binds to membrane lipids but does not bind to the alpha7 nicotinic acetylcholine receptor. *J. Neurochem.* **2007**, *101*, 1527–1538.

[234] Boland, K.; Manias, K.; Perlmutter, D. H. Specificity in recognition of amyloid-

beta peptide by the serpin-enzyme complex receptor in hepatoma cells and neuronal cells. *J. Biol. Chem.* **1995**, *270*, 28022–28028.

[235] Joslin, G.; Griffin, G. L.; August, A. M.; Adams, S.; Fallon, R. J.; Senior, R. M.; Perlmutter, D. H. The serpin-enzyme complex (SEC) receptor mediates the neutrophil chemotactic effect of alpha-1 antitrypsin-elastase complexes and amyloid-beta peptide. *J. Clin. Invest.* **1992**, *90*, 1150–1154.

[236] Schmidt, A. M.; Sahagan, B.; Nelson, R. B.; Selmer, J.; Rothlein, R.; Bell, J. M. The role of RAGE in amyloid-beta peptide-mediated pathology in Alzheimer's disease. *Curr. Opin. Investig Drugs* **2009**, *10*, 672–680.

[237] S, S. B.; Fioravanzo, L.; C, C. G.; Liddo, R. D.; Parnigotto, P. P.; Folin, M. Involvement of the receptor for advanced glycation-end products (RAGE) in beta-amyloid-induced toxic effects in rat cerebromicrovascular endothelial cells cultured in vitro. *Int. J. Mol. Med.* **2009**, *24*, 9–15.

[238] Knowles, J. K.; Rajadas, J.; Nguyen, T.-V. V.; Yang, T.; LeMieux, M. C.; Griend, L. V.; Ishikawa, C.; Massa, S. M.; Wyss-Coray, T.; Longo, F. M. The p75 neurotrophin receptor promotes amyloid-β(1-42)-induced neuritic dystrophy in vitro and in vivo. *J. Neurosci.* **2009**, *29*, 10627–10637.

[239] Bengoechea, T. G.; Chen, Z.; O'Learya, D. A.; Masliahb, E.; Lee, K.-F. p75 reduces β-amyloid-induced sympathetic innervation deficits in an Alzheimer's disease mouse model. *Proc. Natl. Acad. Sci. U.S.A.* **2009**, *106*, 7870–7675.

[240] Prk, L.; Wng, G.; Zhou, P.; Zhou, J.; Pitstick, R.; Previtic, M. L.; Younkind, L.; Younkind, S. G.; Nostrndc, W. E. V.; Choe, S.; Anrther, J.; Crlson, G. A.; Idecol, C. Scavenger receptor CD36 is essential for the cerebrovascular oxidative stress and neurovascular dysfunction induced by amyloid-β. *Proc. Natl. Acad. Sci. U.S.A.* **2011**, *108*, 5063–5068.

[241] Silverstein, R. L.; Febbraio, M. CD36, a scavenger receptor involved in immunity, metabolism, angiogenesis, and behavior. *Sci. Signal* **2009**, *2*, 1–8.

[242] Coraci, I. S.; Husemann, J.; Berman, J. W.; Hulette, C.; Dufour, J. H.; Campanella, G. K.; Luster, A. D.; Silverstein, S. C.; El-Khoury, J. B. CD36, a class B scavenger receptor, is expressed on microglia in Alzheimer's disease brains and can mediate production of reactive oxygen species in response to beta-amyloid fibrils. *Am. J. Pathol.* **2002**, *160*, 101–112.

[243] Varadarajan, S.; Yatin, S.; M, M. A.; Butterfield, D. A. Review: Alzheimer's amyloid β-peptide-associated free radical oxidative stress and neurotoxicity. *Journal of Structural Biology* **2000**, *130*, 184–208.

[244] Butterfield, D. A.; Reed, T.; Newman, S. F.; Sultana, R. Roles of amyloid β-peptide-associated oxidative stress and brain protein modifications in the pathogenesis of Alzheimer's disease and mild cognitive impairment. *Free Radical Biology and Medicine* **2007**, *43*, 658–677.

[245] Jo, D.-G. et al. Evidence that γ-secretase mediates oxidative stress-induced β-secretase expression in Alzheimer's disease. *Neurobiology of Aging* **2010**, *31*, 917–925.

[246] Zheng, L.; Kågedal, K.; Dehvari, N.; Benedikz, E.; Cowburn, R.; Marcusson, J.; Terman, A. Oxidative stress induces macroautophagy of amyloid β-protein and ensuing apoptosis. *Free Radical Biology and Medicine* **2009**, *46*, 422–429.

[247] Abdul, H. M.; Butterfield, D. A. Involvement of PI3K/PKG/ERK1/2 signaling pathways in cortical neurons to trigger protection by cotreatment of acetyl-l-carnitine and α-lipoic acid against HNE-mediated oxidative stress and neurotoxicity: implications for Alzheimer's disease. *Free Radical Biology and Medicine* **2007**, *42*, 371–384.

[248] Naoi, M.; Maruyama, W.; Shamoto-Nagai, M.; Yi, H.; Akao, Y.; Tanaka, M. Oxidative stress in mitochondria: decision to survive and death of neurons in neurodegenerative disorder. *Mol. Neurobiol.* **2005**, *31*, 81–93.

[249] Castegna, A.; Aksenov, M.; Aksenova, M.; Thongboonkerd, V.; Klein, J. B.; Pierce, W. M.; Booze, R.; Markesbery, W. R.; Butterfield, D. A. Proteomic identification of oxidatively modified proteins in Alzheimer's disease brain. Part I. Creatine kinase BB, glutamine synthase, and ubiquitin carboxy-terminal hydrolase L-1. *Free Radical Biology and Medicine* **2002**, *33*, 562–571.

[250] Castegna, A.; Aksenov, M.; Thongboonkerd, V.; Klein, J. B.; Pierce, W. M.; Booze, R.; Markesbery, W. R.; Butterfield, D. A. Proteomic identification of oxidatively modified proteins in Alzheimer's disease brain. Part II. Dihydropyrimidinase-related protein 2, alpha-enolase and heat shock cognate 71. *J. Neurochem.* **2002**, *82*, 1524–1532.

[251] Sultana, R.; Perluigi, M.; Butterfield, D. A. Redox proteomics identification of oxidatively modified proteins in Alzheimer's disease brain and in vivo and in vitro models of AD centered around Abeta(1-42). *J. Chromatogr. B Anal. Technol. Biomed. Life Sci.* **2006**, *833*, 3–11.

[252] Butterfield, D. A.; Boyd-Kimball, D. The critical role of methionine 35 in Alzheimer's amyloid β-peptide (1-42)-induced oxidative stress and neurotoxicity. *BBA - Protein Proteom.* **2005**, *1703*, 149–156.

[253] Butterfield, D. A.; Galvan, V.; Lange, M. B.; Tang, H.; Sowell, R. A.; Spilman, P.; Fombonne, J.; Gorostiza, O.; Zhang, J.; Sultana, R.; Bredesen, D. E. In vivo oxidative stress in brain of Alzheimer disease transgenic mice: Requirement for methionine 35 in amyloid β-peptide of APP. *Free Radical Biology and Medicine* **2010**, *48*, 136–144.

[254] Muthaiyah, B.; Essa, M. M.; Chauhan, V.; Chauhan, A. Protective effects of walnut extract against amyloid beta peptide-induced cell death and oxidative stress in PC12 cells. *Biomedical and Life Science* **2011**, *36*, 2096–2103.

[255] Barten, D. M.; Albright, C. F. Therapeutic strategies for Alzheimer's disease. *Mol. Neurobiol.* **2008**, *37*, 171–186.

[256] Kagan, B. L. Amyloidosis and protein folding. *Science* **2005**, *307*, 42–43.

[257] Chang, Z.; Luo, Y.; Zhang, Y.; Wei, G. Interactions of Aβ25-35 β-barrel-like oligomers with anionic lipid bilayer and resulting membrane leakage: An all-atom molecular dynamics study. *J. Phys. Chem. B* **2011**, *115*, 1165–1174.

[258] Melquiond, A.; Dong, X.; Mousseau, N.; Derreumaux, P. Role of the region 23-28 in Aβ fibril formation: Insights from simulations of the monomers and dimers of Alzheimer's peptides Aβ40 and Aβ42. *Curr. Alzheimer Res.* **2008**, *5*, 244–250.

[259] Bellesia, G.; Shea, J.-E. Diversity of kinetic pathways in amyloid fibril formation. *J. Chem. Phys.* **2009**, *131*, 111102.

[260] Urbanc, B.; Betnel, M.; Cruz, L.; Bitan, G.; Teplow, D. B. Elucidation of amyloid β-protein oligomerization mechanisms: discrete molecular dynamics study. *J. Am. Chem. Soc.* **2010**, *132*, 4266–4280.

[261] Davis, C. H.; Berkowitz, M. L. Structure of the Amyloid-β (1-42) monomer absorbed to model phospholipid bilayers: A molecular dynamics study. *J. Phys. Chem. B* **2009**, *113*, 14480–14486.

[262] Nikolic, A.; Baud, S.; Rauscher, S.; Pomes, R. Molecular mechanism of β-sheet self-organization at water-hydrophobic interfaces. *Proteins: Structure, Function, and Bioinformatics* **2011**, *79*, 1–22.

[263] Wang, Q.; Zhao, C.; Zhao, J.; Wang, J.; Yang, J.-C.; Yu, X.; Zheng, J. Com-

parative molecular dynamics study of Aβ adsorption on the self-assembled monolayers. *Langmuir* **2010**, *26*, 3308–3316.

[264] Kumar, A.; Bullard, R. L.; Patel, P.; Paslay, L. C.; Singh, D.; Bienkiewicz, E. A.; Morgan, S. E.; Rangachari, V. Non-Esterified fatty acids generate distinct low-molecular weight Amyloid-β (Aβ42) oligomers along pathway different from fibril formation. *PLoS One* **2011**, *6*, e18759.

[265] Ashley, R. H.; Harroun, T. A.; Hauss, T.; Breen, K. C.; Bradshaw, J. P. Autoinsertion of soluble oligomers of Alzheimer's Aβ(1-42) peptide into cholesterol-containing membranes is accompanied by relocation of the sterol towards the bilayer surface. *BMC Struct. Biol.* **2006**, *6*, 21.

[266] Kakio, A.; Yano, Y.; Takai, D.; Kuroda, Y.; Matsumoto, O.; Kozutsumi, Y.; Matsuzaki, K. Interaction between amyloid beta-protein aggregates and membranes. *J. Pept. Sci.* **2004**, *10*, 612–21.

[267] Soscia, S. J.; Kirby, J. E.; Washicosky, K. J.; Tucker, S. M.; Ingelsson, M.; Hyman, B.; Burton, M. A.; Goldstein, L. E.; Duong, S.; Tanzi, R. E.; Moir, R. D. The Alzheimer's disease-associated amyloid β-protein is an antimicrobial peptide. *PLoS One* **2010**, *5*, e9505.

[268] Norton, W. T.; Abe, T.; Poduslo, S. E.; Devries, G. H. lipid-composition of isolated brain-cells and axons. *J. Neurosci. Res.* **1975**, *1*, 57–75.

[269] Nagle, J. F.; Tristram-Nagle, S. Lipid bilayer structure. *Curr. Opin. Struct. Biol.* **2000**, *10*, 474–480.

[270] Essmann, U.; Perera, L.; Berkowitz, M. L.; Darden, T.; Lee, H.; Pedersen, L. G. A smooth particle mesh Ewald method. *J. Chem. Phys.* **1995**, *103*, 8577–8593.

[271] DeLano, W. L. The PyMOL Molecular Graphics System, Version 1.4, Schrödinger, LLC. 2011.

[272] Humphrey, W.; Dalke, A.; Schulten, K. VMD - Visual Molecular Dynamics. *J. Mol. Graphics* **1996**, *14*, 33–38.

[273] Anna, S.; Joachim, S. Dynamic structure of fatty acyl chains in a phospholipid bilayer measured by deuterium magnetic resonance. *Biochemistry* **1974**, *13*, 4839–4845.

[274] Petkova, A. T.; Ishii, Y.; Balbach, J. J.; Antzutkin, O. N.; Leapman, R. D.; Delaglio, F.; Tycko, R. A structural model for Alzheimer's β-amyloid fibrils based on experimental constraints from solid state NMR. *Proc. Natl. Acad. Sci. U.S.A.* **2002**, *99*, 16742–16747.

[275] Plumley, J. A.; Dannenberg, J. J. The importance of hydrogen bonding between the glutamine side chains to the formation of Amyloid VQIVYK parallel β-sheets: An ONIOM DFT/AM1 study. *J. Am. Chem. Soc.* **2010**, *132*, 1758–1759.

[276] Chiu, S. W.; Jakobsson, E.; Mashi, R. J.; Scott, H. L. Cholesterol-induced modification in lipid bilayers: A simulation study. *Biophys. J.* **2002**, *83*, 1842–1853.

[277] Friedrich, R. P.; Tepper, K.; Rönicke, R.; Soom, M.; Westermann, M.; Reymann, K.; Kaether, C.; Fändrich, M. Mechanism of amyloid plaque formation suggests an intracellular basis of Aβ pathogenicity. *Proc. Natl. Acad. Sci. U.S.A.* **2010**, *107*, 1942–1947.

[278] Nguyen, P. H.; Li, M. S.; Derreumaux, P. Effects of all-atom force fields on amyloid oligomerization: replica exchange molecular dynamics simulations of the Aβ16-22 dimer and trimer. *Phys. Chem. Chem. Phys.* **2011**, *13*, 9778–9788.

[279] Jiang, P.; Xu, W. X.; Mu, Y. G. Amyloidogenesis abolished by proline substitutions but enhanced by lipid binding. *PLoS Comput. Biol.* **2009**, *5*, e1000357.

[280] Barry, J.; Fritz, M.; Brender, J. R.; Smith, P. E. S.; Lee, D.-K.; Ramamoorthy, A. Determining the effects of lipophilic drugs on membrane structure by solid-state NMR spectroscopy: The case of the antioxidant curcumin. *J. Am. Chem. Soc.* **2009**, *131*, 4490–4498.

[281] Ingolfsson, H. I.; Koeppe, R. E.; Andersen, O. S. Curcumin is a Modulator of Bilayer Material Properties. *Biochemistry* **2007**, *46*, 10384–10391.

[282] Varghese, K.; Molnar, P.; Das, M.; Bhargava, N.; Lambert, S.; Kindy, M. S.; Hickman, J. J. A new target for amyloid beta toxicity validated by standard and high-throughput electrophysiology. *PLoS One* **2010**, *5*, e8643.

[283] Ahmed, T.; Gilani, A.-H.; Hosseinmardi, N.; Semnanian, S.; Enam, S. A.; Fathollahi, Y. Curcuminoids rescue long-term potentiation impaired by amyloid peptide in rat hippocampal slices. *Synapse* **2011**, *65*, 572–582.

[284] Park, S. Y.; Kim, D. S. Discovery of natural products from Curcuma longa that protect cells from beta-amyloid insult: A drug discovery effort against Alzheimer's disease. *J. Nat. Prod.* **2002**, *65*, 1227–1231.

[285] Wang, L.; Li, C.; Guo, H.; Kern, T. S.; Huang, K.; Zheng, L. Curcumin inhibits neuronal and vascular degeneration in retina after ischemia and reperfusion injury. *PLoS One* **2011**, *6*, e23194.

[286] Lee, I.; Yang, J.; Lee, J. H.; Choe, Y. S. Synthesis and evaluation of 1-(4-[18F]fluoroethyl)-7-(4'-methyl)curcumin with improved brain permeability for β-amyloid plaque imaging. *Bioorg. Med. Chem. Lett.* **2011**, *21*, 5765–5769.

[287] Ortica, F.; Rodgers, M. A. J. A laser flash photolysis study of curcumin in dioxane-water mixtures. *Photochem. Photobiol.* **2001**, *74*, 745–751.

[288] Mague, J. T.; Alworth, W. L.; Payton, F. L. Curcumin and derivatives. *Acta Cryst.* **2004**, *60*, 608–610.

[289] Payton, F.; Sandusky, P.; Alworth, W. L. NMR study of the solution structure of curcumin. *J. Nat. Prod.* **2007**, *70*, 143–146.

[290] Gordon, J. C.; Myers, J. B.; Folta, T.; Shoja, V.; Heath, L. S.; Onufriev, A. H++: A server for estimating pKas and adding missing hydrogens to macromolecules. *Nucleic Acids. Res.* **2005**, *33*, 368–371.

[291] Myers, J.; Grothaus, G.; Narayanan, S.; Onufriev, A. A simple clustering algorithm can be accurate enough for use in calculations of pKs in macromolecules. *Proteins* **2006**, *63*, 928–938.

[292] Irwin, J. J.; Shoichet, B. K. ZINC-A free aatabase of commercially available compounds for virtual screening. *J. Chem. Inf. Model* **2005**, *45*, 177–182.

[293] Schuttelkopf, A. W.; van Aalten, D. M. F. PRODRG - A tool for high-throughput crystallography of protein-ligand complexes. *Acta. Crystallogr. D* **2004**, *60*, 1355–1363.

[294] Olubiyi, O. O.; Strodel, B. Structures of the amyloid β-peptides Aβ_{1-40} and Aβ_{1-42} as influenced by pH and a D-peptide. *J. Phys. Chem. B* **2012**, *116*, 3280–3291.

[295] Sanner, M. F. Python: A programming language for software integration and development. *J. Mol. Graphics Mod.* **1999**, *17*, 57–61.

[296] Berendsen, H. J. C.; van Gunsteren J. P. M. Postma, W. F.; Hermans, J. Interaction models for water in relation to protein hydration. *Intermolecular Forces* **1981**, 331–342.

[297] Fraser, C. M.; Fernández, A.; Scott, L. R. WRAPPA: A simple screening tool for candidate dehydron identification. *University of Chicago Technical Report TR-2011-05* **2011**,

[298] Gazit, E. A possible role for π-stacking in the self-assembly of amyloid fibrils.

FASEB J **2002**, *16*, 77–83.

[299] Porat, Y.; Abramowitz, A.; Gazit, E. Inhibition of amyloid fibril formation by polyphenols: structural similarity and aromatic interactions as a common inhibition mechanism. *Chemical Biology & Drug Design* **2006**, *67*, 27–37.

[300] Scrutton, N. S.; Raine, A. R. Cation-pi bonding and amino-aromatic interactions in the biomolecular recognition of substituted ammonium ligands. *Biochem. J.* **1996**, *319*, 1–8.

[301] Hunter, C. A.; Sanders, J. K. M. The nature of pi-pi interactions. *J. Am. Chem. Soc.* **1990**, *112*, 5525–5534.

[302] Xia, Z.; Zhu, Z.; Zhu, J.; Zhou, R. Recognition mechanism of siRNA by viral p19 suppressor of RNA silencing: A molecular dynamics study. *Biophys. J.* **2009**, *96*, 1761–1769.

[303] Dua, J.; Du, J.; Zhao, L.; Wang, L.; Liu, Y.; Li, D.; Yang, Y.; Zhou, R.; Zhao, Y.; Chai, Z.; Chen, C. Binding of blood proteins to carbon nanotubes reduces cytotoxicity. *Proc. Natl. Acad. Sci. U.S.A.* **2011**, *108*, 16968–16973.

[304] Zuo, G.; Gu, W.; Fang, H.; Zhou, R. Carbon nanotube wins the competitive binding over proline-rich motif ligand on SH3 domain. *J. Phys. Chem. C* **2011**, *115*, 12322–12328.

[305] Fernández, A.; Scott, R. Dehydron: A structurally encoded signal for protein interaction. *Biophys. J.* **2003**, *85*, 1914–1928.

[306] Chen, J. P.; Zhang, X.; Fernandez, A. Molecular basis for specificity in the druggable kinome: Sequence-based analysis. *Bioinformatics* **2007**, *23*, 563–572.

[307] Crespo, A.; Fernandez, A. Induced disorder in protein-ligand complexes as a drug-design strategy. *Molecular Pharmaceutics* **2008**, *5*, 430–437.

[308] Fraser, C. M.; Fernández, A.; Scott, L. R. *Advances in computational biology*; Springer: New York, 2010; Chapter 53, pp 473–479.

[309] Betts, M. J.; Russell, R. B. *Bioinformatics for geneticists*; Wiley, 2003.

[310] Young, T.; Abel, R.; Kim, B.; Berne, B. J.; Friesner, R. A. Motifs for molecular recognition exploiting hydrophobic enclosure in protein-ligand binding. *Proc. Natl. Acad. Sci. U.S.A.* **2007**, *104*, 808–813.

[311] Liu, P.; Huang, X.; Zhou, R.; Berne, B. J. Observation of a dewetting transition in the collapse of the melittin tetramer. *Nature* **2005**, *437*, 159–162.

[312] Zhou, R.; Huang, X.; Margulis, C. J.; Berne, B. J. Hydrophobic collapse in multidomain protein folding. *Science* **2004**, *305*, 1605–1609.

[313] Avramovich-Tirosh, Y.; Amit, T.; Bar-Am, O.; Weinreb, O.; Youdim, M. B. Physiological and pathological aspects of Aβ in iron homeostasis via 5'UTR in the APP mRNA and the therapeutic use of iron-chelators. *BMC neuroscience* **2008**, *9*, S2.

[314] Mantyh, P. W.; Ghilardi, J. R.; Rogers, S.; DeMaster, E.; Allen, C. J.; Stimson, E. R.; Maggio, J. E. Aluminum, iron, and zinc ions promote aggregation of physiological concentrations of β-amyloid peptide. *J. Neurochem.* **1993**, *61*, 1171–1174.

[315] Lovell, M. A.; Robertson, J. D.; Teesdale, W. J.; Campbell, J. L.; Markesbery, W. R. Copper, iron and zinc in Alzheimer's disease senile plaques. *J. Neurol. Sci.* **1998**, *158*, 47–52.

[316] Bush, A. I.; Tanzi, R. E. Therapeutics for Alzheimer's disease based on the metal hypothesis. *Neurotherapeutics* **2008**, *5*, 421–432.

[317] Smith, D. G.; Cappai, R.; Barnham, K. J. The redox chemistry of the Alzheimer's disease amyloid β peptide. *BBA - Protein Proteom.* **2007**, *1768*,

1976–1990.

[318] Halliwell, B.; Gutterer, J. M. *Free Radicals in Biology and Medicine*; Oxford University Press, USA, 1999.

[319] Honda, K.; Casadesus, G.; Petersen, R. B.; Perry, G.; Smith, M. A. Oxidative stress and redox-active iron in Alzheimer's disease. *Annals of the New York Academy of Sciences* **2006**, *1012*, 179–182.

[320] Rottkamp, C. A.; Raina, A. K.; Zhu, X.; Gaier, E.; Bush, A. I.; Atwood, C. S.; Chevion, M.; Perry, G.; Smith, M. A. Redox-active iron mediates amyloid-β toxicity. *Free Radical Biology and Medicine* **2001**, *30*, 447–450.

[321] Liu, G.; Men, P.; Kudo, W.; Perry, G.; Smith, M. A. Nanoparticle-chelator conjugates as inhibitors of amyloid-β aggregation and neurotoxicity: A novel therapeutic approach for Alzheimer disease. *Neuroscience Letters* **2009**, *455*, 187–190.

[322] Castellani, R. J.; Moreira, P. I.; Zhu, G. P. X. The role of iron as a mediator of oxidative stress in Alzheimer disease. *BioFactors* **2012**, *38*, 133–138.

[323] Hou, S.; Mark F Reynolds, Frank T Horrigan, Stefan H Heinemann,; Hoshi, T. Reversible binding of heme to proteins in cellular signal transduction. *Acc. Chem. Res.* **2006**, *39*, 918–924.

[324] Parker, W. D. J.; Parks, J.; Filley, C. M.; Kleinschmidt-DeMasters, B. K. Electron transport chain defects in Alzheimer's disease brain. *Neurology* **1994**, *44*, 1090–1096.

[325] Bjelkmar, P.; Larsson, P.; Cuendet, M. A.; Hess, B.; Lindahl, E. Implementation of the CHARMM force field in GROMACS: Analysis of protein stability effects from correction maps, virtual interaction sites, and water models. *J. Chem. Theory Comput.* **2010**, *6*, 459–466.

[326] Berendsen, H. J. C.; van der Spoel, D.; van Drunen, R. GROMACS: A message-passing parallel molecular dynamics implementation. *Comput. Phys. Comm.* **1995**, *91*, 43–56.

[327] Lindahl, E.; Hess, B.; van der Spoel, D. Gromacs 3.0: A package for molecular simulation and trajectory analysis. *J. Mol. Model* **2001**, *7*, 306–317.

[328] Spoel, D. V. D.; Lindahl, E.; Hess, B.; Groenhof, G.; Mark, A. E.; Berendsen, H. J. C. GROMACS: Fast, flexible, and free. *J. Comput. Chem.* **2005**, *26*, 1701–1718.

[329] Daura, X.; Gademann, K.; Jaun, B.; Seebach, D.; van Gunsteren, W. F.; Mark, A. E. Peptide folding: when simulation meets experiment. *Angew. Chem. Int. Ed.* **1999**, *38*, 236–240.

[330] Xu, W.; Zhang, C.; Derreumaux, P.; Graslund, A.; Morozova-Roche, L.; Mu, Y. Intrinsic determinants of $A\beta_{12-24}$ pH-dependent self-assembly revealed by combined computational and experimental studies. *PLoS One* **2011**, *6*, e24329.

[331] Pramanik, D.; Dey, S. G. Active site environment of heme-bound amyloid β peptide associated with Alzheimer's disease. *J. Am. Chem. Soc.* **2011**, *133*, 81–87.

[332] Azimi, S.; Rauk, A. The binding of Fe(II)-heme to the amyloid beta peptide of Alzheimer's disease: QM/MM investigations. *J. Chem. Theory Comput.* **2012**, *8*, 5150–5158.

[333] Tuppo, E. E.; Arias, H. R. The role of inflammation in Alzheimer's disease. *The International Journal of Biochemistry and Cell Biology* **2005**, *37*, 289–305.

[334] Tan, Z. S.; Seshadri, S. Inflammation in the Alzheimer's disease cascade: culprit or innocent bystander? *Alzheimers Res. Ther.* **2010**, *2*, 6.

[335] Holmes, C.; Cunningham, C.; Zotova, E.; Woolford, J.; Dean, C.; Kerr, S.;

Culliford, D.; Perry, V. H. Systemic inflammation and disease progression in Alzheimer disease. *Neurology* **2009**, *73*, 768–774.

[336] Shankar, G. M.; Li, S. M.; Mehta, T. H.; Garcia-Munoz, A.; Shepardson, N. E.; Smith, I.; Brett, F. M.; Farrell, M. A.; Rowan, M. J.; Lemere, C. A.; Regan, C. M.; Walsh, D. M.; Sabatini, B. L.; Selkoe, D. J. Amyloid-beta protein dimers isolated directly from Alzheimer's brains impair synaptic plasticity and memory. *Nature Med.* **2008**, *14*, 837–842.

[337] Heizmann, G. F. C. W.; Schäfer, B. W. S100 proteins: structure, functions and pathology. *Frontiers in Bioscience* **2002**, *7*, 1356–1368.

[338] Itou, H.; Yao, M.; Fujita, I.; Watanabe, N.; Suzuki, M.; Nishihira, J.; Tanaka, I. The crystal structure of human MRP14 (S100A9), a Ca^{2+}-dependent regulator protein in inflammatory process. *J. Mol. Biol.* **2002**, *316*, 265–276.

[339] Vogl, T.; Gharibyan, A. L.; Morozova-Roche, L. A. Pro-inflammatory S100A8 and S100A9 proteins: Self-assembly into multifunctional native and amyloid complexes. *Int. J. Mol. Sci.* **2012**, *13*, 2893–2917.

[340] Foell, D.; Wittkowski, H.; Vogl, T.; Roth, J. S100 proteins expressed in phagocytes: A novel group of damage-associated molecular pattern molecules. *Journal of Leukocyte Biology* **2007**, *81*, 28–37.

[341] Ma, B.; Nussinov, R. Simulations as analytical tools to understand protein aggregation and predict amyloid conformation. *Curr. Opin. Chem. Biol.* **2006**, *10*, 445–452.

[342] Korndörfer, I. P.; Brueckner, F.; Skerra, A. The crystal structure of the human $(S100A8/S100A9)_2$ heterotetramer, calprotectin, illustrates how conformational changes of interacting α-helices can determine specific association of two EF-hand proteins. *J. Mol. Biol.* **2007**, *370*, 887–898.

[343] Abe, H.; Kawasaki, K.; Nakanishi, H. pH-dependent aggregate forms and conformation of Alzheimer amyloid beta-peptide (12-24). *J. Biochem.* **2002**, *132*, 863–874.

[344] Ma, B.; Nussinov, R. Stabilities and conformations of Alzheimer's beta - amyloid peptide oligomers (Abeta 16-22, Abeta 16-35, and Abeta 10-35): Sequence effects. *Proc. Natl. Acad. Sci. U.S.A.* **2002**, *99*, 14126–14131.

[345] Balbach, J. J.; Ishii, Y.; Antzutkin, O. N.; Leapman, R. D.; Rizzo, N. W.; Dyda, F.; Reed, J.; Tycko, R. Amyloid fibril formation by $A\beta_{16-22}$, a seven-residue fragment of the Alzheimer's β-amyloid peptide, and structural characterization by solid state NMR. *Biochemistry* **2000**, *39*, 13748–13759.

[346] Lu, Y.; Wei, G.; Derreumaux, P. Effects of G33A and G33I mutations on the structures of monomer and dimer of the amyloid-β fragment 29-42 by replica exchange molecular dynamics simulations. *J. Phys. Chem. B* **2011**, *115*, 1282–1288.

[347] Mu, Y.; Nguyen, P. H.; Stock, G. Energy landscape of a small peptide revealed by dihedral angle principal component analysis. *Proteins: Struct. Funct. Bioinf.* **2005**, *58*, 45–52.

[348] Anitha, S. Studies on DNA topology and DNA-amyloid beta ($A\beta$) peptides interaction in relevance to Alzheimer's disease. Ph.D. thesis, University of Mysore, 2005.

[349] Ahn, B. W.; Song, D. U.; Jung, Y. D.; Chay, K. O.; Chung, M. A.; Yang, S. Y.; Shin, B. A. Detection of β-amyloid peptide aggregation using DNA electrophoresis. *Analytical Chemistry* **2000**, *284*, 401–405.

[350] Barrantes, A.; Rejas, M. T.; Benítez, M. J.; Jiménez, J. S. Interaction between Alzheimer's $A\beta 1-42$ peptide and DNA detected by surface plasmon

resonance. *J. Alzheimers Dis.* **2007**, *12*, 345–355.

[351] Hegde, M. L.; Anitha, S.; Latha, K. S.; Mustak, M. S.; Stein, R.; Ravid, R.; Rao, K. S. J. First evidence for helical transitions in supercoiled DNA by amyloid beta peptide $(1-42)$ and aluminum: a new insight in understanding Alzheimer's disease. *J. Mol. Neurosci.* **2004**, *2004*, 19–31.

[352] Suram, A.; Hegde, M. L.; Rao, K. S. J. A new evidence for DNA nicking property of amyloid beta-peptide $(1-42)$: relevance to Alzheimer's disease. *Arch. Biochem. Biophys.* **2007**, *463*, 245–252.

[353] Haijia Yu, Jinsong Ren,; Qu, X. Time-dependent DNA condensation induced by amyloid β-peptide. *Biophys. J.* **2007**, *92*, 185–191.

[354] Geng, J.; Zhao, C.; Ren, J.; Qu, X. Alzheimer's disease amyloid beta converting left-handed Z-DNA back to right-handed B-form. *Chem. Commun.* **2010**, *46*, 7187–7189.

[355] Domizio, J. D.; Zhang, R.; Stagg, L. J.; Gagea, M.; Zhuo, M.; Ladbury, J. E.; Cao, W. Binding with nucleic acids or glycosaminoglycans converts soluble protein oligomers to amyloid. *J. Biol. Chem.* **2011**, *287*, 736–747.

[356] van Dijk, M.; Bonvin, A. M. J. J. 3D-DART: A DNA structure modelling server. *Nucleic Acids. Res.* **2009**, *37*, W235–W239.

[357] Brzezinski, K.; Brzuszkiewicz, A.; Dauter, M.; Kubicki, M.; Jaskolski, M.; Dauter, Z. High regularity of Z-DNA revealed by ultra high-resolution crystal structure at 0.55$\mathring{A}$. *Nucleic Acids. Res.* **2011**, *39*, 6238–6248.

[358] Phillips, J. C.; Braun, R.; Wang, W.; Gumbart, J.; Tajkhorshid, E.; Villa, E.; Chipot, C.; Skeel, R. D.; Kalé, L.; Schulten, K. Scalable molecular dynamics with NAMD. *J. Comput. Chem.* **2005**, *26*, 1781–1802.

[359] Bernedo, V.; Insua, D.; Suárez, M.; Santamarina, G.; Sarasa, M.; Pesini, P. β-

amyloid cortical deposits are accompanied by the loss of serotonergic neurons in the dog. *J. Comp. Neurol.* **2009**, *513*, 417–429.

[360] Cirrito, J. R.; Disabato, B. M.; Restivo, J. L.; Verges, D. K.; Goebel, W. D.; Sathyan, A.; Hayreh, D.; D'Angelo, G.; Benzinger, T.; Yoon, H.; Kim, J.; Morris, J. C.; Mintun, M. A.; Sheline, Y. I. Serotonin signaling is associated with lower amyloid-β levels and plaques in transgenic mice and humans. *Proc. Natl. Acad. Sci. U.S.A.* **2011**, *108*, 14968–14973.

Publications

1. **L. N. Zhao**, T. Zhang, C. Zhang, C. Wang, L. A. Morozova-Roche, L. Y. Chew and Y. G. Mu. S100A9 induces aggregation-prone conformation in Abeta peptides: A combined experimental and simulation study. RSC Advances, 3, 24081-24089 (2013).

2. **L. N. Zhao**, Y. G. Mu and L. Y. Chew. Heme prevents Abeta peptides aggregation through hydrophobic interaction based on molecular dynamics simulation. Phys. Chem. Chem. Phys., 15(33):14098 (2013).

3. **L. N. Zhao**, S. W. Chiu, J. Benoit, L. Y. Chew and Y. G. Mu, The effect of curcumin on the stability of Aβ dimers. J. Phys. Chem. B, 116(25), 7428-7435 (2012).

4. **L. N. Zhao**, H. W. Leong, Y. G. Mu and L. Y. Chew, The toxicity of amyloid β oligomers. Int. J. Mol. Sci., 13, 7303 (2012).

5. **L. N. Zhao**, S. W. Chiu, J. Benoit, L. Y. Chew and Y. G. Mu, Amyloid beta peptides aggregation in a mixed membrane bilayer: a molecular dynamics study. J. Phys. Chem. B, 115(42), 12247-12256 (2011).